

**ASSESSMENT OF A NEXT GENERATION  
GRAVITY MISSION FOR MONITORING THE  
VARIATIONS OF EARTH'S GRAVITY FIELD**

**TN4: Mission Analysis and AOCS Concepts**

<b>Written by</b>	<b>Responsibility</b> + handwritten signature if no electronic workflow tool
G. Sechi	Author
	Author
	Author
<b>Verified by</b>	
A. Anselmi	Checker
<b>Approved by</b>	
A. Anselmi	Study Manager
<b>Documentation Manager</b>	
R. Cavaglià	

Approval evidence is kept within the documentation management system.

**CHANGE RECORDS**

<b>ISSUE</b>	<b>DATE</b>	<b>§ CHANGE RECORDS</b>	<b>AUTHOR</b>
1	July 10		G. Sechi

## TABLE OF CONTENTS

<b>1. INTRODUCTION .....</b>	<b>5</b>
1.1 Scope and Purpose .....	5
<b>2. DOCUMENTS.....</b>	<b>5</b>
2.1 Applicable Documents.....	5
2.2 ESA Reference Documents.....	5
2.3 NGGM Study Notes .....	6
2.4 Further Reference Documents.....	6
<b>3. SYNTHESIS OF CONTROL REQUIREMENTS .....</b>	<b>7</b>
3.1 Introduction.....	7
3.2 Linear acceleration control requirements .....	7
3.3 Relative position control requirements .....	7
3.4 Attitude control requirements.....	8
<b>4. CONTROL ARCHITECTURE AND DESIGN UPDATES .....</b>	<b>11</b>
4.1 Introduction.....	11
4.2 Drag-free control algorithms.....	11
4.2.1 Results from previous design and updates.....	11
4.2.2 Design algorithm description.....	11
4.2.3 Simulation results.....	12
4.3 Formation control algorithms .....	16
4.3.1 Results from previous design and updates.....	16
4.3.2 Design justification .....	17
4.3.3 Design algorithm description.....	26
4.3.4 Simulation results.....	27
4.4 Attitude control.....	33
4.4.1 Pointing control requirements .....	33
4.4.2 Laser pointing by satellite .....	38
4.4.2.1 Requirement and accuracy of the metrology .....	38
4.4.2.2 Design algorithm description.....	43
4.4.2.3 Simulation results .....	46
<b>5. NEW STAR-TRACKER MODEL .....</b>	<b>56</b>
5.1 Introduction.....	56

5.2	Computation of the spectral density of attitude error .....	57
6.	POST-PROCESSING EMULATOR.....	60
6.1	Introduction.....	60
6.2	Algorithm description .....	60
7.	EQUIPMENT REQUIREMENT .....	66
7.1	Thrusters requirements .....	66
8.	APPENDIX A –ATTITUDE MOTION IN PENDULUM FORMATION.....	69
8.1	Justification of the attitude motion .....	69
9.	ACRONYMS.....	72

## 1. INTRODUCTION

### 1.1 Scope and Purpose

This document is submitted in fulfilment of WP 2220 of the Next Generation Gravity Mission (NGGM) study. It constitutes the output of Task 3 of the NGGM statement of work.

The purpose of the document is to report on the work and on the results concerning the attitude and orbit control concepts introduced in the frame of the study.

With respect to the previous study phase, new formation geometries have been considered like in-line with baseline up to 100km (10km in previous study phase), pendulum and cartwheel. Moreover, the laser pointing mechanism has been cancel leaving laser pointing function in charge of the attitude control.

## 2. DOCUMENTS

### 2.1 Applicable Documents

- [AD-1] Assessment of a Next Generation Gravity Mission to monitor the variations of Earth's gravity field, Statement of Work, EOP-SF/2008-09-1334, Issue 2, 20 November 2008, Appendix 1 to AO/1-5914/09/NL/CT
- [AD-2] Special Conditions of Tender, Appendix 3 to AO/1-5914/09/NL/CT
- [AD-3] Draft Contract. Appendix 2 to AO/1-5914/09/NL/CT.

### 2.2 ESA Reference Documents

- [RD-1] Rummel et al. (2003), Scientific objectives for Future Geopotential Missions, Technical Note, Version 6 from the ESA contract No: 16668/02/NL/MM "Enabling Observation Techniques for Future Solid Earth Missions"
- [RD-2] Koop, R., Rummel, R. (2007), The Future of Satellite Gravimetry, Final Report of the Future Gravity Mission Workshop, 12-13 April 2007 ESA/ESTEC, Noordwijk, Netherlands
- [RD-3] Laser Doppler Interferometry Mission for determination of the Earth's Gravity Field, ESTEC Contract 18456/04/NL/CP, Final Report, Issue 1, 19 December 2005
- [RD-4] Laser Interferometry High Precision Tracking for LEO, ESA Contract No. 0512/06/NL/IA, Final Report, July 2008
- [RD-5] System Support to Laser Interferometry Tracking Technology Development for Gravity Field Monitoring, ESA Contract No. 20846/07/NL/FF, Final report, September 2008
- [RD-6] Bender P.L., Wiese D.N., and Nerem R.S., "A Possible Dual-GRACE Mission With 90 Degree And 63 Degree Inclination Orbits", Proceedings of the 3rd International Symposium on Formation Flying, Missions and Technologies, Noordwijk (NL), April 2008

- [RD-7] T. van Dam et al., Monitoring and Modelling Individual Sources of Mass Distribution and Transport in the Earth System by Means of Satellites, Final Report, ESA Contract No. 20403, November 2008
- [RD-8] Variable Earth Model Description and Product Specification Document, ESA Contract No. 20403, November 2008
- [RD-9] Enabling Observation Techniques for Future Solid Earth Missions, ESA Contract No: 16668/02/ NL/MM, Final report, Issue 2, 15 July 2004.A

### 2.3 NGGM Study Notes

- [RD-10] NGGM TN1 "Requirement Analysis", University of Luxembourg, Issue 1, Revision 1, 8 February 2010
- [RD-11] NGGM TN2 "System Drivers", Thales Alenia Space, SD-TN-AI-1262, 4 December 2010
- [RD-12] NGGM TN3 Part 1 "Instrument Concepts", Thales Alenia Space Italy, SD-TN-AI-1289, in preparation
- [RD-13] NGGM TN3 Part 2 "Observing Techniques", IAPG, in preparation
- [RD-14] NGGM TN4 Part 1 "AOCS concepts", Thales Alenia Space Italy, SD-TN-AI-1290, in preparation
- [RD-15] NGGM TN4 Part 2 "Mission Analysis of Candidate Scenarios", Deimos, in preparation
- [RD-16] NGGM TN5 Part 1 "Multi-Satellite Simulation Tool for SST Mission", Thales Alenia Space Italy, SD-TN-AI-1291, in preparation
- [RD-17] NGGM TN5 Part 2 "Scientific Simulation Tool", DEOS, in preparation
- [RD-18] NGGM TN5 Part 3 "Variable Gravity Model", IAPG, in preparation
- [RD-19] NGGM TN6 Part 1 "Candidate System Concepts and Mission Architecture outlines, trade-off's and favourite mission concept", Thales Alenia Space Italy, SD-TN-AI-1292, in preparation
- [RD-20] NGGM TN6 Part 2 "Scientific Assessment of Mission Architectures", GIS, in preparation
- [RD-21] NGGM TN7 "Conclusions and Recommendations", Thales Alenia Space Italy, to be initiated

### 2.4 Further Reference Documents

- [RD-22] Enrico Canuto, "TR4 – Drag-free, relative satellite position and attitude control strategies investigation", LiGRA-PoliTo-Part I -19.0/08, 30 October 2008.
- [RD-23] Enrico Canuto, "CCN-1 – Optimal formation control", LiGRA-PoliTo-25.0-1/09, 25 August 2008.
- [RD-24] Handout of the PM2 presentation, 18 March 2010.
- [RD-25] E. Canuto, "Embedded Model Control: outline of the theory", ISA Transaction, 44(7), June 2007, 46(3), p.363-377
- [RD-26] J.L. Beaupellet, S. De Sanctis, G. Sechi, B. Girouart, "ATTITUDE DETERMINATION TAILORED TO MULTIPLE HEADS STAR-TRACKER", in Proceedings of the 7<sup>th</sup> International ESA Conference on Guidance, Navigation & Control Systems, 2-5 June 2008, Tralee, County Kerry, Ireland

### 3. SYNTHESIS OF CONTROL REQUIREMENTS

#### 3.1 Introduction

The following chapter reports all the requirements relevant for the design of the control systems, as coming from [RD-12].

#### 3.2 Linear acceleration control requirements

The linear acceleration control (drag-free control) has in charge the virtualization of the environment (drag-free) by the compensation of environmental forces in order to limit the residual linear.

Two requirements have been provided:

- the magnitude of the residual linear acceleration shall be lower than  $10^{-6}$  m/s<sup>2</sup> (each axis);
- the stability of the residual linear acceleration as indicated in Figure 3.2-1 (each axis).

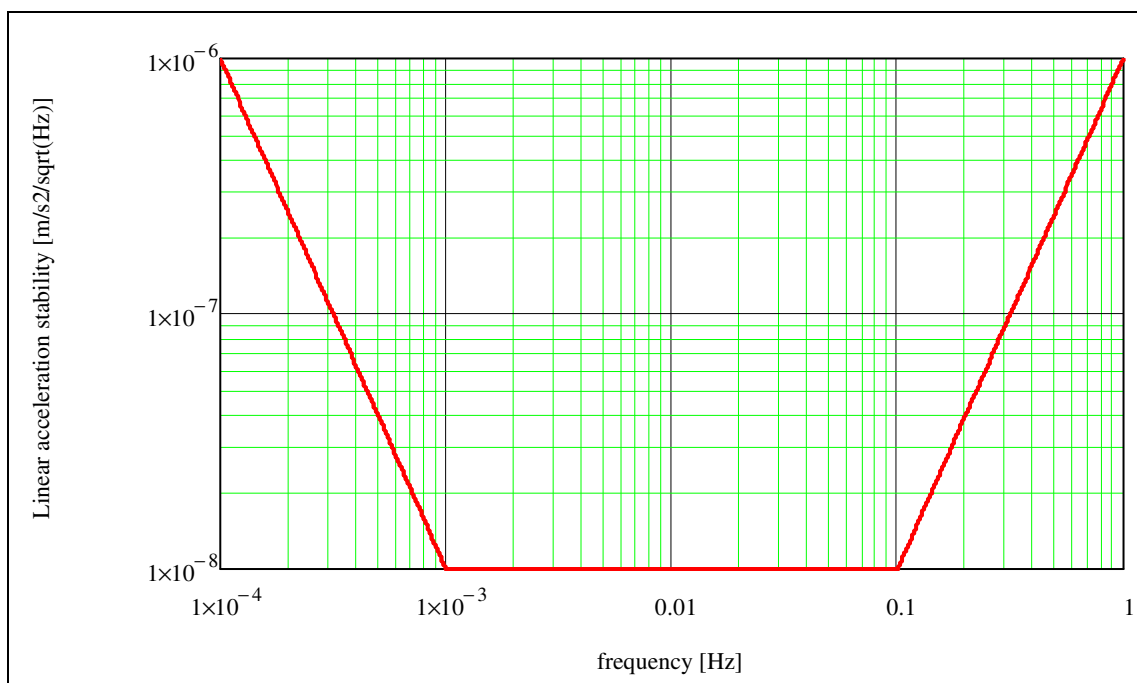


Figure 3.2-1 Requirement of the linear acceleration stability.

#### 3.3 Relative position control requirements

The relative position requirements are in charge of the formation control. They outcome from two different objectives:

- to cope with the required sensitivity on the Earth gravity field, the magnitude of the distance between the satellites shall not be lower than a 50÷100km;

- the maximum distance shall be compatible with the laser operating conditions. It is worth notice that the power required to laser increases with the square value of the distance.

In the frame of the study, different formation geometries have been considered: in-line, pendulum and cart-wheel. Table 3.3-1 summaries the requirement on the relative position components for each foreseen formation. The relative position is given in Local Orbital Reference Frame (LORF) of the Satellite 1 (see Figure 3.3-1).

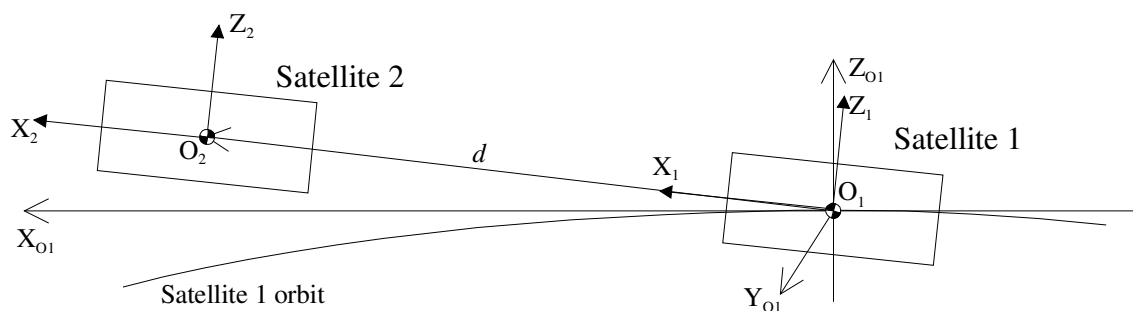


Figure 3.3-1 Definition of the satellite-to-satellite alignment.

Table 3.3-1 – Requirements on the satellite relative position expressed in the Satellite 1 LORF.

	Nominal values [km]			Allowed errors [km]		
	X	Y	Z	X	Y	Z
<b>In-line</b>	75	0	0	+/-10	+/-1	+/-1
<b>Pendulum</b>	62÷88	+/-62	0	+/-10	+/-10	+/-1
<b>Cart-wheel</b>	+/-100	0	+/-50	+/-10	+/-1	+/-10

### 3.4 Attitude control requirements

The attitude control design has cope with the following objectives:

- to keep the X axis aligned with the satellite-to-satellite direction with the following absolute errors:
  - Satellite 2:  $\leq 1^\circ$  (the laser shall be inside the retro-reflector field-of-view);
  - Satellite 1:  $\leq 2 \cdot 10^{-5}$  rad (driven by the required laser beam pointing).
- to keep the satellite-to-satellite direction by satellite X axis with the stability provided in Figure 3.4-1 and Figure 3.4-2.
- to constrain the magnitude of the angular acceleration and rate error below  $1e-6$  rad/s<sup>2</sup> and  $1e-4$  rad/s respectively;
- to constrain the angular rate and acceleration stability below the values reported in Figure 3.4-3 and Figure 3.4-4.

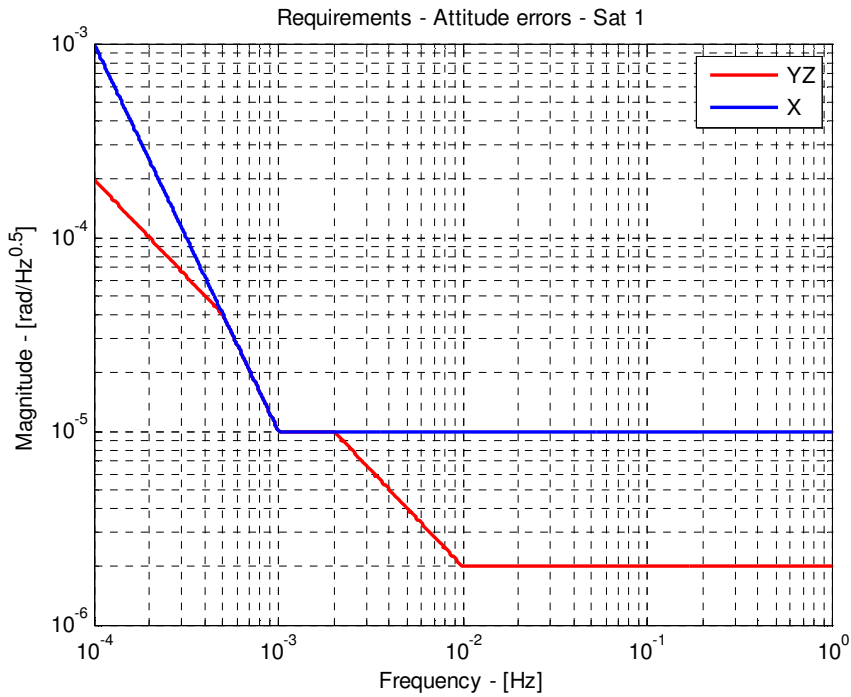


Figure 3.4-1 Requirement on the pointing stability (Satellite 1).

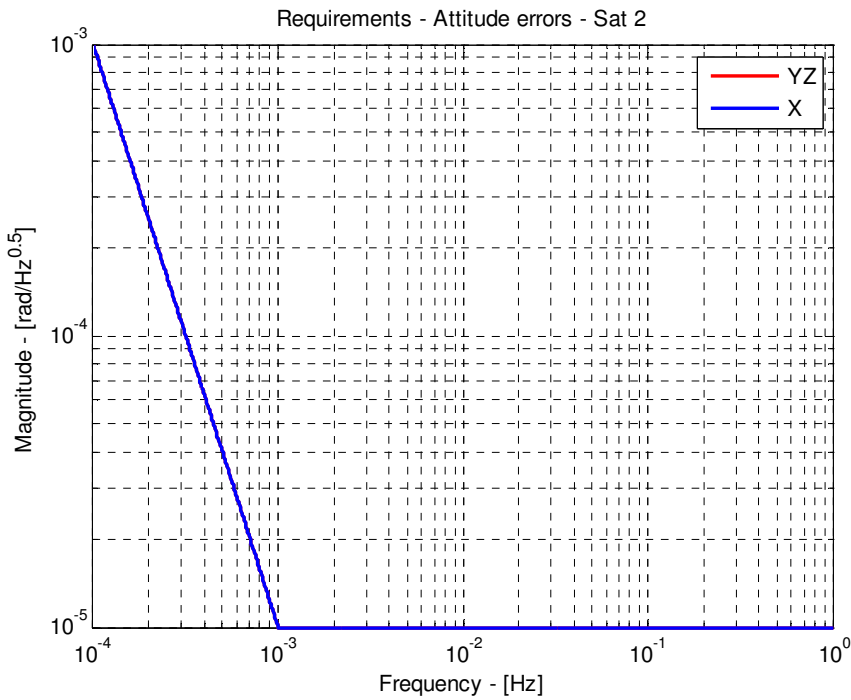


Figure 3.4-2 Requirement on the pointing stability (Satellite 2).

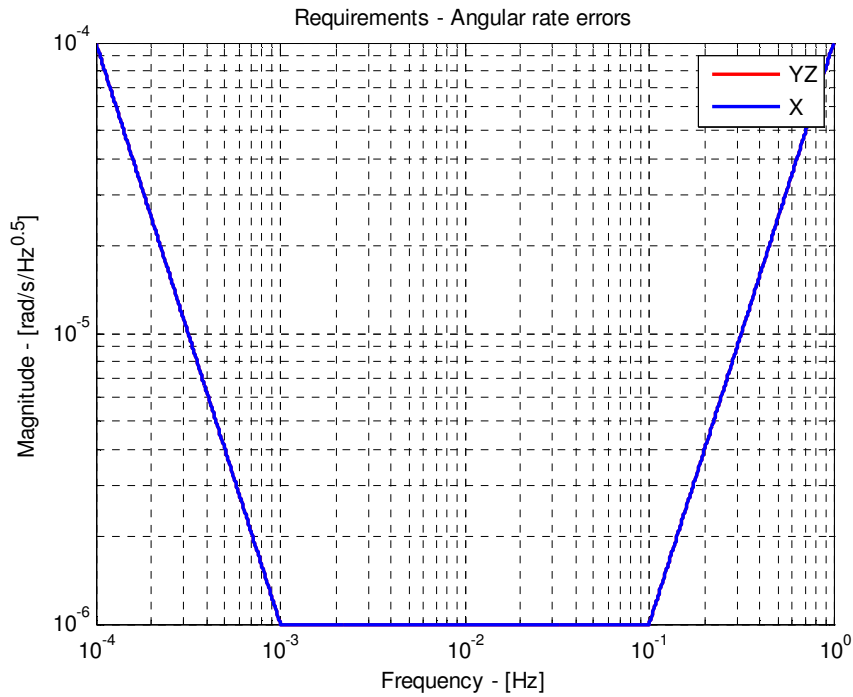


Figure 3.4-3 Requirement on the angular rate errors (Satellite 1 and Satellite 2).

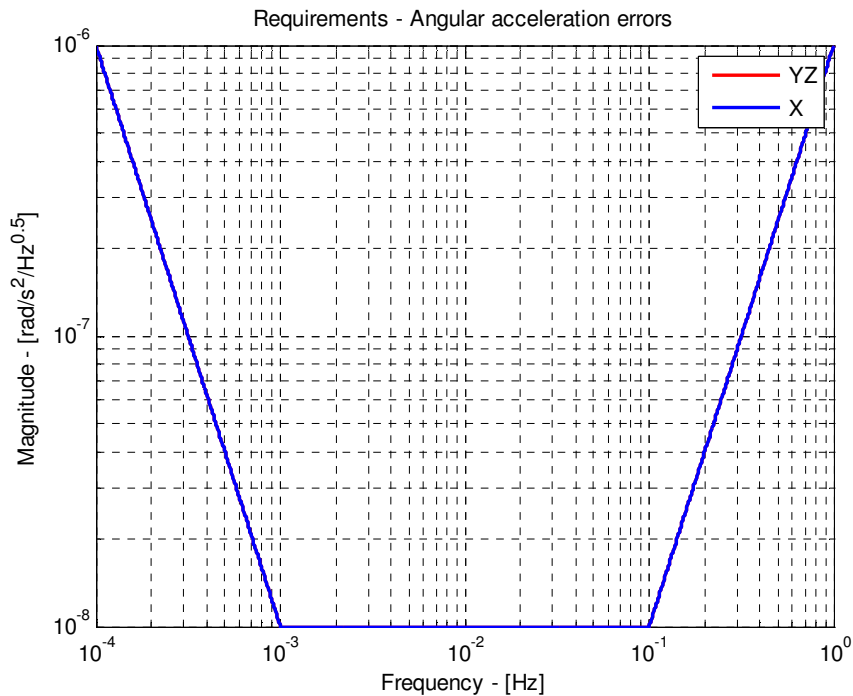


Figure 3.4-4 Requirement on the angular acceleration errors (Satellite 1 and Satellite 2).

## 4. CONTROL ARCHITECTURE AND DESIGN UPDATES

### 4.1 Introduction

Both the control architecture and the algorithms start from the work done during the previous study phase and described in [RD-22] and [RD-23].

All introduced changes and up-dates have been done to cope with the actual accelerometers' drag-free channel (not considered during previous study phase), the new control requirements and formation geometries.

Hereafter, description and justification of the improvements will be provided. Not too much emphasis has been put on the rigorous presentation of the algorithms since it is considered outside the scope of the study. This should be interesting to be done in next studies.

### 4.2 Drag-free control algorithms

#### 4.2.1 Results from previous design and updates

The activities involving the linear acceleration controls (drag-free) have been:

- re-tuning of the acceleration predictors (see [RD-22]) of each linear axis to take into account the anti-aliasing filter on accelerometer's outputs;
- increasing of the order of the X and Y axes acceleration predictors to permits a greater low-frequency rejection with the same control bandwidth (similar margins with respect to the requirements provided by Z axis acceleration predictors for in-line and pendulum formation geometries).

The re-tuning has been necessary since the previous drag-free control parameters have not taken into account the anti-aliasing filter at the end of the DFAC channel of each accelerometer that is instead present inside the E2E simulator. The anti-aliasing filter is the same considered for the DFAC channel present on the GOCE electrostatic gradiometer, i.e. 3rd order Butterworth low-pass digital filter, 3.5 Hz cut-off frequency.

Figure 4.2-3 shows the one-sided spectral density of the X-axis linear acceleration as before the tuning update. This has been done taking into account all the requirements, providing enough robustness toward plant uncertainty, and still improvement capabilities.

#### 4.2.2 Design algorithm description

The new X and Y axes acceleration predictor has the same structure given at pag. 53 of the [RD-22]. It embeds a simplified model of the thruster-to-accelerometer dynamics (first order) and a stochastic model of the disturbance (2<sup>nd</sup> order in previous design, 3<sup>rd</sup> order now).

The 4<sup>th</sup> order embedded model is the following:

$$\begin{bmatrix} x(i+1) \\ a(i+1) \\ s(i+1) \\ \Delta s(i+1) \end{bmatrix} = \begin{bmatrix} 0 & 1 & 0 & 0 \\ 0 & 1 & 1 & 0 \\ 0 & 0 & 1 & 1 \\ 0 & 0 & 0 & 1 \end{bmatrix} \begin{bmatrix} x(i) \\ a(i) \\ s(i) \\ \Delta s(i) \end{bmatrix} + \begin{bmatrix} 1 \\ 0 \\ 0 \\ 0 \end{bmatrix} u(i) + \begin{bmatrix} 1 & 0 & 0 & 0 \\ 0 & 1 & 0 & 0 \\ 0 & 0 & 1 & 0 \\ 0 & 0 & 0 & 1 \end{bmatrix} \begin{bmatrix} w_0(i) \\ w_1(i) \\ w_2(i) \\ w_3(i) \end{bmatrix}$$

$$y(i) = x(i) + e(i)$$

$e(i)$  takes into account the acceleration measurement error and model error.

The corresponding state predictor reads:

$$\begin{bmatrix} \hat{x}(i+1) \\ \hat{a}(i+1) \\ \hat{s}(i+1) \\ \Delta \hat{s}(i+1) \end{bmatrix} = \begin{bmatrix} -l_0 & 1 & 0 & 0 \\ -l_1 & 1 & 1 & 0 \\ -l_2 & 0 & 1 & 1 \\ -l_3 & 0 & 0 & 1 \end{bmatrix} \begin{bmatrix} \hat{x}(i) \\ \hat{a}(i) \\ \hat{s}(i) \\ \Delta \hat{s}(i) \end{bmatrix} + \begin{bmatrix} 1 \\ 0 \\ 0 \\ 0 \end{bmatrix} u(i) + \begin{bmatrix} l_0 \\ l_1 \\ l_2 \\ l_3 \end{bmatrix} \tilde{y}(i)$$

The X and Y controllers sensitivity function is given in Figure 4.2-1: it has a low-frequency asymptote of the 3<sup>rd</sup> order. Figure 4.2-2 shows the sensitivity function for the Z axis controller.

Table 4.2-1 provides the values of the gains as for the actual tuning of the linear acceleration predictors.

### 4.2.3 Simulation results

Table 4.2-1 – Parameters of the linear acceleration controls (10Hz sampling frequency).

Axis	Gains	Value
<b>X</b>	$l_0$	0.08
	$l_1$	0.36
	$l_2$	0.0464
	$l_3$	0.00192
<b>Y</b>	$l_0$	0.08
	$l_1$	0.36
	$l_2$	0.0464
	$l_3$	0.00192
<b>Z</b>	$l_0$	0.1
	$l_1$	0.32
	$l_2$	0.028

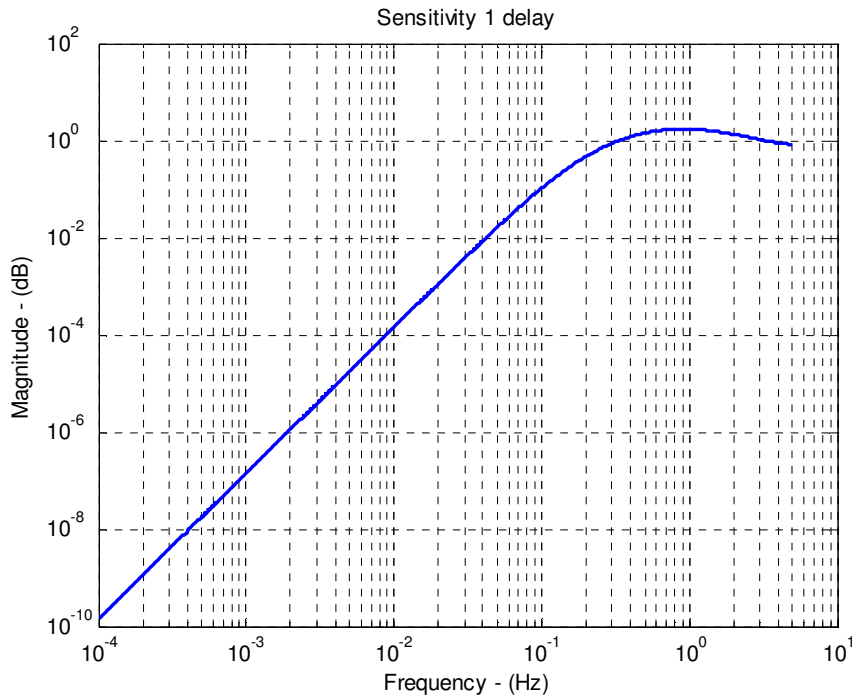


Figure 4.2-1 Sensitivity function of the X and Y axes linear acceleration controllers.

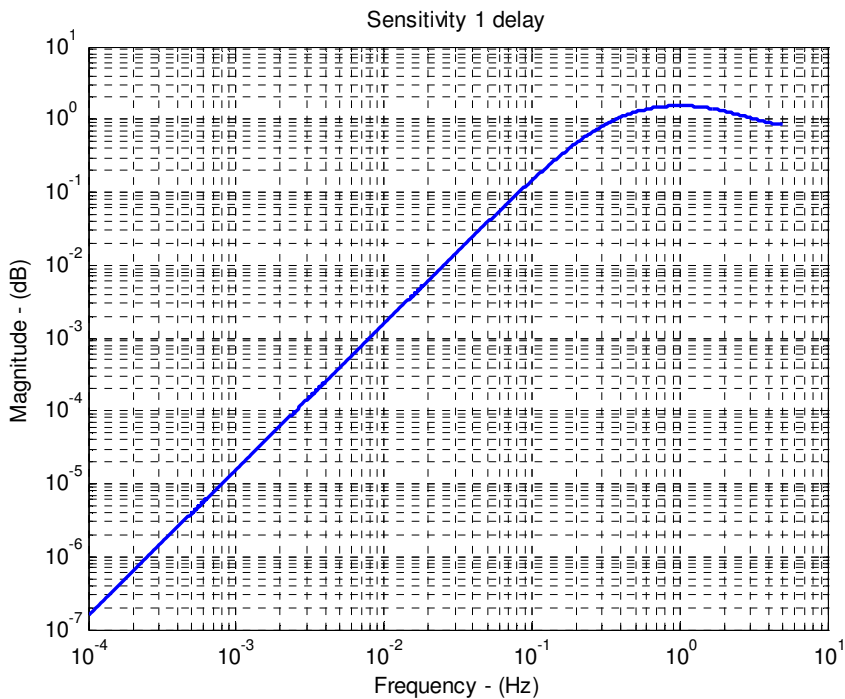


Figure 4.2-2 Sensitivity function of the Z axis linear acceleration controller.

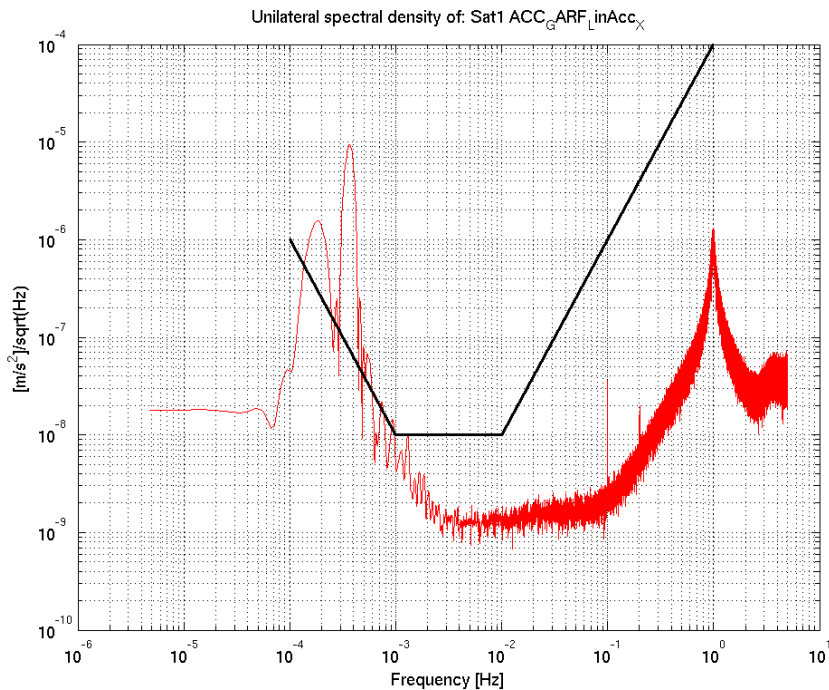


Figure 4.2-3 One-sided spectral density of the X-axis linear acceleration in the previous solution after the introduction of the DFAC channel (in-line formation with 10km baseline),(the black line is the requirement considered in previous study phase).

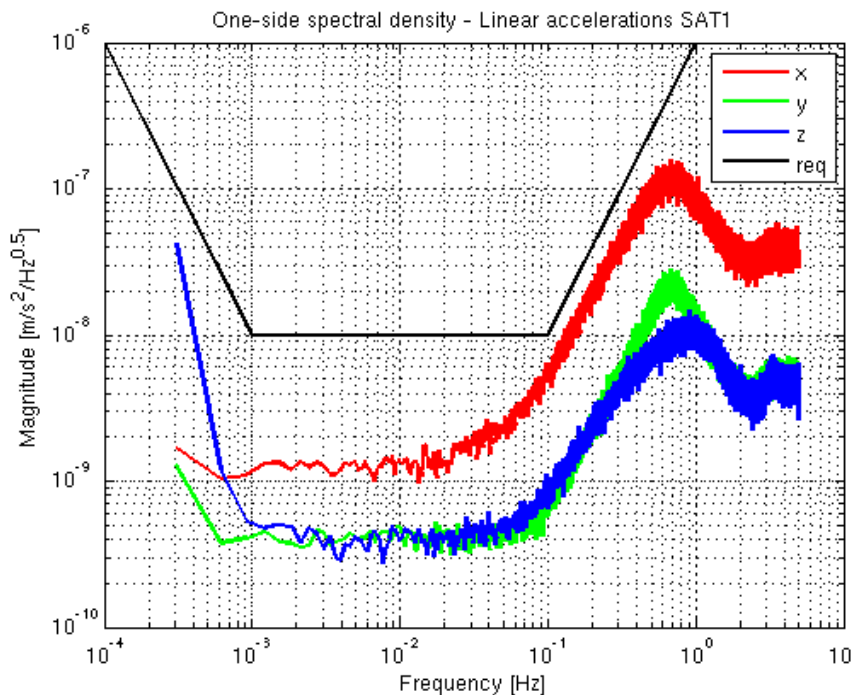


Figure 4.2-4 One-sided spectral density of the SAT1 linear accelerations after the introduction of the DFAC channel and for new design (formation control not activated).

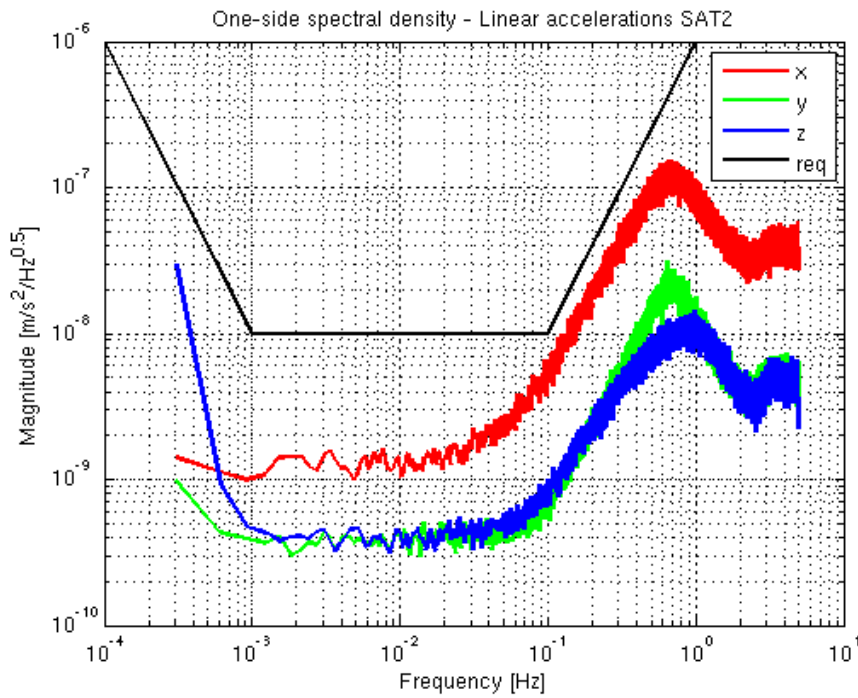


Figure 4.2-5 One-sided spectral density of the SAT 2 linear accelerations after the introduction of the DFAC channel and for new design (formation control not activated).

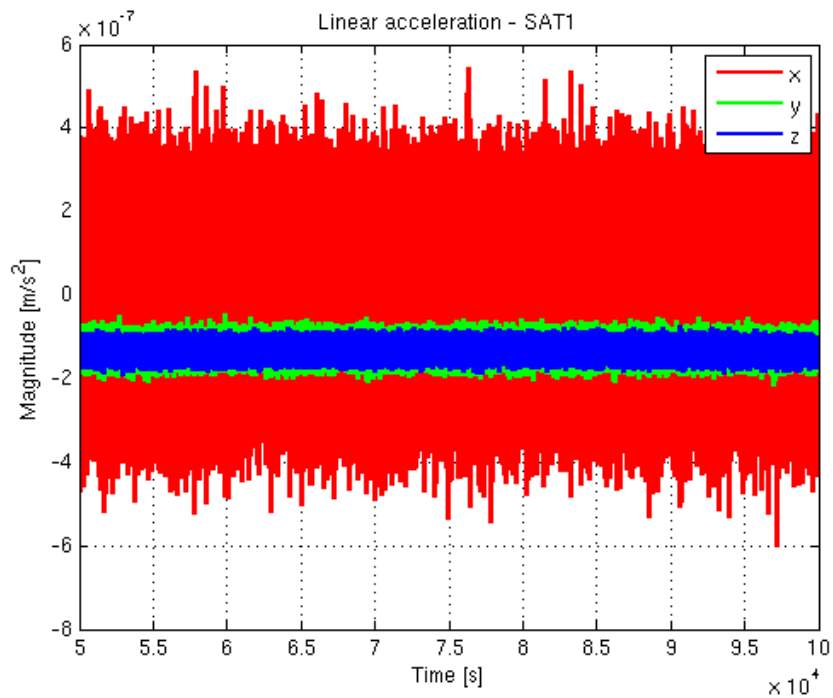


Figure 4.2-6 Time series of the SAT1 linear accelerations after the introduction of the DFAC channel and for new design (formation control not activated).

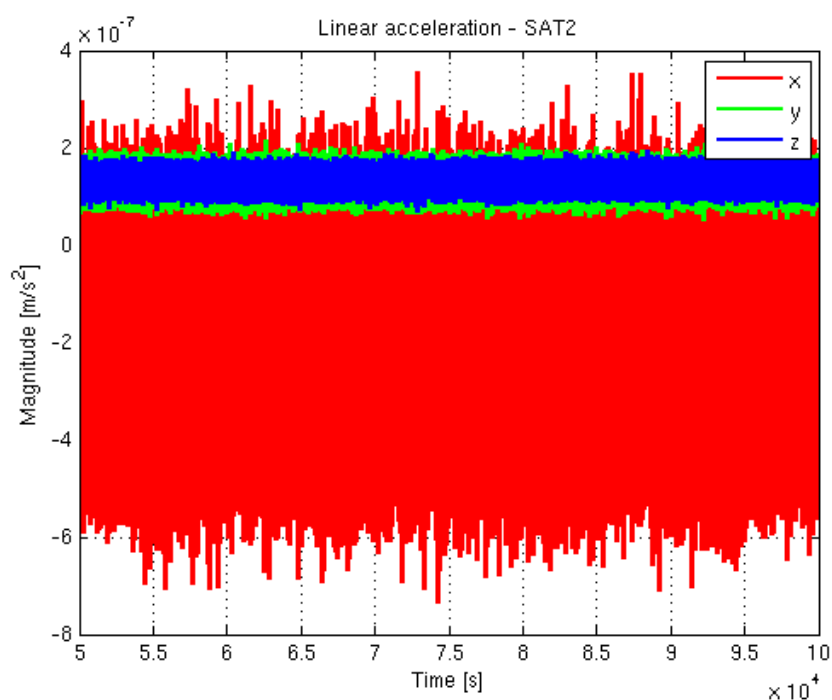


Figure 4.2-7 Time series of the SAT2 linear accelerations after the introduction of the DFAC channel and for new design (formation control not activated).

### 4.3 Formation control algorithms

#### 4.3.1 Results from previous design and updates

In the frame of the previous study, the formation flying control for the in-line geometry with baseline equals to 10km has been studied.

As shown in [RD-23], the expected performances were all met. With the extension of the baseline from 10km up to 75÷100km required for the considered new formations, without any additional tuning the obtained results were as provided in Figure 4.3-1. To reduce the computer simulation time, the Earth gravity model was truncated at 10<sup>th</sup> order and degree as clearly shown by the sudden change in the spectral density of the linear acceleration at about 4mHz.

It is clear that the spectral density of the residual linear acceleration at frequencies close to 1mHz is too high. The worsening of the performance is due to the action of the formation control. In fact, the formation control command (and then the required acceleration that shall not be destroyed by drag-free) is proportional to the amplitude of the detected disturbance that, in turn, is proportional to the baseline length. To cope with the linear acceleration requirement and longer baseline it is necessary to reduce the control authority at least of a factor 10.

At first, formation control parameters have been modified but without to much success. Then, by a more deep understanding of the control algorithm, it was clear that the architecture carried out during the previous study phase was not able to cope with new requirement.

In the previous control architecture, a damping action has been introduced on radial and out-of-plane directions, and a PID-like control on along-track directions. The radial and along-track controls were designed taking into account the coupling and following a thrust optimal multivariate control approach (see [RD-23]).

The damping action has been designed to be effective at the orbital frequency, i.e. at about 0.2mHz, 1/5 of the lower frequency for the MBW.

Two options appear possible:

- to change the control design without introducing any damping action and limiting the control bandwidth to lower frequency;
- to have a fine characterization of the overall control loop (magnitude and phase delay of the transfer function), in order to recover the actual signal by post-processing.

Of course, those options are not reciprocally exclusive; the first one will be addressed hereafter.

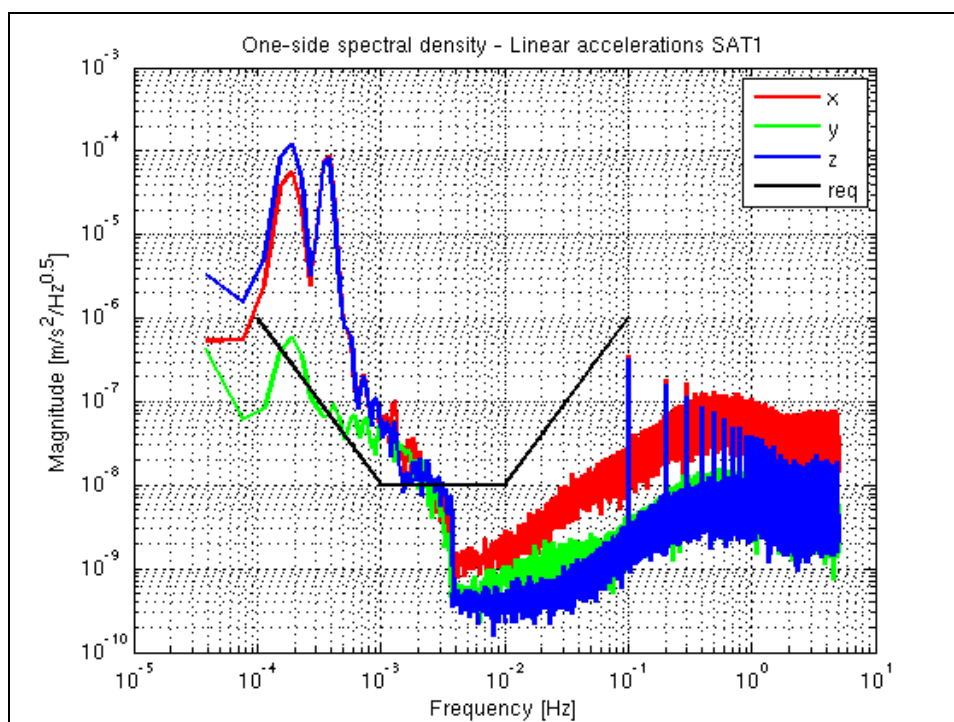


Figure 4.3-1 One-sided spectral density of the linear acceleration on Satellite 1 ),(the black line is the requirement considered in previous study phase).

### 4.3.2 Design justification

Starting from a given init state vector, the formation geometry changes in time according to:

- perturbation due to gravity field (non-spherical components like J2, etc.), drag, solar pressure, etc.
- differential linear acceleration bias due to drag-free;
- not exact initialization of the state variables (relative position and/or velocity) due to GNC sub-system.

The basic ideas have been started considering the evolution of the in-line (relative distance 75km) and pendulum formation (relative mean distance 75km) geometries considering the following additional perturbations:

- A. Earth gravity only: Earth gravity model (30x30);
- B. Full gravity: Earth gravity model (30x30), Sun and Moon;
- C. Full gravity and differential bias: Earth gravity model (30x30), Sun, Moon and a residual differential bias due to drag-free controls ( $\pm 10^{-7}$  m/s<sup>2</sup>).

The error on state variables initialization related to GNC sub-system was not taken into account. One month simulation time has been considered to assess the formation motion.

The motion for the in-line and pendulum formations have been analysed by Deimos (see [RD-24]) and the major results have been reported in the following.

From the shown results, it is possible to conclude that:

- 3rd body perturbations have small impact;
- differential bias destabilizes all formations in few days;
- the pendulum formation built starting with  $\Delta i$  formation shows almost linear drift from the init relative mean distance;
- pendulum formation is more stable with  $\Delta \Omega$  delta in RAAN.

It is clear that the control law shall embed at least the capability to compensate the differential biases. The bias estimator shall be enough fast to follow the low frequency drift of the differential biases, and, at the same time, enough slow to do not provide disturbances at the frequency relevant for the scientific mission.

Since the control shall be operating at low-frequency (i.e. less than the orbit frequency), the model on which to design the controller may be very simple, without take into account J2 effects and other: the Hill-Clohessy-Wiltshire (HCW) model (chief motion almost circular, differential effects related to J2, drag, etc. are not taken into account) is considered good enough.

Let consider:

- $x$  : along track relative distance;
- $y$  : out-of-plane (across track) relative distance;
- $z$  : radial relative distance;
- $a_x$  : along track acceleration;
- $a_y$  : out-of-plane acceleration;
- $a_z$  : radial acceleration;
- $n$  : orbit angular rate.

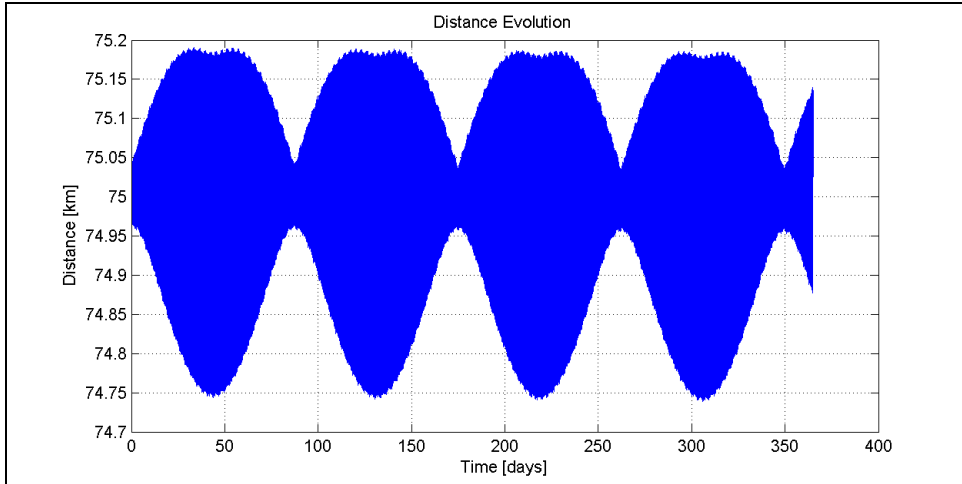


Figure 4.3-2 – In-line formation - Earth gravity only – Along track motion (1 year).

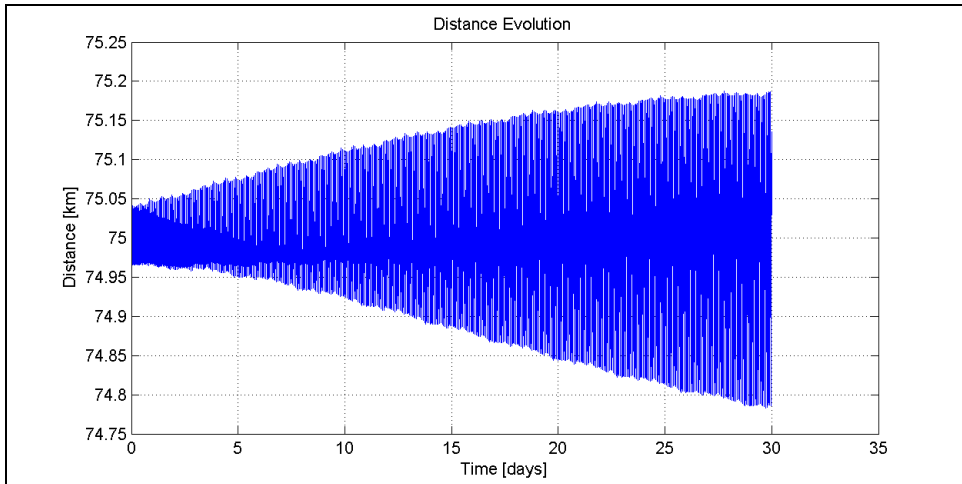


Figure 4.3-3 - In-line formation - Earth gravity only – Zoom on the first month for the along track motion.

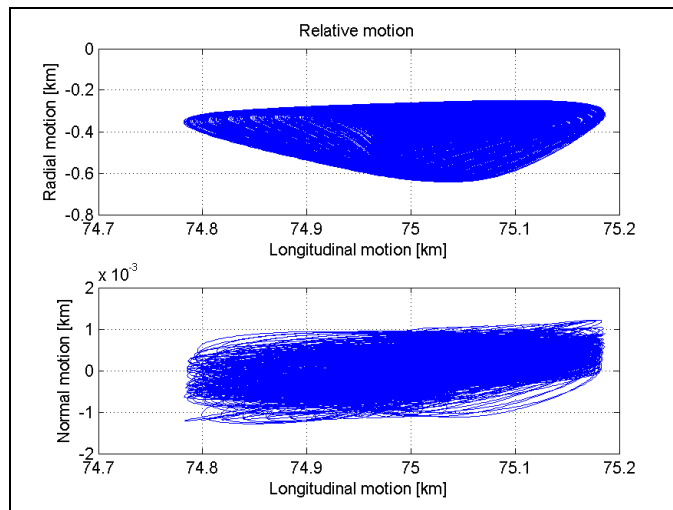


Figure 4.3-4 - In-line formation - Earth gravity only – Radial and out-of-plane motion.

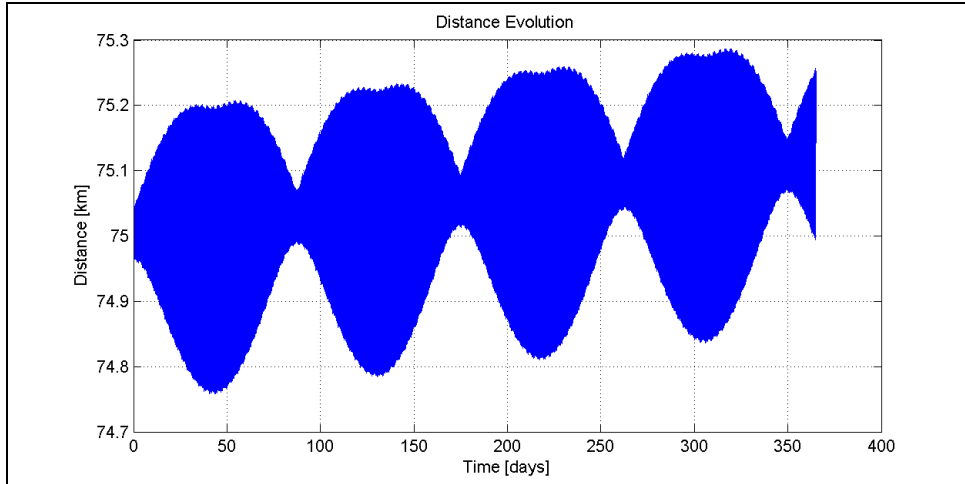


Figure 4.3-5 – In-line formation - Full gravity – Along track motion (1 year)

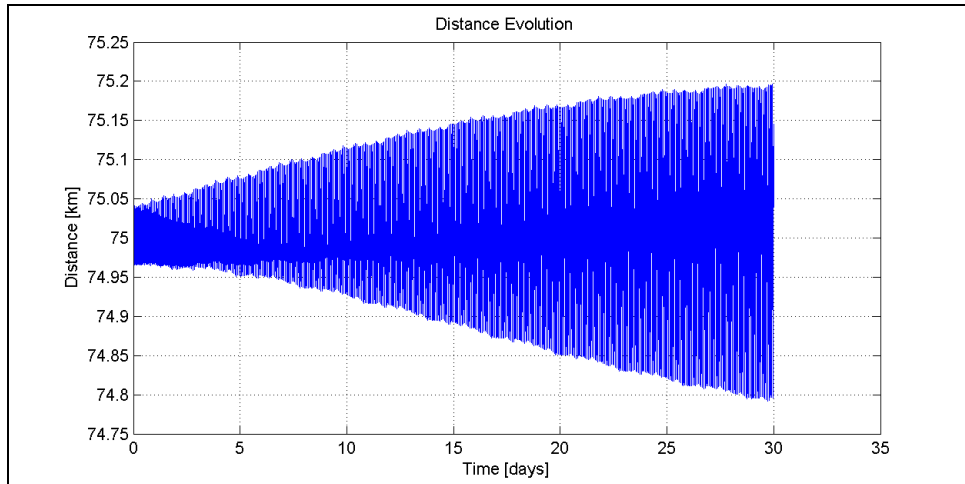


Figure 4.3-6 - In-line formation - Full gravity – Zoom on the first month for the along track motion.

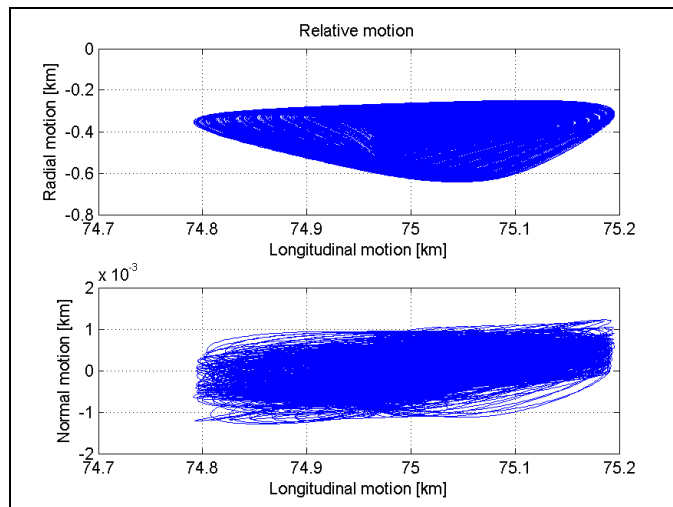


Figure 4.3-7 - In-line formation - Full gravity – Radial and out-of-plane motion.

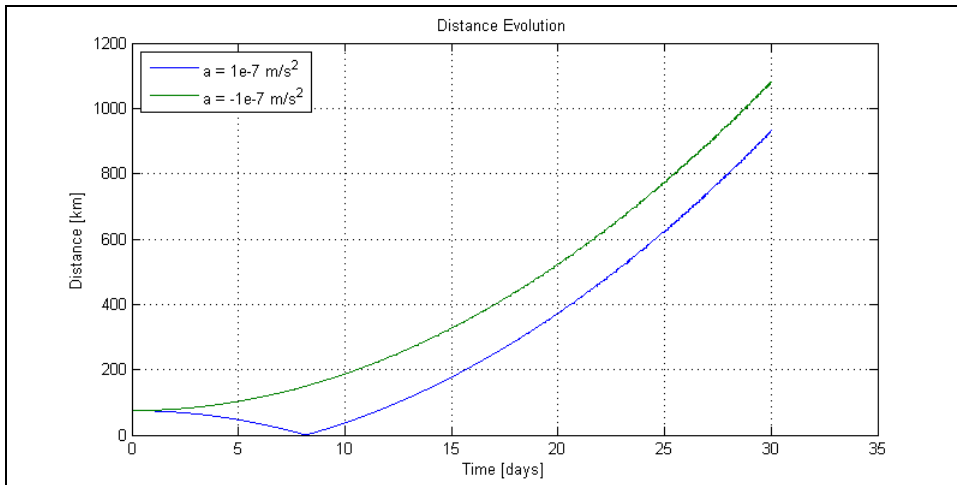


Figure 4.3-8 - In-line formation - Full gravity and differential bias – Along track motion.

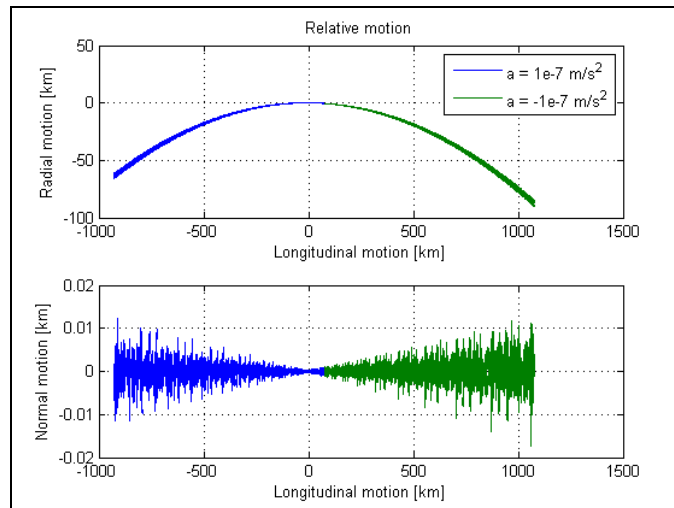


Figure 4.3-9 - In-line formation - Full gravity and differential bias – Radial and out-of-plane motion.

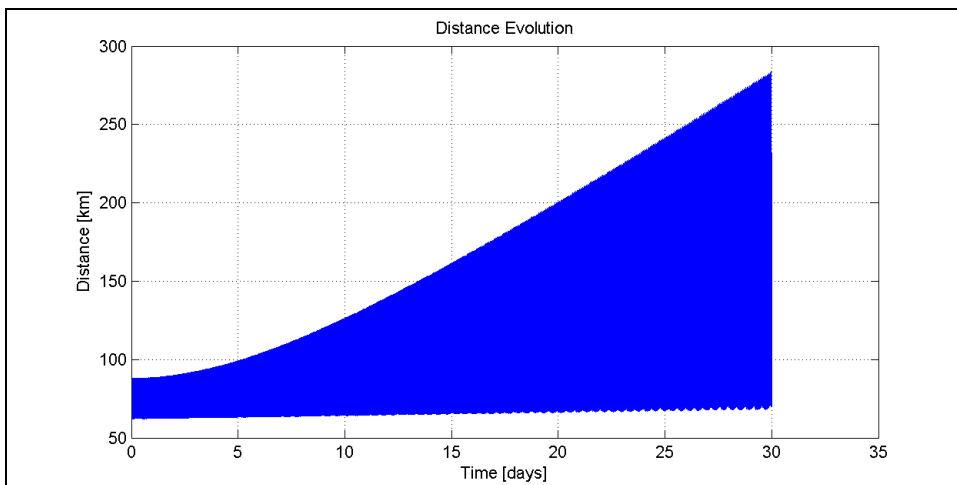


Figure 4.3-10 – Pendulum with  $\Delta i$  formation - Earth gravity only – Along track motion.

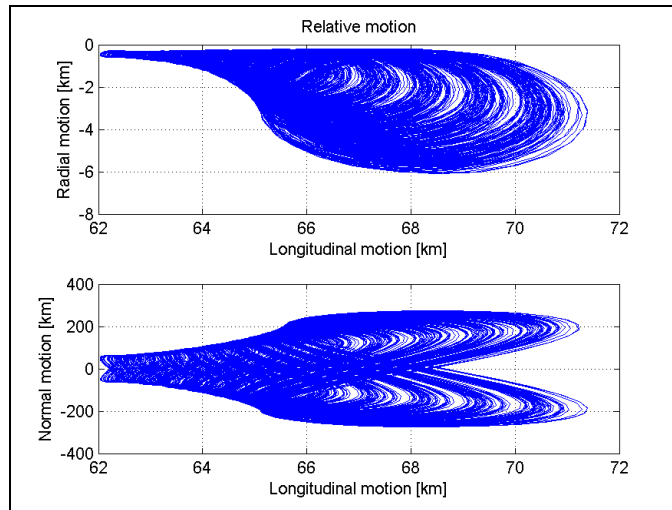


Figure 4.3-11 – Pendulum with  $\Delta i$  formation - Earth gravity only – Radial and out-of-plane motion.

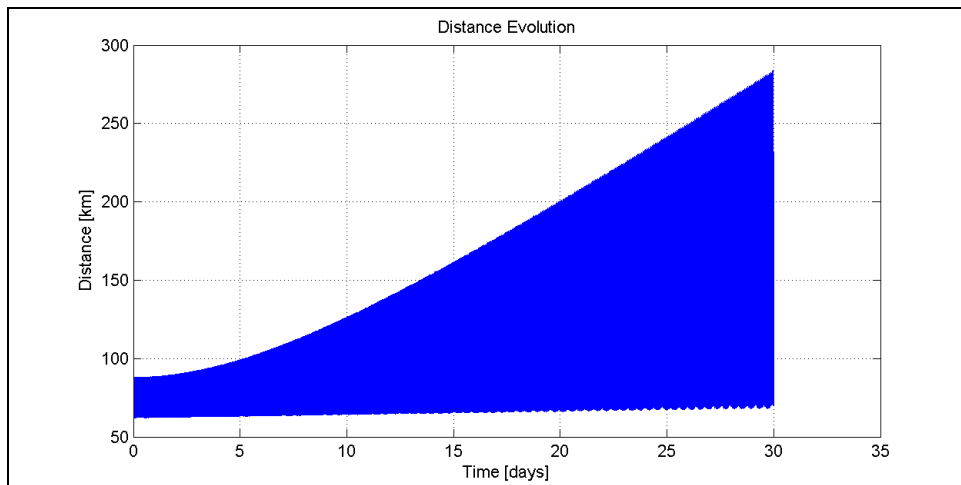


Figure 4.3-12 – Pendulum with  $\Delta i$  formation - Full gravity – Along track motion.

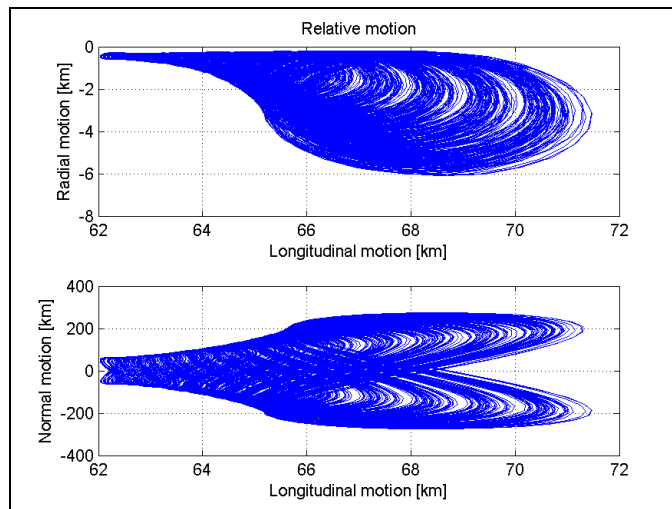


Figure 4.3-13 – Pendulum with  $\Delta i$  formation - Full gravity – Radial and out-of-plane motion.

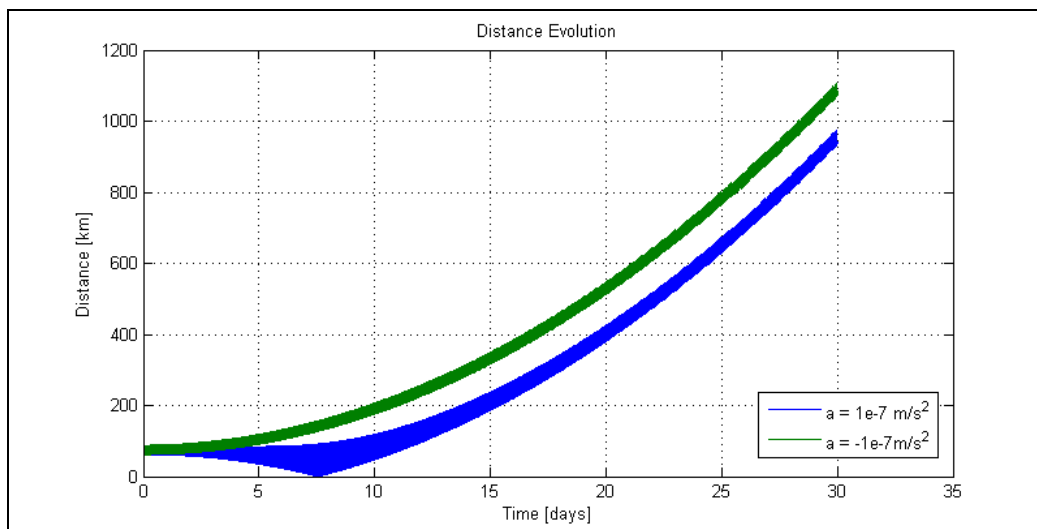


Figure 4.3-14 – Pendulum with  $\Delta i$  formation - Full gravity and differential bias – Along track motion.

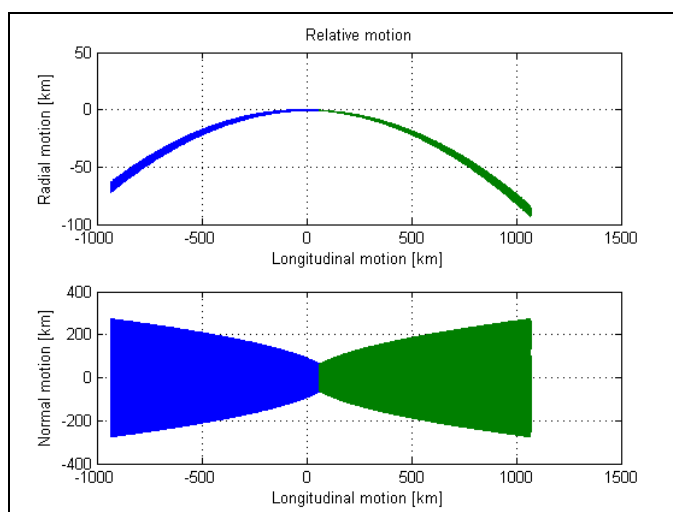


Figure 4.3-15 – Pendulum with  $\Delta i$  formation - Full gravity and differential bias – Radial and out-of-plane motion.

Table 4.3-1 – Summary of the formation motion under different classes of perturbations.

	Perturbations [km]	Deviation wrt 75 km [km]	Deviation wrt max. design distances [km]
In-line formation	Earth Gravity	0.2	-
	Full Gravity	0.2	-
	Full Gravity + Differential Bias	1000	-
Pendulum with $\Delta i$	Earth Gravity	200	-
	Full Gravity	200	-
	Full Gravity + Differential Bias	1000	-
Pendulum with $\Delta \Omega$	Earth Gravity	13	0.3
	Full Gravity	13	0.3
	Full Gravity + Differential Bias	1000	-

The HCW equation reads:

- in plane (along track and radial) motion

$$\begin{bmatrix} \dot{x} \\ \ddot{x} \\ \dot{z} \\ \ddot{z} \end{bmatrix} = \begin{bmatrix} 0 & 1 & 0 & 0 \\ 0 & 0 & 0 & -2n \\ 0 & 0 & 0 & 1 \\ 0 & 2n & 3n^2 & 0 \end{bmatrix} \begin{bmatrix} x \\ \dot{x} \\ z \\ \dot{z} \end{bmatrix} + \begin{bmatrix} 0 & 0 \\ 1 & 0 \\ 0 & 0 \\ 0 & 1 \end{bmatrix} \begin{bmatrix} a_x \\ a_z \end{bmatrix}$$

- out of plane/ across-track motion

$$\begin{bmatrix} \dot{y} \\ \ddot{y} \end{bmatrix} = \begin{bmatrix} 0 & 1 \\ -n^2 & 0 \end{bmatrix} \begin{bmatrix} y \\ \dot{y} \end{bmatrix} + a_y$$

CWH model puts in evidence coupling between XZ axes (along-track/ radial) while Y axis (across track) is uncoupled. The eigenvalues of the HCW equation are:

- along-track and radial (coupled axis):  $0, 0, \pm jn$
- across-track:  $\pm jn$

The system is not asymptotically stable.

Starting from the linear time invariant HCW model, it has been derived at first the solution of the homogeneous differential equations, and then the transfer functions and the step responses.

The solution of the homogeneous differential equations reads:

$$x(t) = -2A_0 \sin(nt + \alpha) - \frac{3}{2}nt y_{off} + x_{off}$$

$$y(t) = A_0 \cos(nt + \alpha) + y_{off}$$

$$z(t) = B_0 \sin(nt + \beta)$$

being  $A_0, B_0, \alpha, \beta, x_{off}, y_{off}$  linked to the init values for relative position and velocity. Bounded relative motion is available if  $y_{off} = 0$ , i.e.  $\dot{x}_0 + 2ny_0 = 0 \Rightarrow \dot{x}_0 = 0$

The MIMO transfer function reads:

$$\begin{bmatrix} X(s) \\ Y(s) \\ Z(s) \end{bmatrix} = \frac{1}{s^2(s^2 + n^2)} \begin{bmatrix} s^2 - 3n^2 & 0 & -2ns \\ 0 & s^2 & 0 \\ 2ns & 0 & s^2 \end{bmatrix} \begin{bmatrix} A_x(s) \\ A_y(s) \\ A_z(s) \end{bmatrix}$$

The motion as consequence of the differential biases reads:

$$x(t) = \frac{\bar{A}_X}{n^2} \left\{ [1 - \cos(nt)] - 3 \left[ -1 + \frac{n^2 t^2}{2} + \frac{1}{n} \cos(nt) \right] \right\} - \frac{2\bar{A}_Z}{n^2} \{nt - \sin(nt)\}$$

$$y(t) = \frac{\bar{A}_Y}{n^2} \{1 - \cos(nt)\}$$

$$z(t) = \frac{2\bar{A}_X}{n^2} \{nt - \sin(nt)\} + \frac{\bar{A}_Z}{n^2} \{1 - \cos(nt)\}$$

where  $\bar{A}_X$ ,  $\bar{A}_Y$  and  $\bar{A}_Z$  are the differential biases amplitude on the  $a_x$ ,  $a_y$  and  $a_z$  accelerations respectively.

It is possible to observe that:

- if we apply a bias on X linear axis (along-track) only, then:
  - X-axis relative position grows in quadratic way;
  - Z-axis relative position grows in linear way.
- if we apply a bias on Z linear axis (radial) only, then:
  - X-axis relative position grows in linear way;
  - Z-axis relative position remains bounded with magnitude related to the applied bias.
- if we apply a bias on Y linear axis (across-track) only, then the Y-axis relative position remains bounded with magnitude related to the applied bias.

As consequence of previous statements, the proposed formation control for the observation phase may be very simple. Only, the along track (X-axis) relative position shall be controlled to maintain the formation geometry on a time horizon to be defined and addressed by simulation. The X-axis controller shall embed the capability to estimate the differential bias and shall provide compensation for it (i.e. PID like controller).

Radial (Z-axis) and across-track (Y-axis) may be left without any specific control law. A differential bias up to  $2 \cdot 10^{-7}$  m/s<sup>2</sup> induces an oscillation with amplitude  $\frac{A}{n^2} = 0.15$ m that is negligible with the formation init error due to GNC sub-system.

The simulations done to support the scientists' activities have shown that the formation geometries like in-line and pendulum may be maintained for more than 60days.

In any case, the formation control architecture shall be based on at least two types of formation controls algorithms to support the formation acquisition and to permit the scientific observation. The observation phase shall be preceded and followed by formation acquisition and re-acquisition phases.

Formation acquisition may be based on control solutions like those considered during the previous study phase and described in [RD-23]. They offer very small relative position and velocity errors formation (indicated before as init error due to GNC sub-system).

### 4.3.3 Design algorithm description

Since the objective of the study has not been the refined design of the control algorithms but to establish the orbit and attitude control concept for each satellite and to support the E2E simulation, a very simple but robust controller has been considered.

The design has not been done according to the approach Embedded Model Control (see [RD-25]) or other state space based approaches. The actual design is based on a very simple PID controller, according to the following discrete state equation:

$$\begin{bmatrix} \hat{x}_0(i+1) \\ \hat{x}_1(i+1) \\ \hat{x}_2(i+1) \end{bmatrix} = \begin{bmatrix} 1-l_0 & 1 & 0 \\ -l_1 & 1 & 0 \\ -1 & 0 & 1 \end{bmatrix} \begin{bmatrix} \hat{x}_0(i) \\ \hat{x}_1(i) \\ \hat{x}_2(i) \end{bmatrix} + \begin{bmatrix} l_0 \\ l_1 \\ 0 \end{bmatrix} \tilde{x}(i) + \begin{bmatrix} 0 \\ 0 \\ 1 \end{bmatrix} \bar{r}(i)$$

$$u_x(i) = k_p(\bar{r}(i) - \hat{x}_0(i)) - k_D(-\hat{x}_1(i)) + k_I \hat{x}_2(i)$$

being

$\hat{x}_0$  : estimator state variables (relative position);

$\hat{x}_1$  : estimator state variables (relative position first difference);

$\hat{x}_2$  : estimator state variables (integrative action);

$l_0, l_1$  : estimator gains;

$u_x$  : commanded X-axis acceleration;

$\bar{r}$  : average reference distance (set-point);

$k_p$  : controller gain proportional to the difference between the average reference distance  $\bar{r}$  and the estimated relative position;

$k_D$  : controller gain proportional to the difference between the estimated relative velocity;

$k_I$  : controller gain proportional to the integral of the difference between the average reference distance  $\bar{r}$  and the estimated relative position.

The considered steady state gains and reference average distances for in-line and pendulum are shown in Table 4.3-2. The proposed control tuning represents only a preliminary solution that of course may be still improved.

The formation control sampling frequency is the same considered during the previous study phase (i.e. 0.1Hz). Since in the current study phase the requirements on residual linear acceleration has been extended up to 0.1Hz, it should be convenient in the frame of next phases to increase the formation control sampling frequency (e.g. 0.5Hz), moving toward high frequency also the image spectrum of the formation control.

To fastener the differential bias estimation and, at the same time, to reduce the time to start the scientific observation, a time-variant gains solution has been implemented inside the E2E simulator.

**Table 4.3-2 – Values of the steady-state parameters of the relative position controller (0.1Hz sampling frequency)**

Formation geometry	Gain	Value
<i>In-line</i>		
	$\bar{r}$	75000m
	$l_0$	2.000000e-02
	$l_1$	1.000000e-04
	$k_P$	1.400000e-11
	$k_D$	7.000000e-07
	$k_I$	8.000111e-17
<i>Pendulum</i>		
	$\bar{r}$	62000m
	$l_0$	2.000000e-02
	$l_1$	1.000000e-04
	$k_P$	1.400000e-11
	$k_D$	7.000000e-07
	$k_I$	8.000111e-17

#### 4.3.4 Simulation results

The results provided hereafter are only to show that the new control architecture is effective. More details are outside the scope of the study; in any case, that formation control has been considered for simulation results provided to the scientists.

The more simple in-line formation has been considered with a baseline equals to 75km. Considered biases on linear acceleration measurement have been considered up to  $\pm 2 \cdot 10^{-7}$  m/sec<sup>2</sup>.

The results have been obtained considering active the satellite-to-satellite pointing strategy (no laser beam pointing mechanism present).

The comparison between Figure 4.3-1 with Figure 4.3-23 and Figure 4.3-24 show the clear improvement achieved with the new control law (it is worth to notice that the spectral density has been computed considering the same length of the time interval).

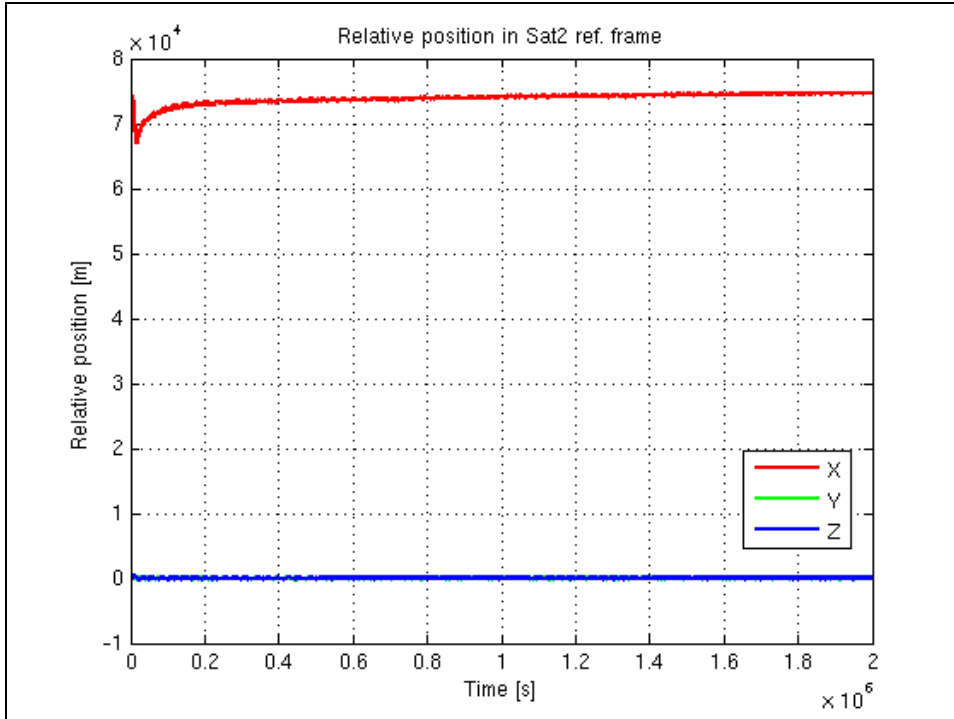


Figure 4.3-16 Relative position of the SAT1 with respect to SAT2, provided in SAT2 body reference frame.

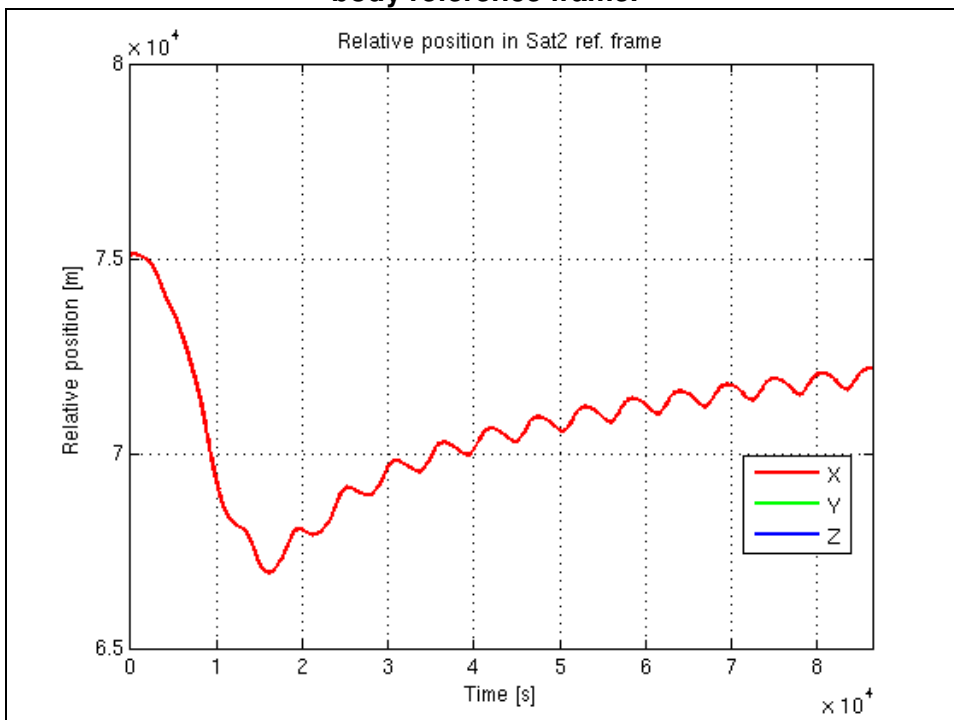


Figure 4.3-17 Relative position of the SAT1 with respect to SAT2, provided in SAT2 body reference frame (transient after formation control activation).

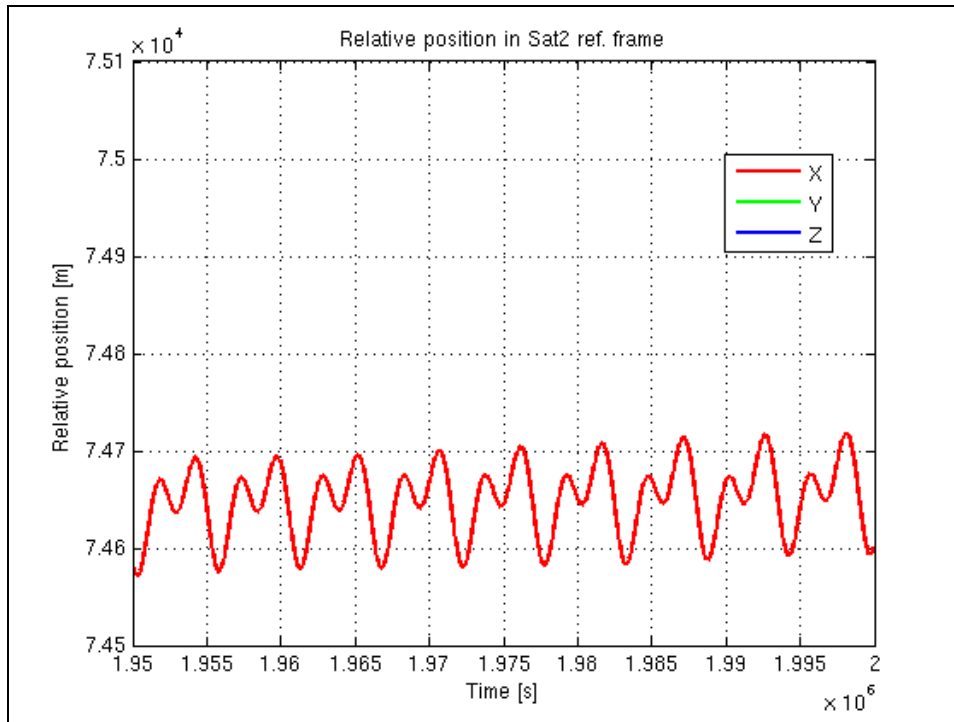


Figure 4.3-18 X-axis component of the relative position of the SAT1 with respect to SAT2, provided in SAT2 body reference frame (steady state).

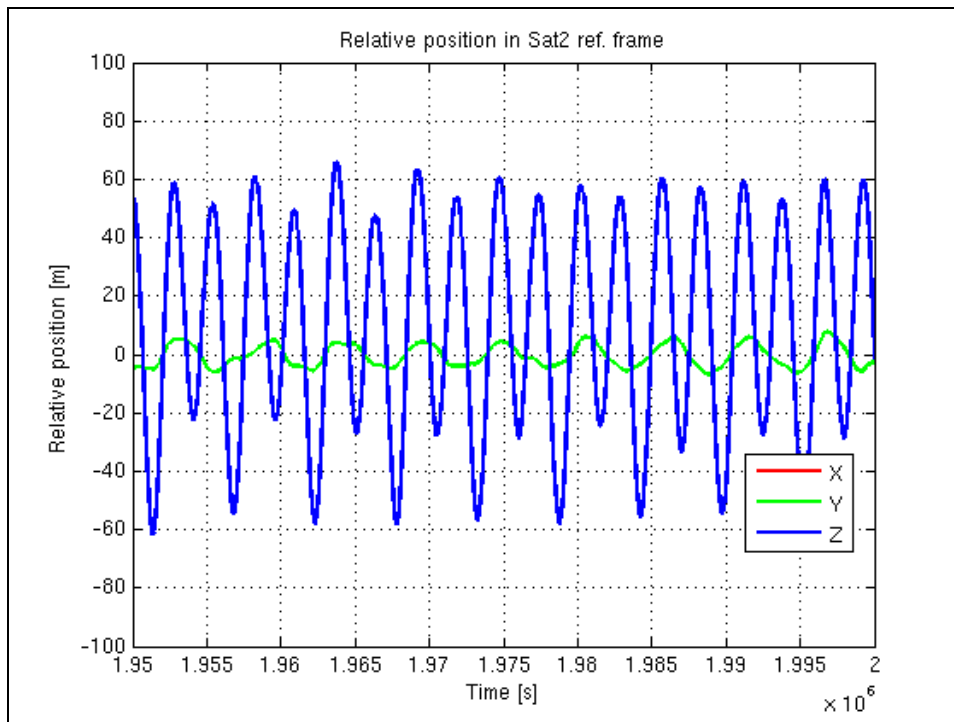


Figure 4.3-19 Y-axis and Z-axis components of the relative position of the SAT1 with respect to SAT2, provided in SAT2 body reference frame (steady state).

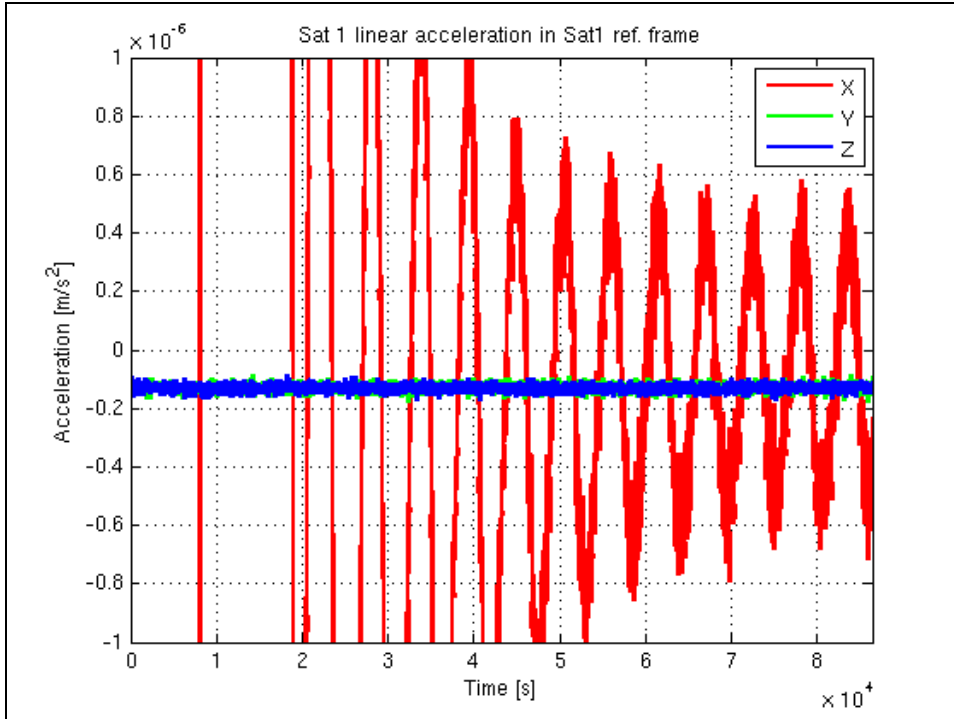


Figure 4.3-20 SAT1 linear acceleration in SAT1 body reference frame (transient after formation control activation).

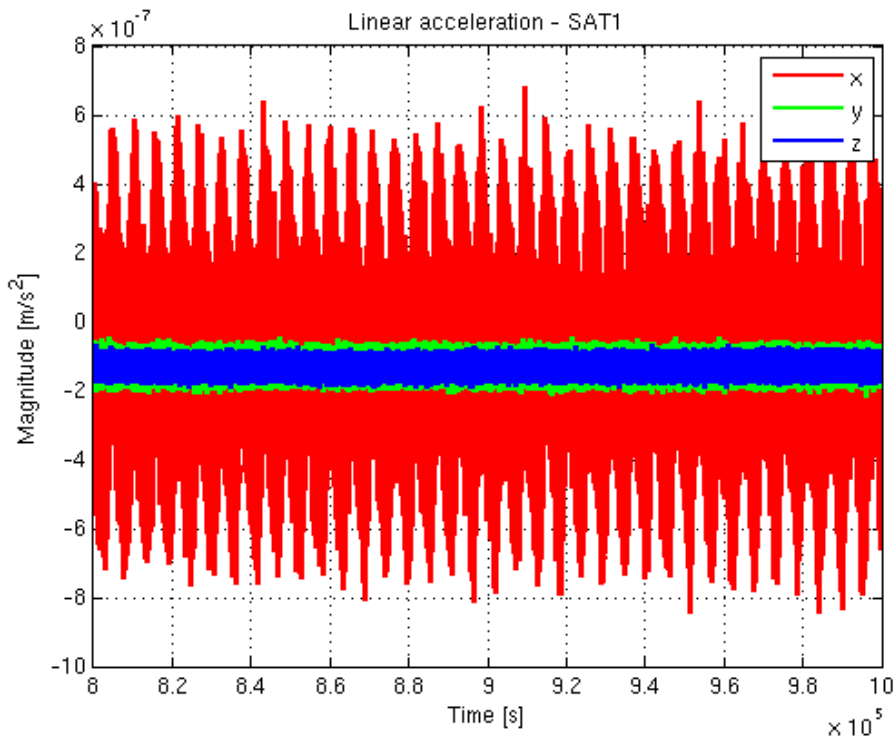


Figure 4.3-21 Time series of the SAT1 linear acceleration in SAT1 body reference frame (steady state).

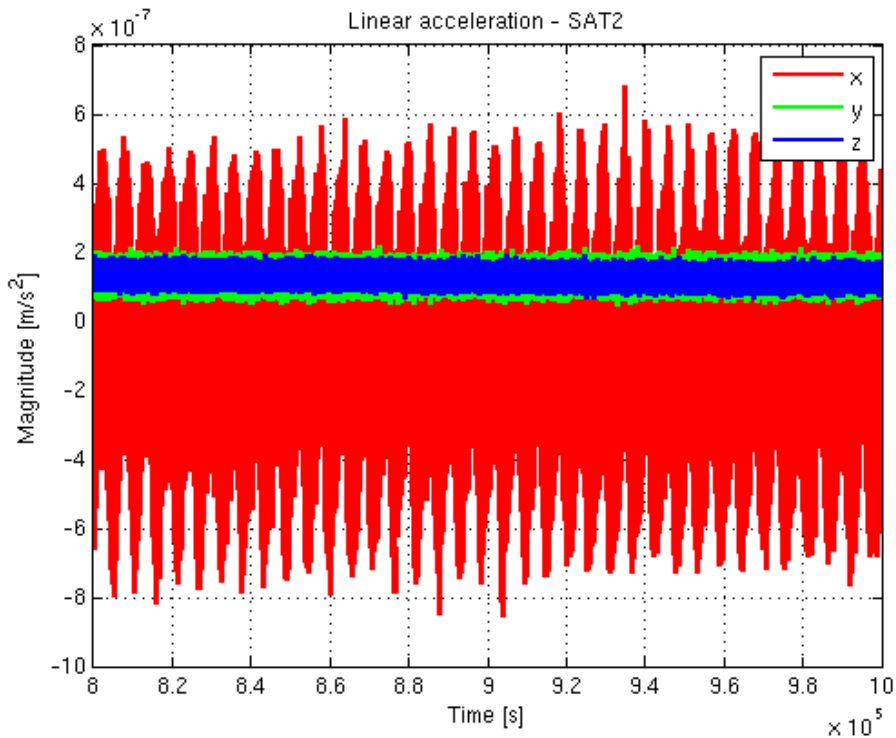


Figure 4.3-22 Time series of the SAT2 linear acceleration in SAT2 body reference frame (steady state).

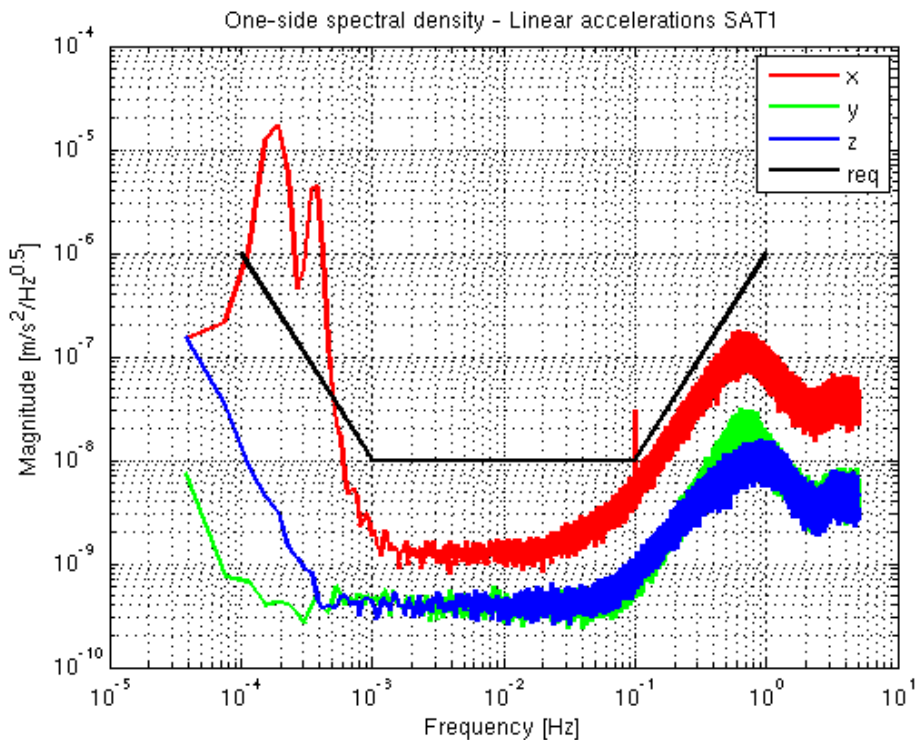


Figure 4.3-23 One-sided spectral density of the SAT1 linear acceleration in SAT1 body reference frame.

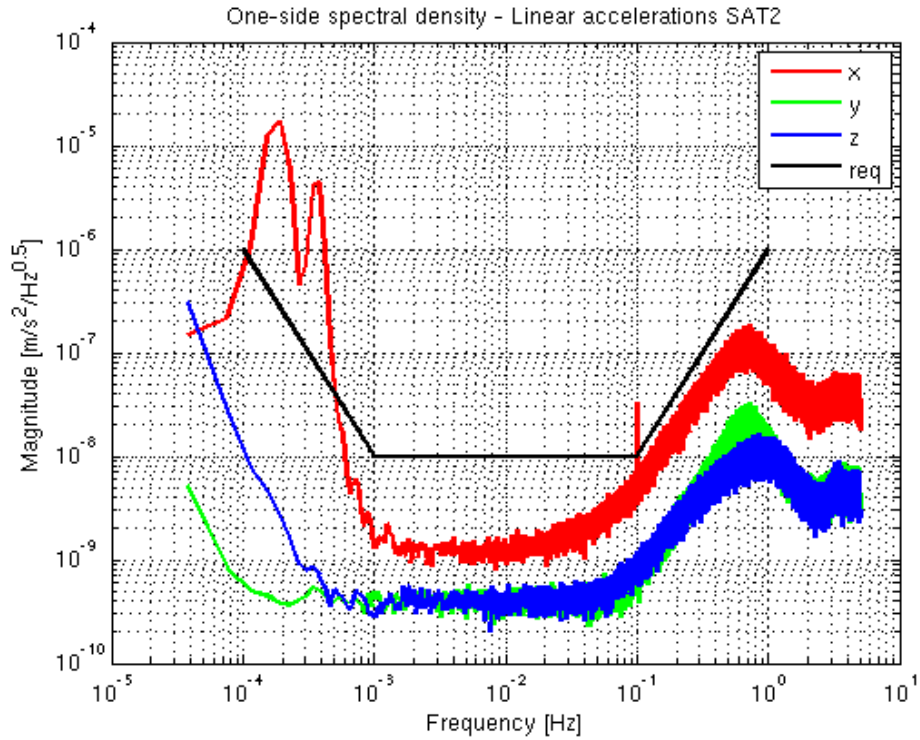


Figure 4.3-24 One-sided spectral density of the SAT2 linear acceleration in SAT2 body reference frame.

## 4.4 Attitude control

### 4.4.1 Pointing control requirements

Figure 3.4-1, Figure 3.4-2, Figure 3.4-3 and Figure 3.4-4 report the pointing requirements as provided for attitude errors, angular rate errors and angular acceleration errors for both satellites, all derived without taking into account the natural link.

Since there exist a kinematics link between errors in attitude, angular rate and angular acceleration, all those have been transformed in a comparable form taking into that link. This permits to address the driver requirement at different frequency.

Figure 4.4-1 and others show that:

- for Satellite 1, at frequencies  $< 0.015\text{Hz}$  (Y and Z axes) and  $< 0.005\text{Hz}$  (X axis), the pointing requirement is driven by the attitude error. Only at high frequency, the requirement on angular acceleration drives the design.
- for Satellite 2, at frequencies  $< 0.005\text{Hz}$  (X, Y and Z axes), the pointing requirement is driven by the attitude error. Only at high frequency, the requirement on angular acceleration drives the design.
- for both satellite, angular rate stability requirement never drives the pointing requirements.

Those observations are very important since:

- they provide clear indications on the requirement to specify on angular acceleration measurements error spectral density;
- they help to address the more complex requirement on star-tracker low-frequency attitude errors, where harmonics errors and stochastic errors are present together.

In the frame of the study, clear indication of how to manage harmonics errors from scientists has not been provided. These errors are essentially at low frequency and are due to:

- residual control action of the formation controller;
- star-tracker FoV errors and thermo-mechanical deformation;
- laser beam pointing by attitude control.

The first one is visible on residual linear acceleration; the third one may be observed on residual angular acceleration and are due to the relative motion of the satellites. Special care shall be done for the second one to implement the correct data-fusion between star-tracker data and accelerometer data (on-board real-time control and on-ground angular rate and attitude reconstitution).

The star-tracker manufacturer for historical reasons and not only, do not provide spectral density and/or spectrum of attitude errors of their equipment. As it will shown in the next chapter, these additional information are instead relevant for any high-performance Earth observation mission.

Starting from that, using the GOCE in-flight data, the spectral densities of GOCE star-trackers (Advanced Stellar Compass by Technical University of Denmark) errors have been reconstituted (see chapter 5). These results have not been used to update the attitude controllers rather to provide reliable errors for on-ground angular rate and attitude reconstitution.

The reason to do not update the attitude controllers was mainly related to the subsequently decision to cancel the beam steering mechanism. Under this condition, for every formation, Y and Z axes of each spacecraft are controlled using optical metrology measurement; only X axis is controlled using star-tracker measurement.

For the specific in-line formation, considering the requirements given in Table 3.3-1, in practise, the laser beam pointed by Satellite 1 remains in the field-of-view of the retro-reflector mounted on Satellite 2, also in the case the Satellite 2 keeps its LORF.

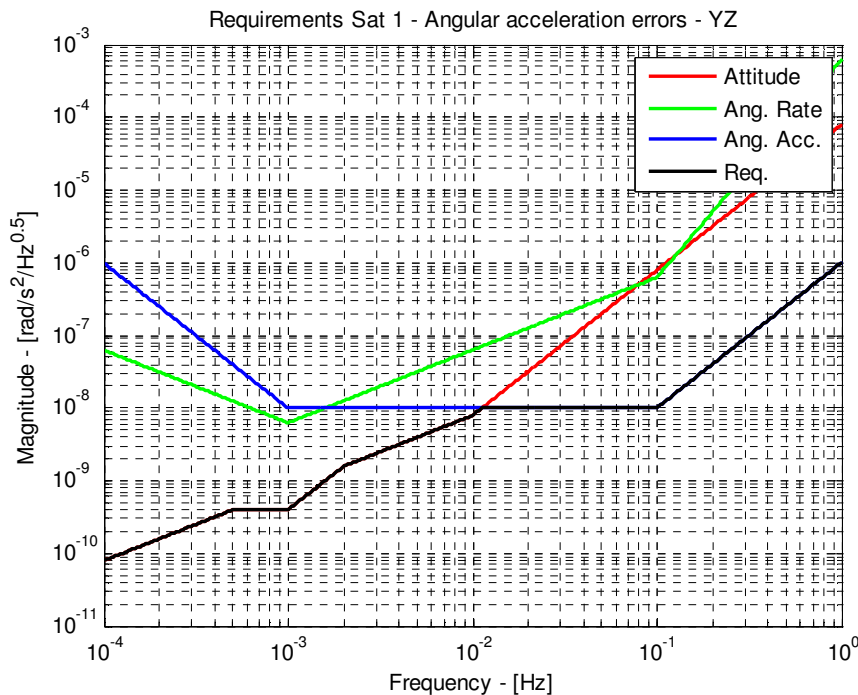


Figure 4.4-1 Y and Z axes Satellite 1 pointing requirements transformed in equivalent angular acceleration.

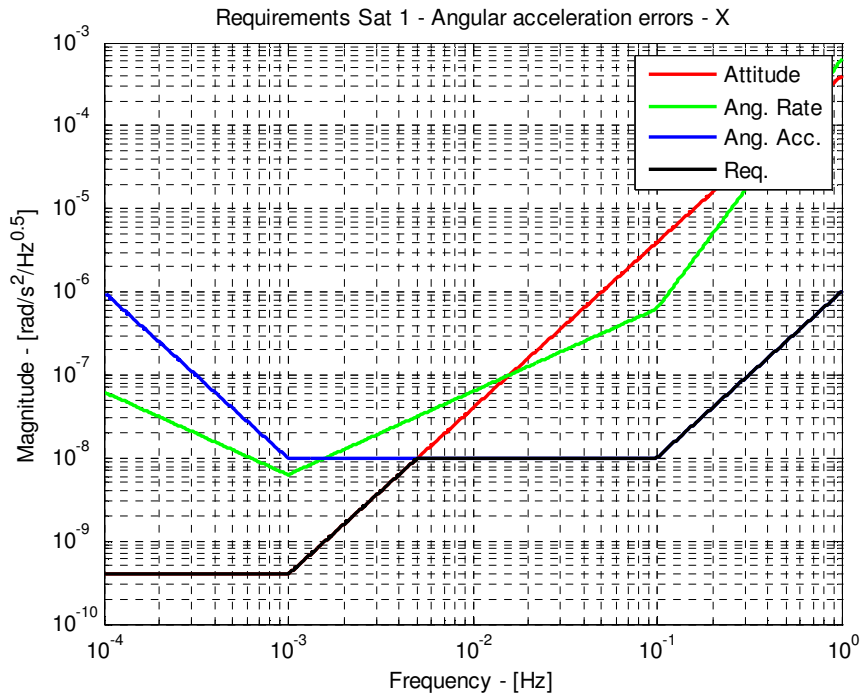


Figure 4.4-2 X axis Satellite 1 pointing requirements reported in equivalent angular acceleration.

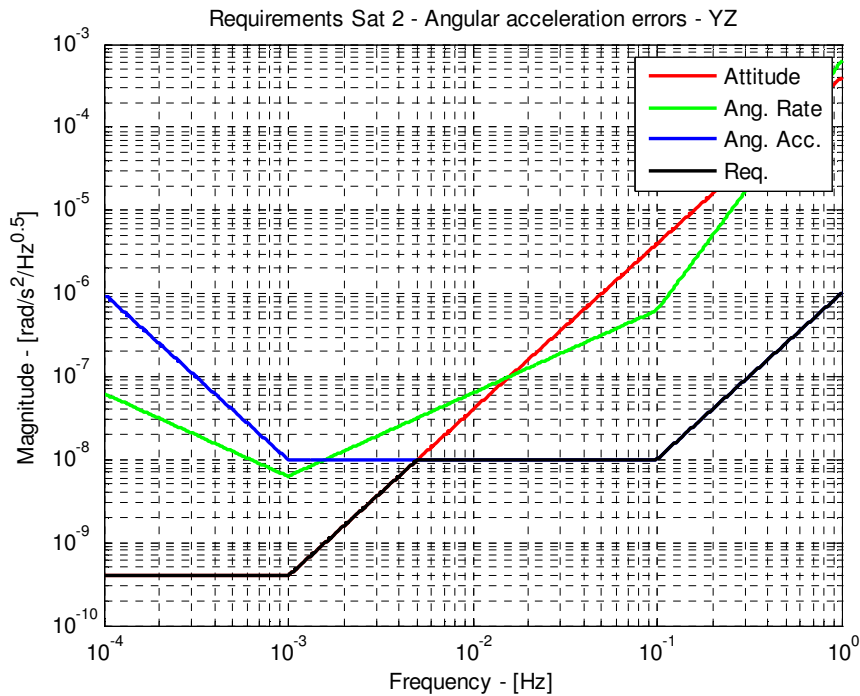


Figure 4.4-3 Y and Z axes Satellite 2 pointing requirements reported in equivalent angular acceleration.

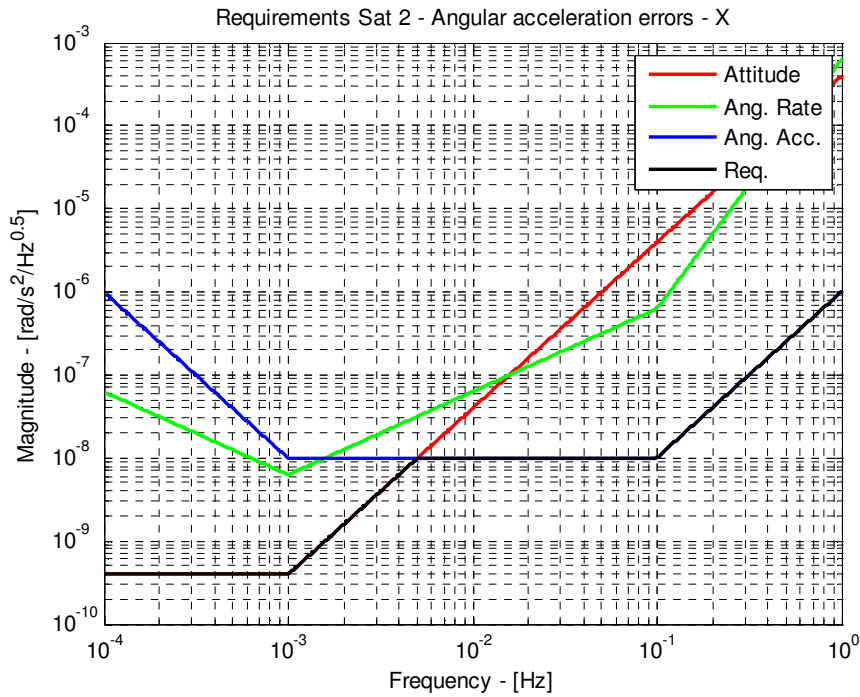


Figure 4.4-4 X axis Satellite 2 pointing requirements reported in equivalent angular acceleration.

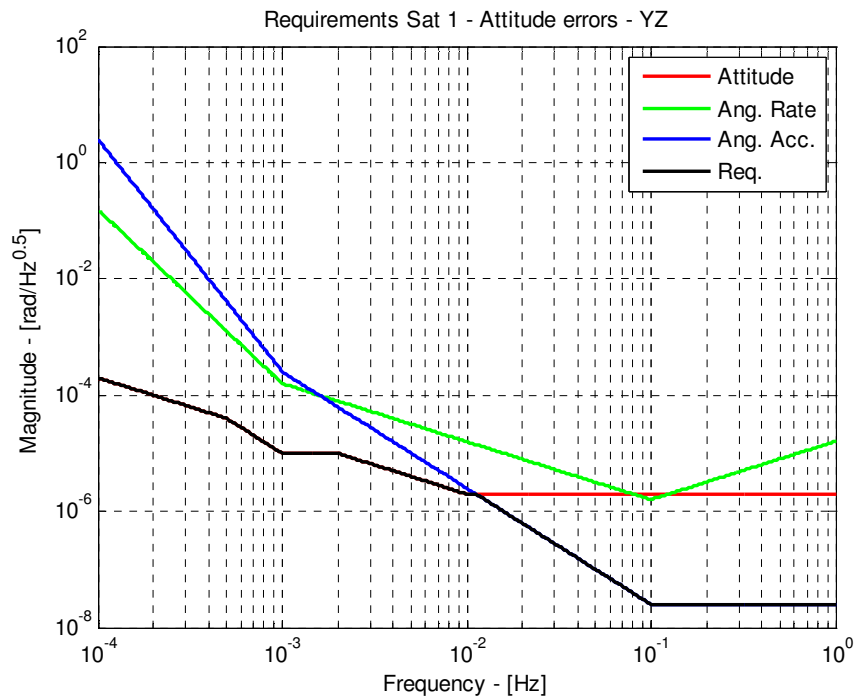


Figure 4.4-5 Y and Z axes Satellite 1 pointing requirements reported in equivalent attitude errors.

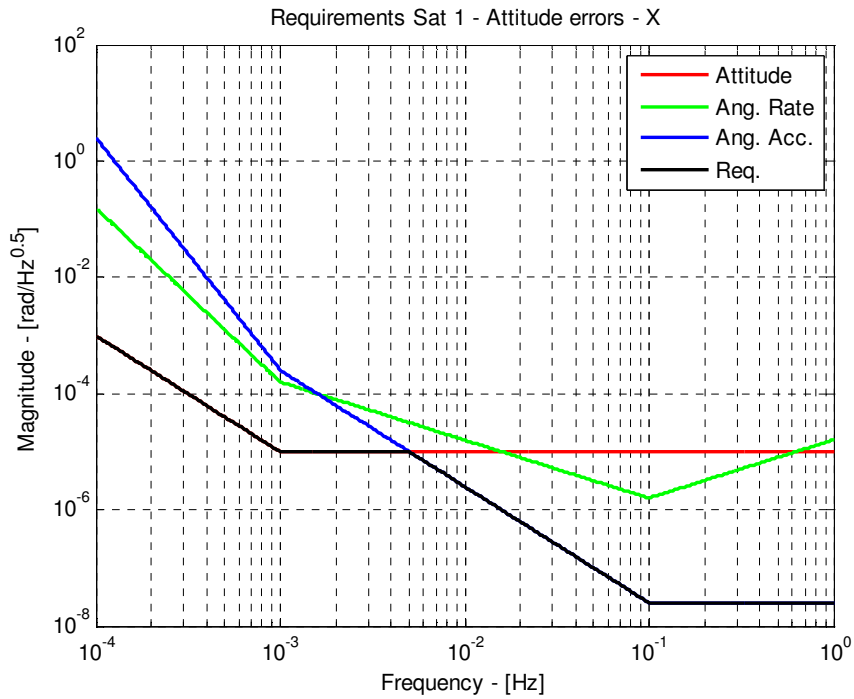


Figure 4.4-6 X axis Satellite 1 pointing requirements reported in equivalent attitude errors.

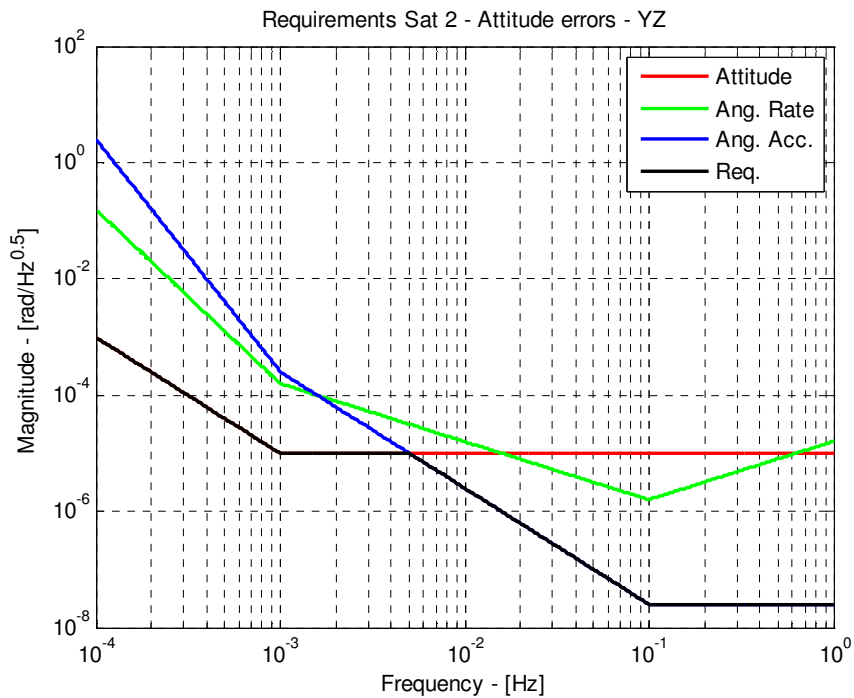


Figure 4.4-7 Y and Z axes Satellite 2 pointing requirements reported in equivalent attitude errors.

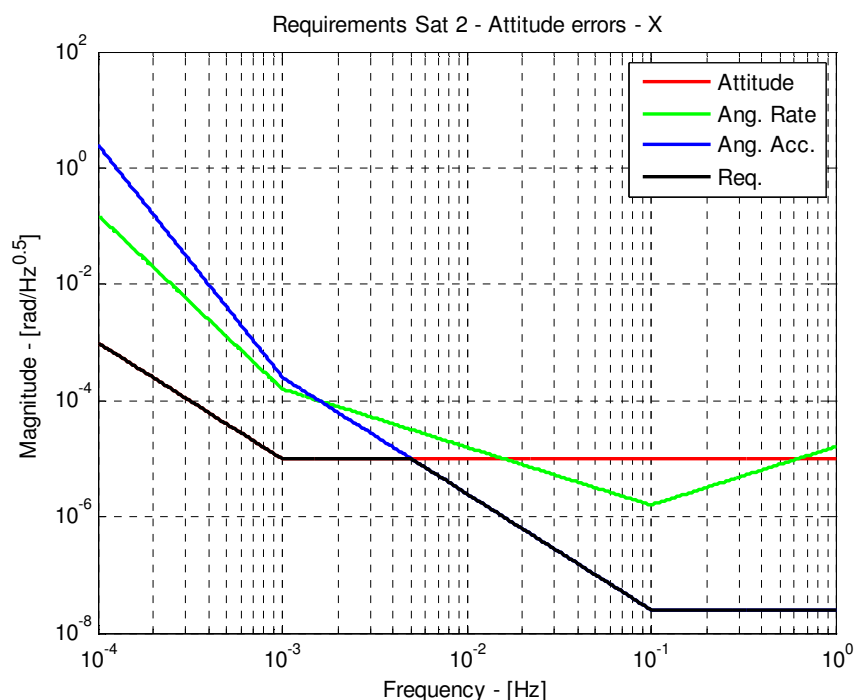


Figure 4.4-8 X axis Satellite 2 pointing requirements reported in equivalent attitude errors.

## 4.4.2 Laser pointing by satellite

### 4.4.2.1 Requirement and accuracy of the metrology

In the frame of the study, it has been considered the possibility to cancel the Beam Steering Mechanism and to execute the tracking by attitude control of Satellite 1.

The general attitude control architecture is the following:

- Satellite 1 executes the tracking of Satellite 2 (Satellite X-axis alignment to the satellite-to-satellite direction), using the displacement measurement provided by optical metrology. The tracking shall be maintained with an error lower than  $2 \cdot 10^{-5}$  rad and with stability as given in Figure 3.4-1.
- Satellite 2 rotates following Satellite 1 movement in order to keep the laser beam pointed by Satellite 1 inside the retro-reflector field-of-view ( $\leq 1^\circ$ ). Stability requirement is given in Figure 3.4-2.

In the following the compatibility of the pointing requirements with available optical metrology performances will be considered.

The optical metrology provides two type of measurement:

- Lateral displacement measurement (lateral metrology):
  - Bias < 1 mm;

- Noise profile as shown in Figure 4.4-9;
- Angular measurement (angular metrology):
  - Bias < 10<sup>-4</sup> rad;
  - Noise profile as shown in Figure 4.4-10;

The lateral metrology provides the mis-pointing measurement to steer the Satellite 1 X axis. The equivalent pointing measurement is given in Figure 4.4-11 compute considering the distance between satellites equals to 40km, 75km and 110km.

The above equivalent pointing measurement noise spectral density have been compared with the requirement derived in previous chapter and reported in Figure 4.4-5 (Satellite 1 attitude error on Y and Z axes), Figure 4.4-6 (Satellite 1 attitude error on X axis, Satellite 2 attitude error on all axes), Figure 4.4-1 (Satellite 1 angular acceleration error on Y and Z axes) and Figure 4.4-2 (Satellite 1 angular acceleration error on X axis, Satellite 2 angular acceleration error on all axes).

Figure 4.4-12 , Figure 4.4-13, Figure 4.4-14 and Figure 4.4-15 offer the comparison between requirements and measurements accuracies. From those, it is possible to observe that:

- the lateral metrology accuracy is substantially compatible with pointing requirements on Y and Z axes. The margins are poor for frequency close to 0.1Hz.
- the angular metrology permits to cope with low frequency pointing requirements (dominated by attitude stability requirement) but it is not enough for frequency higher than 0.02Hz (dominated by angular acceleration stability requirement).

It is worth to notice that in case of in-line formation, the Satellite 2 attitude control may be based on the LORF tracking, as done in previous study phase. This is possible since the allowed Y and Z relative position error still permit to cope with the field-of-view of the retro-reflector<sup>1</sup>.

The measurement biases are fully compatible with the requirements.

<sup>1</sup> Requirement on relative position error is provided in Table 3.3-1; from that, the maximum off-pointing is 1deg (@ 75km). Numerical simulations show results much better.

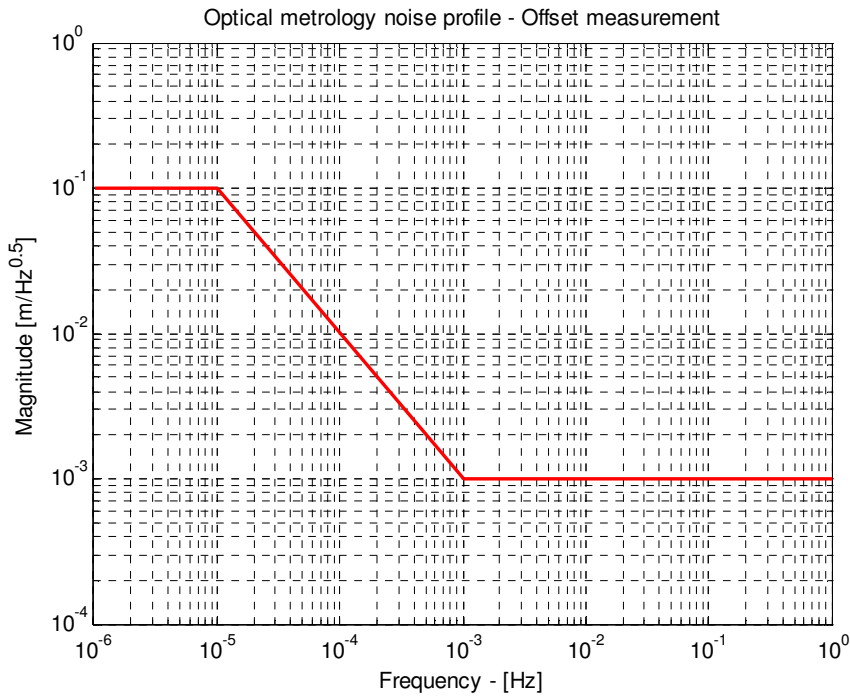


Figure 4.4-9 Noise profile considered for the measurement provided by lateral optical metrology.

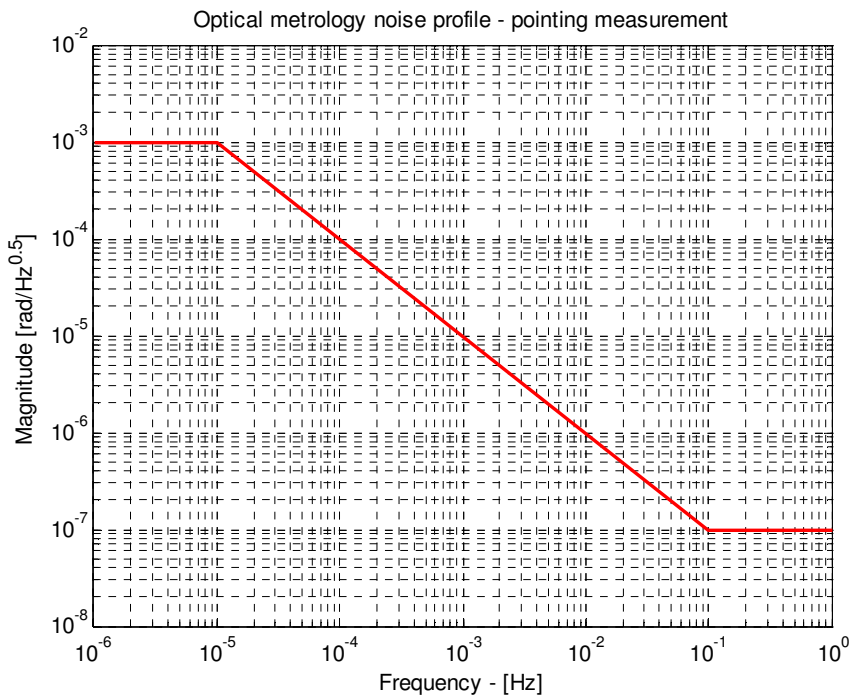


Figure 4.4-10 Noise profile considered for the pointing measurement provided by angular optical metrology.

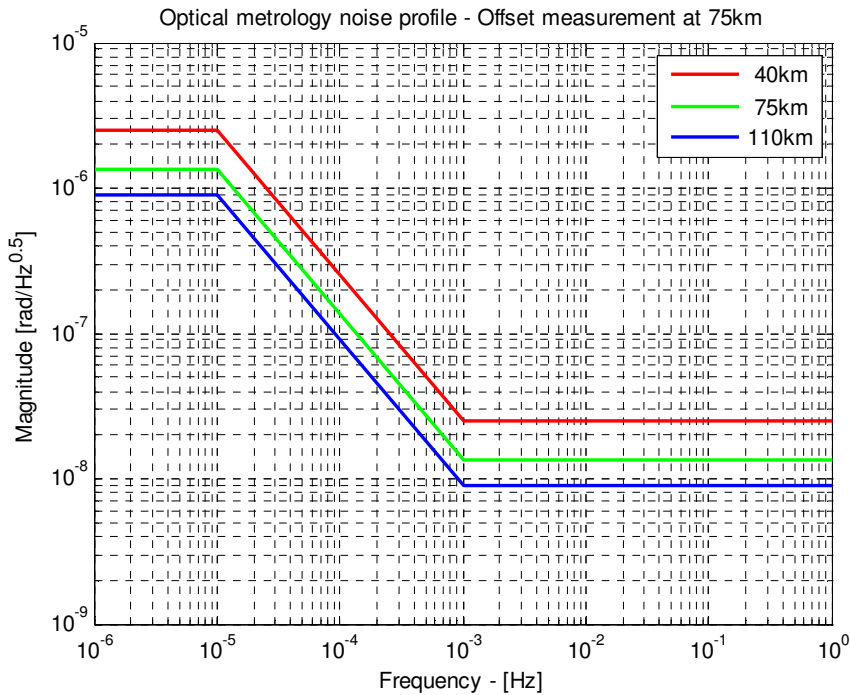


Figure 4.4-11 Noise profile considered for the lateral metrology reported in equivalent angle at 40, 75 and 110km distance.

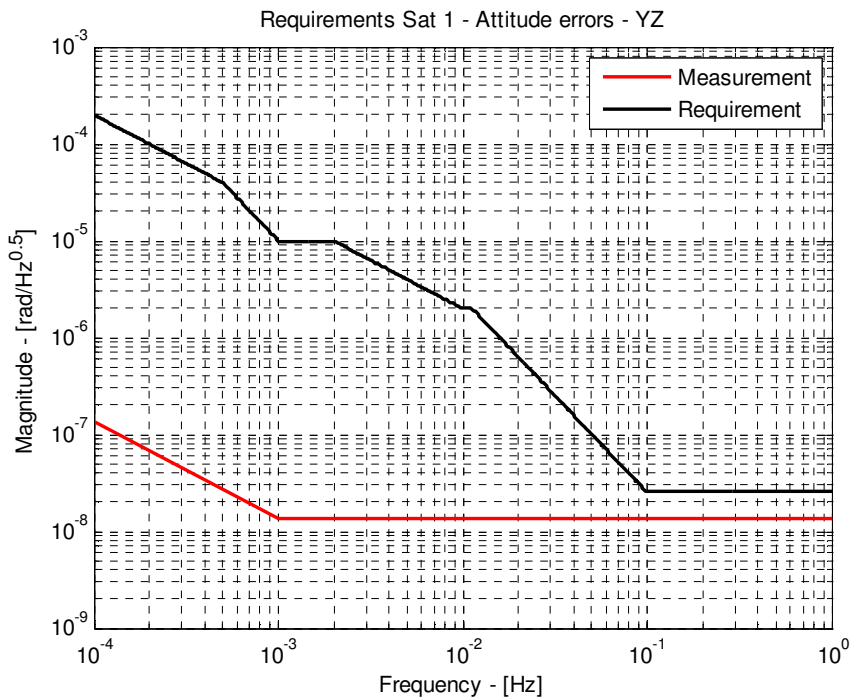


Figure 4.4-12 Comparison between the requirement and the measurement performance (75km) in terms of attitude errors – Satellite 1 Y and Z axes.

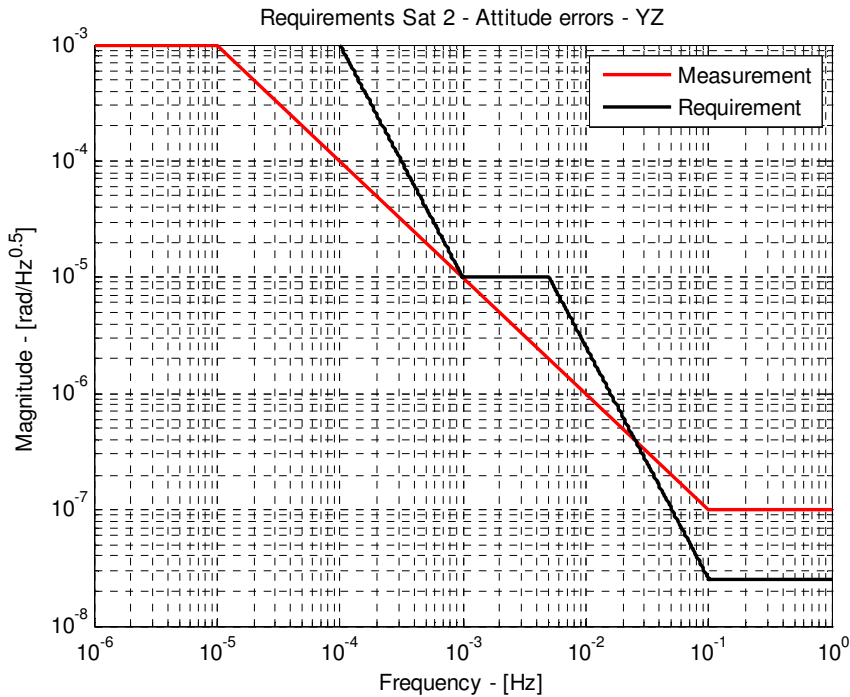


Figure 4.4-13 Comparison between the requirement and the measurement performance in terms of attitude errors – Satellite 2 Y and Z axes.

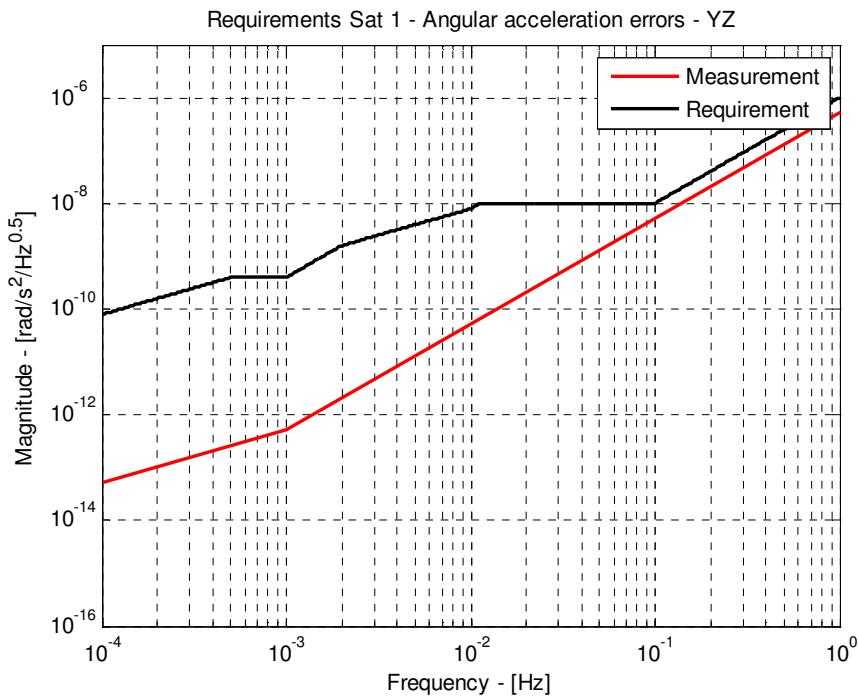


Figure 4.4-14 Comparison between the requirement and the measurement performance (75km) in terms of angular acceleration errors – Satellite 1 Y and Z axes.

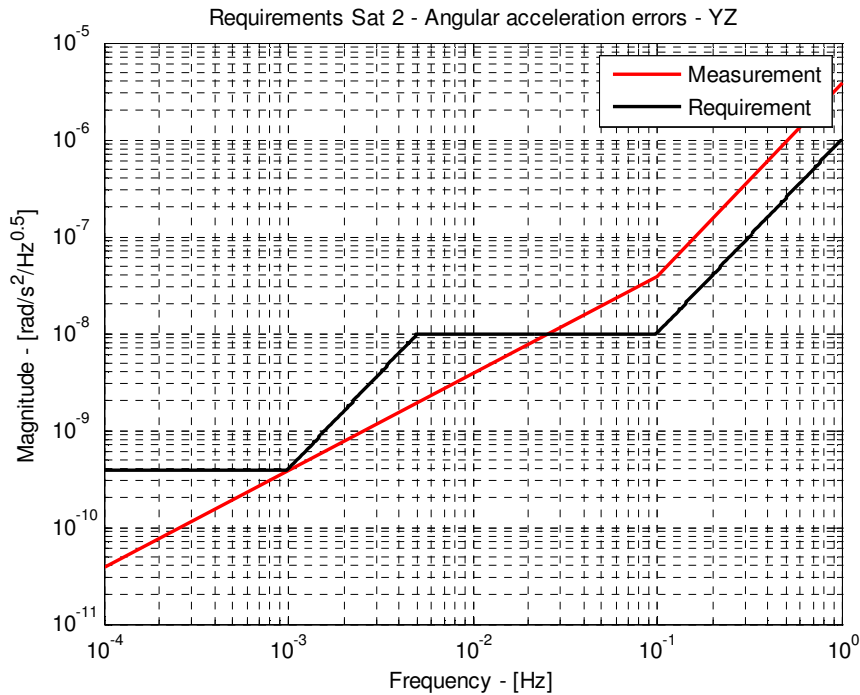


Figure 4.4-15 Comparison between the requirement and the measurement performance in terms of angular acceleration errors –Satellite 2 Y and Z axes.

#### 4.4.2.2 Design algorithm description

The reference attitude  ${}_I \mathbf{R}_{TARGET1}$  to be maintained by the Satellite 1 may be described as follows:

$${}_I \mathbf{R}_{LORF1} = \begin{bmatrix} \frac{\mathbf{v}_1}{\|\mathbf{v}_1\|} & \frac{\mathbf{r}_1 \times \mathbf{v}_1}{\|\mathbf{r}_1 \times \mathbf{v}_1\|} & \frac{\mathbf{v}_1}{\|\mathbf{v}_1\|} \times \frac{\mathbf{r}_1 \times \mathbf{v}_1}{\|\mathbf{r}_1 \times \mathbf{v}_1\|} \end{bmatrix}$$

$$\hat{\mathbf{n}}_{21}^I = \frac{\mathbf{r}_2^I - \mathbf{r}_1^I}{\|\mathbf{r}_2^I - \mathbf{r}_1^I\|}$$

$$\hat{\mathbf{n}}_{21}^{LORF1} = ({}_I \mathbf{R}_{LORF1})^T \hat{\mathbf{n}}_{21}^I$$

$${}_{LORF1} \mathbf{R}_{TARGET1} = \begin{bmatrix} \hat{\mathbf{n}}_{21}^{LORF1} & \begin{pmatrix} \hat{\mathbf{n}}_{21}^{LORF1} \times \mathbf{v}_1 \\ \|\hat{\mathbf{n}}_{21}^{LORF1} \times \mathbf{v}_1\| \end{pmatrix} & \begin{pmatrix} \hat{\mathbf{n}}_{21}^{LORF1} \times \mathbf{v}_1 \\ \|\hat{\mathbf{n}}_{21}^{LORF1} \times \mathbf{v}_1\| \end{pmatrix} \end{bmatrix}$$

$${}_I \mathbf{R}_{TARGET1} = ({}_I \mathbf{R}_{LORF1}) ({}_{LORF1} \mathbf{R}_{TARGET1})$$

The attitude error feeding the attitude observer has been computed according to the following steps:

$${}_{B1} \Delta \mathbf{R}_{TARGET1} = [{}_I \mathbf{R}_{B1}(\tilde{\mathbf{q}}_1)]^T {}_I \mathbf{R}_{TARGET1}$$

$\tilde{\mathbf{q}}_1$  attitude quaternion measurement

$${}_{B1} \Delta \mathbf{R}_{TARGET1} \Rightarrow \begin{bmatrix} \tilde{\vartheta}_X \\ \tilde{\vartheta}_Y \\ \tilde{\vartheta}_Z \end{bmatrix}$$

The error in the rotation around Y and Z axes are substituted the mispointing measurement provided by optical metrology ( $\tilde{\delta}_X, \tilde{\delta}_Y$ ):

$$\begin{bmatrix} \tilde{\vartheta}_X \\ \tilde{\vartheta}_Y \\ \tilde{\vartheta}_Z \end{bmatrix} \Rightarrow \begin{bmatrix} \tilde{\vartheta}_X \\ -\frac{\tilde{\delta}_Y}{\|\hat{\mathbf{r}}_2^I - \hat{\mathbf{r}}_1^I\|} \\ \frac{\tilde{\delta}_X}{\|\hat{\mathbf{r}}_2^I - \hat{\mathbf{r}}_1^I\|} \end{bmatrix}$$

$\hat{\mathbf{r}}_2^I$  and  $\hat{\mathbf{r}}_1^I$  are provided by LORF quaternion estimator module (see [RD-22]).

The same formulas have been used to define the reference attitude for the Satellite 2. The attitude errors have been computed considering the angles measurement provided by optical metrology ( $\tilde{\alpha}, \tilde{\beta}$ ):

$$\begin{bmatrix} \tilde{\vartheta}_X \\ \tilde{\vartheta}_Y \\ \tilde{\vartheta}_Z \end{bmatrix} \Rightarrow \begin{bmatrix} \tilde{\vartheta}_X \\ -\tilde{\beta} \\ -\tilde{\alpha} \end{bmatrix}$$

With respect to the design of the attitude control described in [RD-22], the following changes have been introduced on attitude control (both satellite, all formation):

- X axis
  - Angular acceleration control : no changes;
  - Attitude control : no changes;
- Y axis
  - Angular acceleration control : deleted;
  - Attitude control : control bandwidth widens;
- Z axis
  - Angular acceleration control : deleted;
  - Attitude control : control bandwidth widens.

In the in-line formation, Satellite 2 may track the LORF allowing the same attitude control architecture described in [RD-22].

Table 4.4-1 . Angular acceleration predictor parameters (10Hz)

Axis	Gain	Value
X	$l_0$	2.500000e-03
	$l_1$	2.500000e-06
	$l_2$	1.250000e-09
Y	$l_0$	0
	$l_1$	0
	$l_2$	0
Z	$l_0$	0
	$l_1$	0
	$l_2$	0

Table 4.4-2 . Attitude predictor parameters (10Hz)

Axis	Gain	Value
X	$l_0$	4.000000e-07
	$m_0$	-3.200000e-10
	$m_1$	8.000000e-15
	$m_2$	3.200000e-19
	$\beta$	1.000000e-03
Y	$l_0$	1.330000e-02
	$m_0$	-3.186000e-03
	$m_1$	2.440000e-06
	$m_2$	8.000000e-09
	$\beta$	2.600000e-01
Z	$l_0$	1.330000e-02
	$m_0$	-3.186000e-03
	$m_1$	2.440000e-06
	$m_2$	8.000000e-09
	$\beta$	2.600000e-01

Table 4.4-3 . Attitude control law parameters (10Hz)

Axis	Gain	Value
X	$k_0$	-1.600000e-05
	$k_1$	8.000000e-03
Y	$k_0$	1.000000e-02
	$k_1$	2.000000e-01

Axis	Gain	Value
Z	$k_0$	1.000000e-02
	$k_1$	2.000000e-01

#### 4.4.2.3 Simulation results

To show the results obtained with the satellite laser tracking solution, both in-line and pendulum formations have been considered.

Relevant results for in-line formation are showed from Figure 4.4-16 to Figure 4.4-25. Pendulum formation results are provided from Figure 4.4-26 to Figure 4.4-35.

The comparison shows that the performances on linear accelerations are the same for both the formations. Big differences may be still observed on the angular acceleration spectral densities, where the relative natural movement between satellites induces high attitude dynamics for tracking. The low-frequency angular acceleration spectral density reduces with pendulum span getting to the values shown for the in-line formation. At first order, the magnitude of the angular acceleration residual spectral density is linear with the pendulum span angle. It means that considering a pendulum formation with the same minimum distance between satellites but with 15deg span, the expected magnitude of angular acceleration at low-frequency reduces by a factor 3.

It is important to remark that at low-frequency, the angular acceleration has essentially a harmonic behavior.

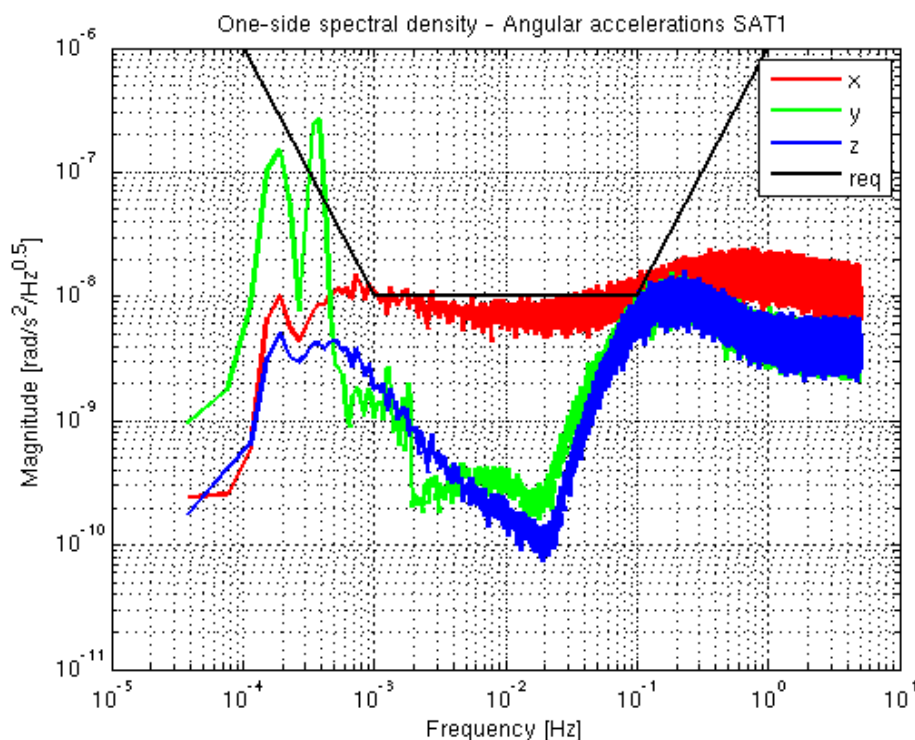


Figure 4.4-16 In-line formation - One-sided spectral density of the SAT1 angular acceleration in SAT1 body reference frame.

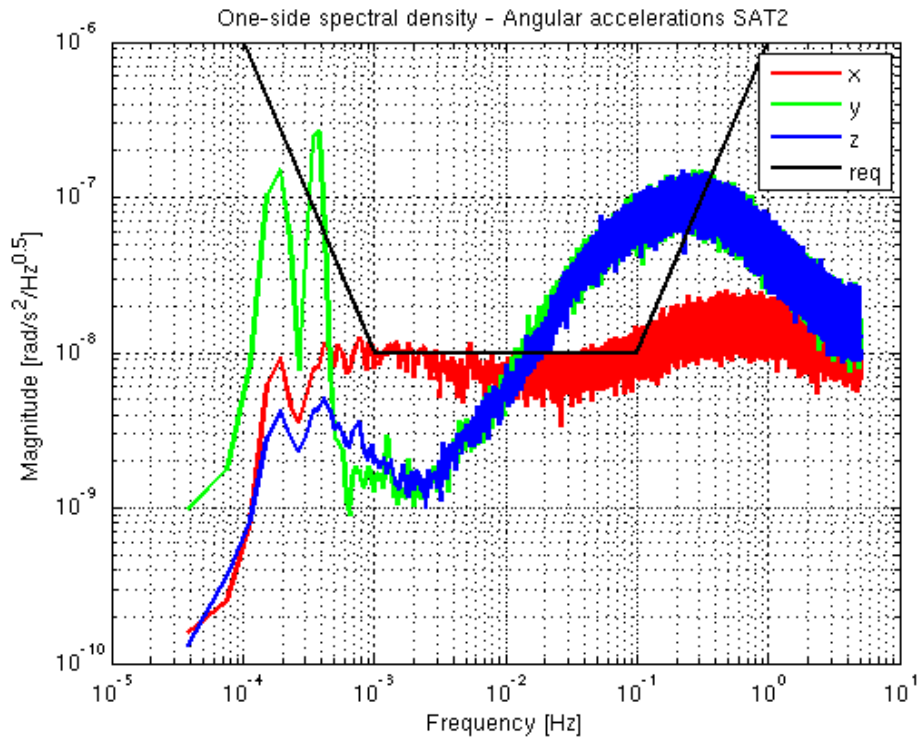


Figure 4.4-17 In-line formation - One-sided spectral density of the SAT2 angular acceleration in SAT2 body reference frame (requirement considered in previous study phase).

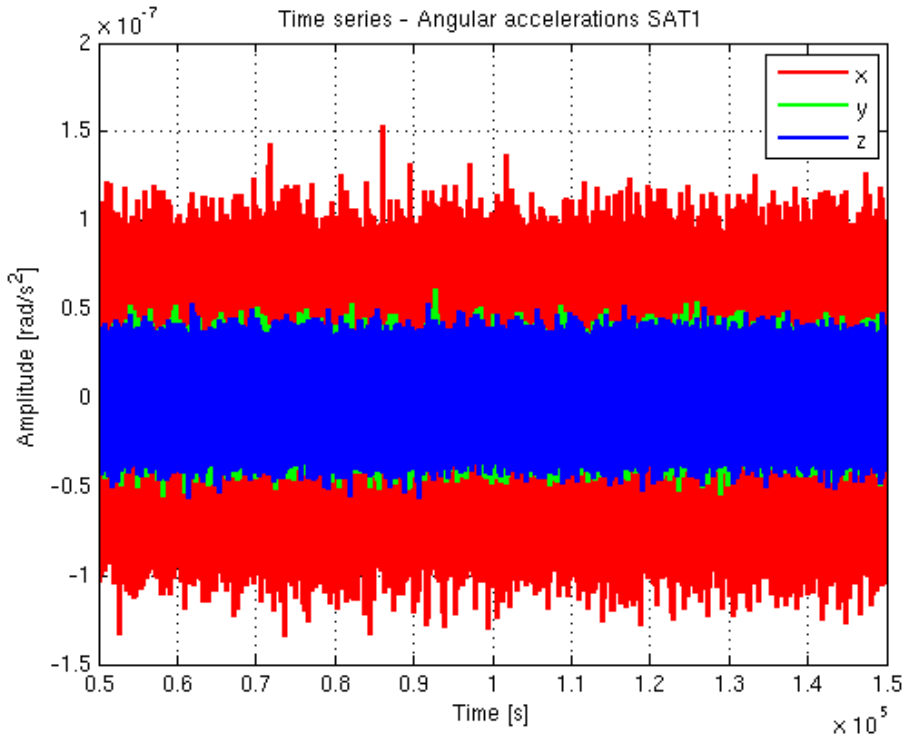


Figure 4.4-18 In-line formation - Time serie of the Satellite 1 angular accelerations.

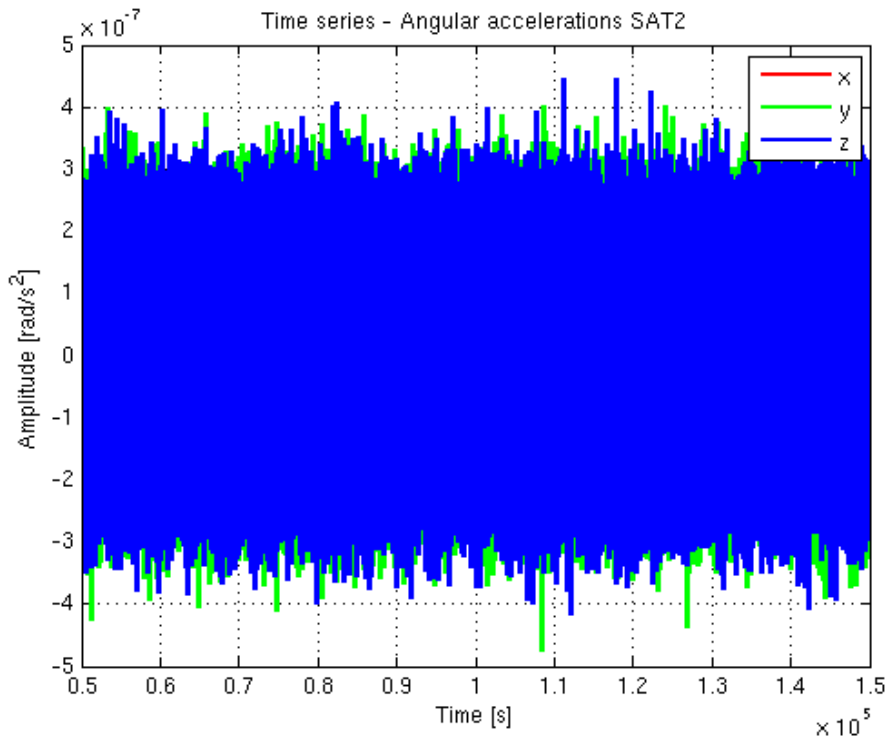


Figure 4.4-19 In-line formation - Time serie of the Satellite 2 angular accelerations.

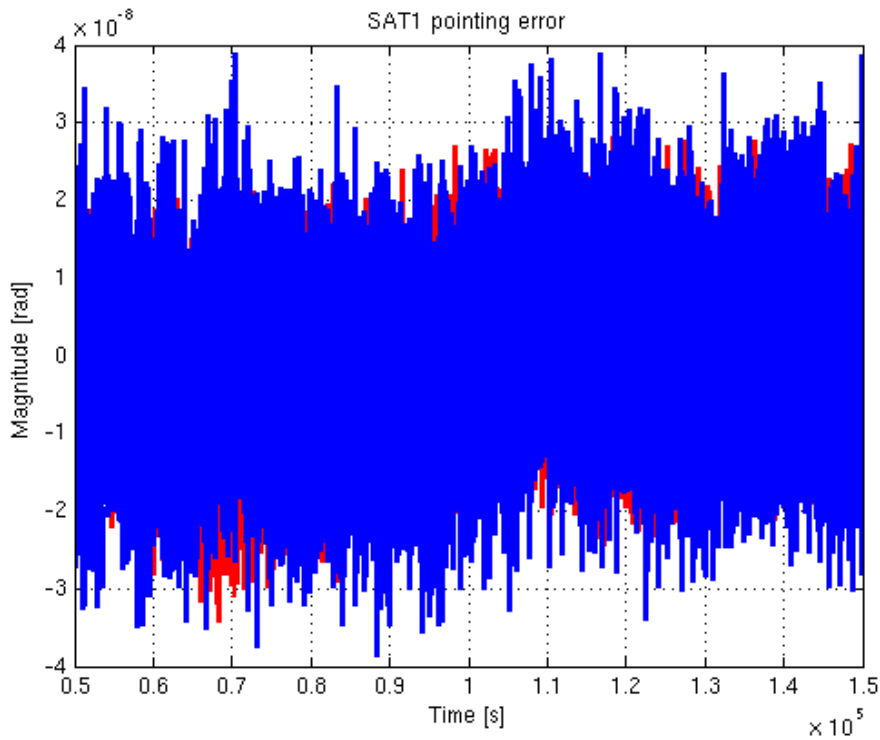


Figure 4.4-20 In-line formation - Time serie of the Satellite 1 pointing errors (Y and Z axes).

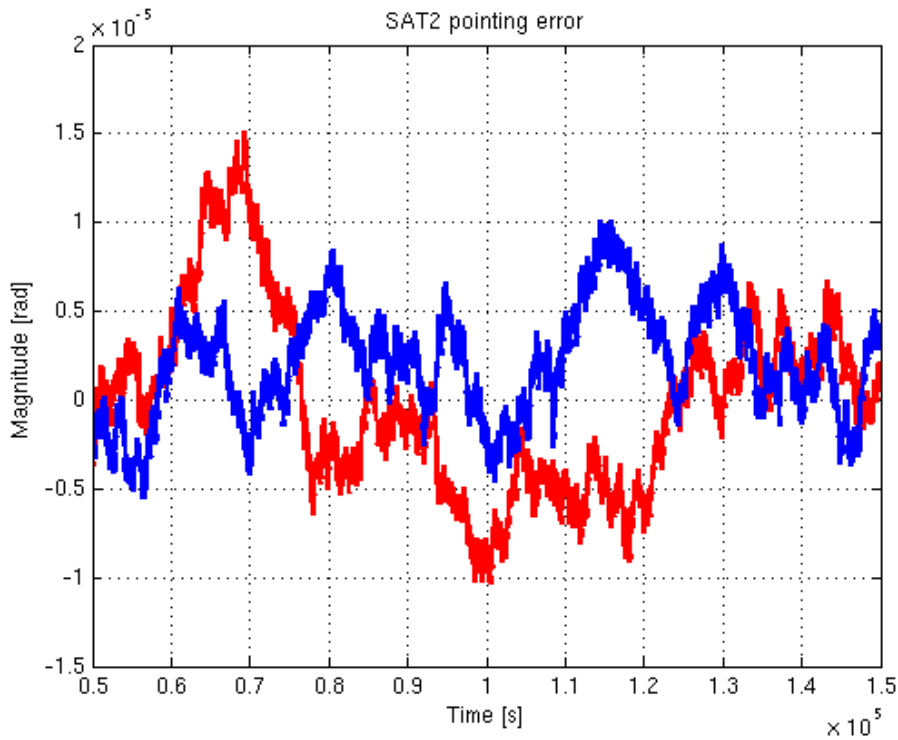


Figure 4.4-21 In-line formation - Time serie of the Satellite 2 pointing errors (Y and Z axes).

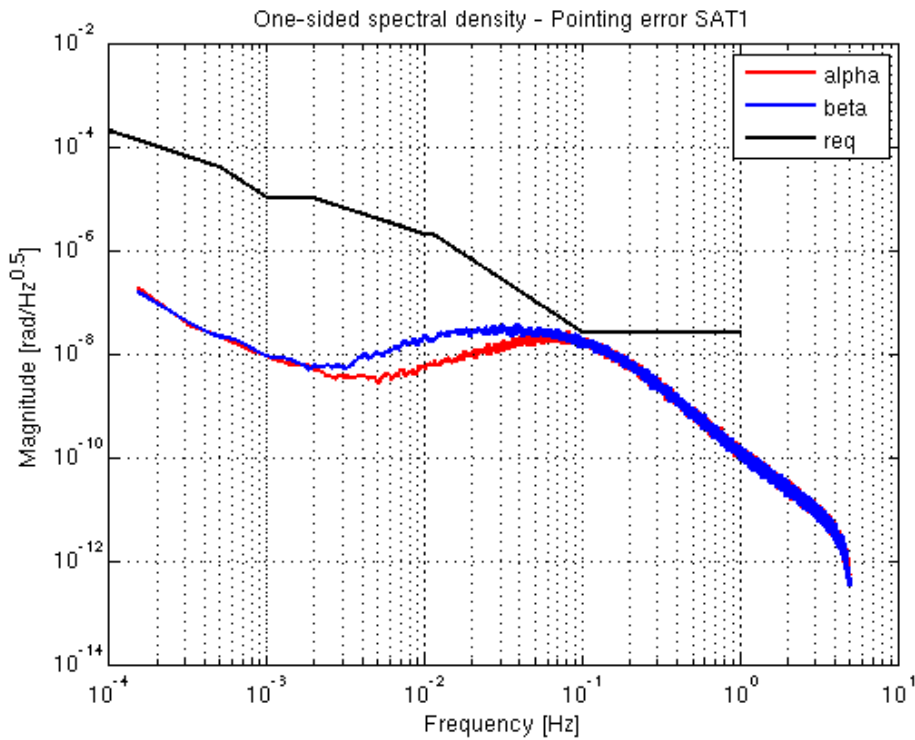


Figure 4.4-22 In-line formation - One-sided spectral of the Satellite 1 pointing errors (alpha=>Z, beta=>Y).

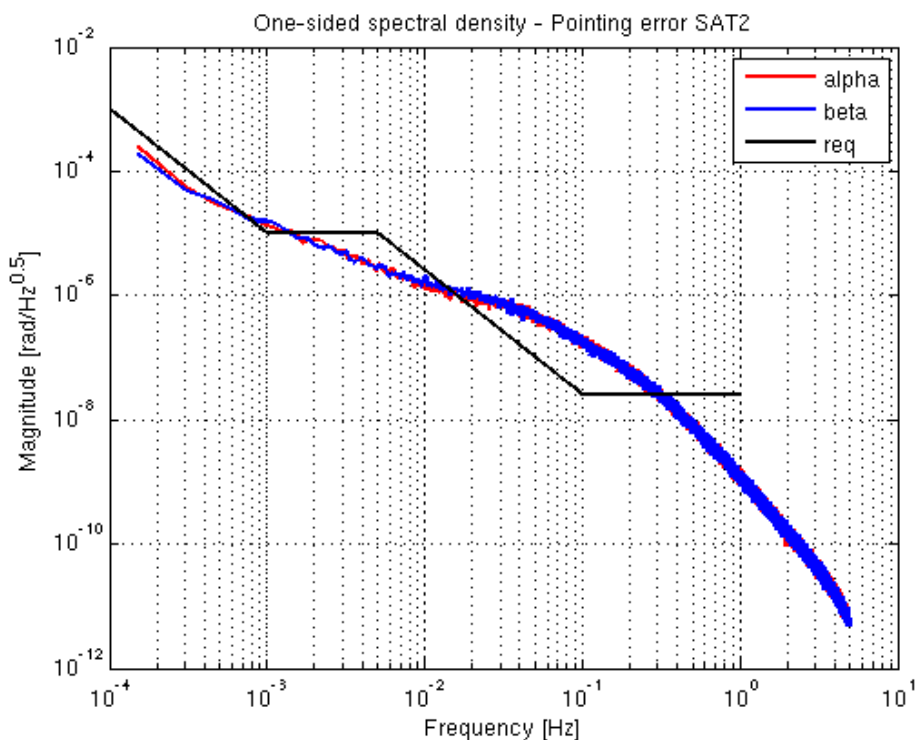


Figure 4.4-23 In-line formation - One-sided spectral of the Satellite 2 pointing errors (alpha=>Z, beta=>Y).

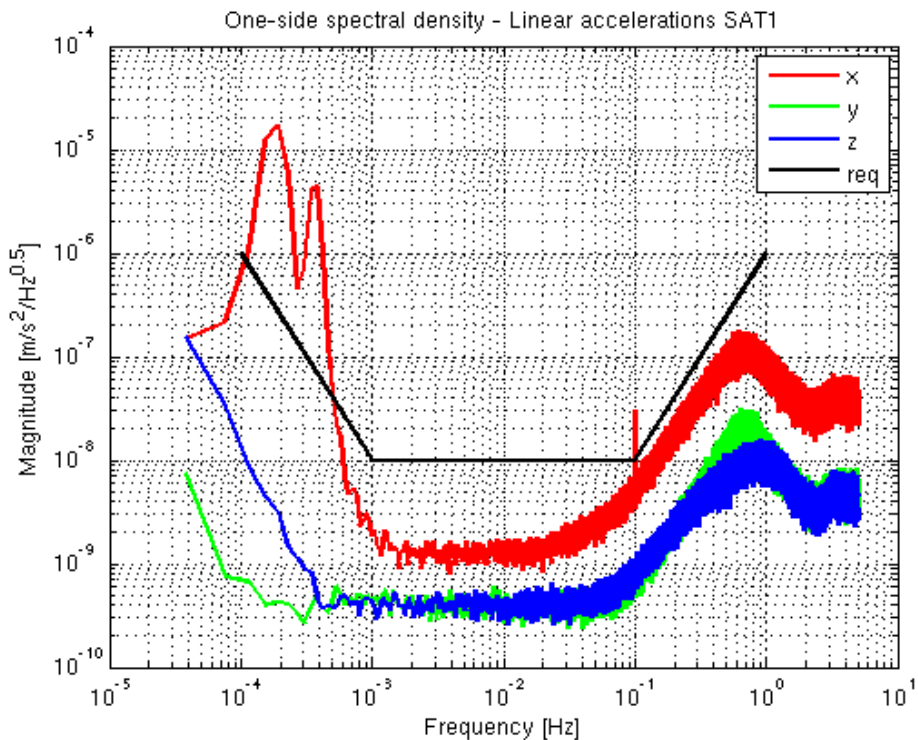


Figure 4.4-24 In-line formation - One-sided spectral density of the SAT1 linear acceleration in SAT1 body reference frame (requirement considered in previous study phase).

Figure 4.4-25 In-line formation - One-sided spectral density of the SAT2 linear acceleration in SAT2 body reference frame (requirement considered in previous study phase).

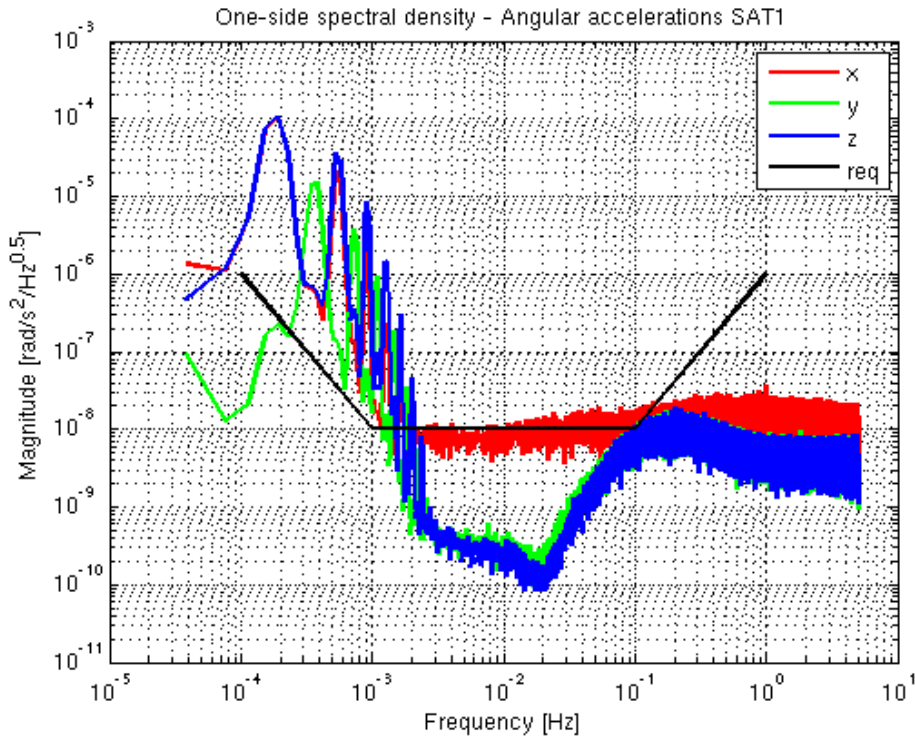


Figure 4.4-26 Pendulum formation - One-sided spectral density of the SAT1 angular acceleration in SAT1 body reference frame.

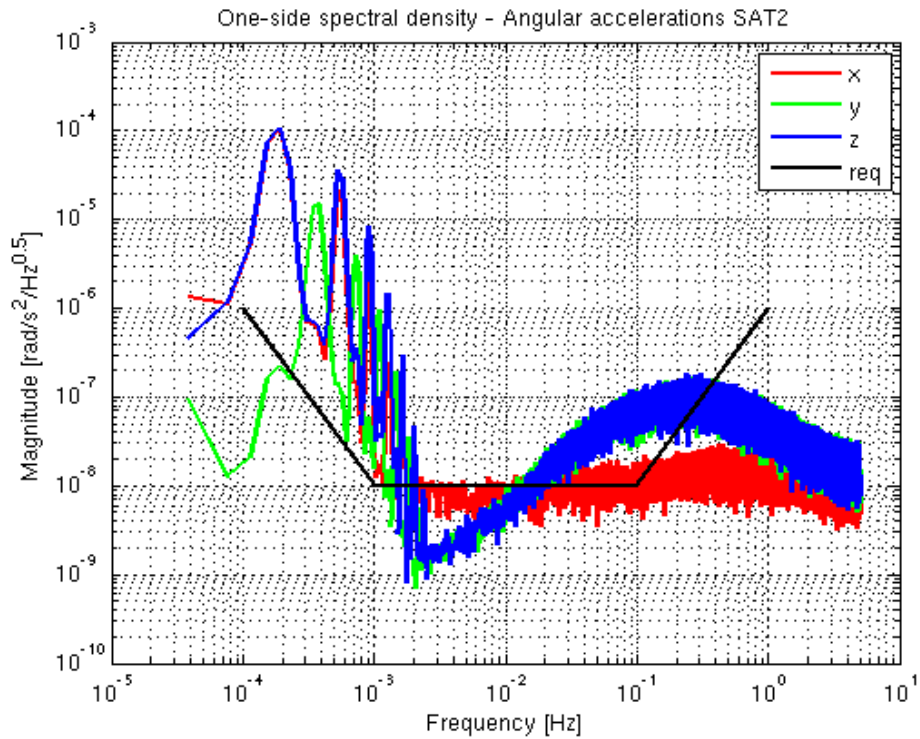


Figure 4.4-27 Pendulum formation - One-sided spectral density of the SAT2 angular acceleration in SAT2 body reference frame (requirement considered in previous study phase).

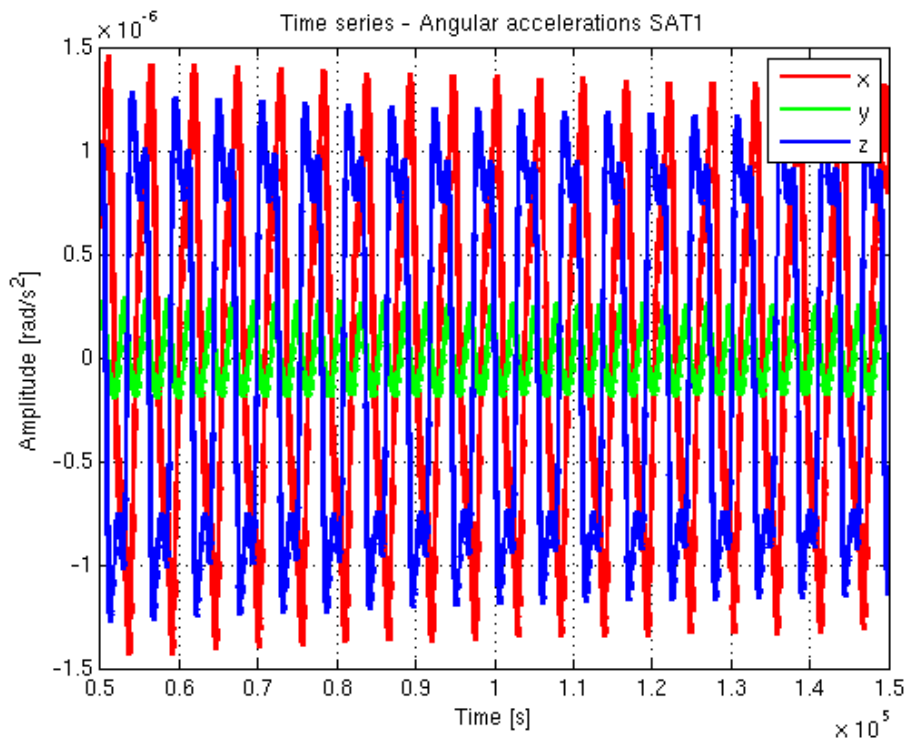


Figure 4.4-28 Pendulum formation - Time serie of the Satellite 1 angular accelerations.

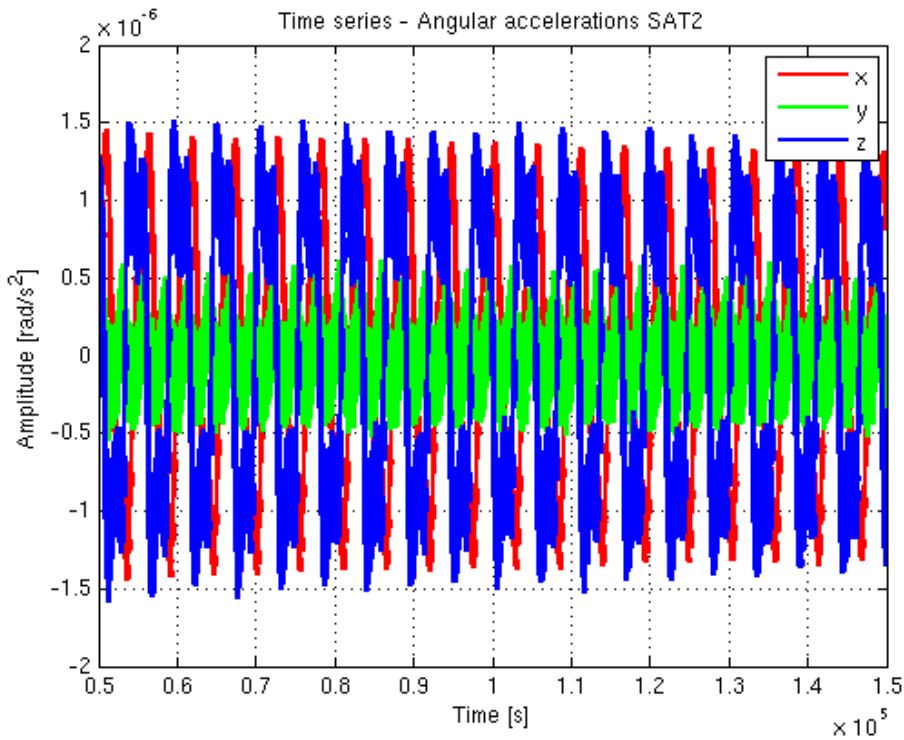


Figure 4.4-29 Pendulum formation - Time serie of the Satellite 2 angular accelerations.

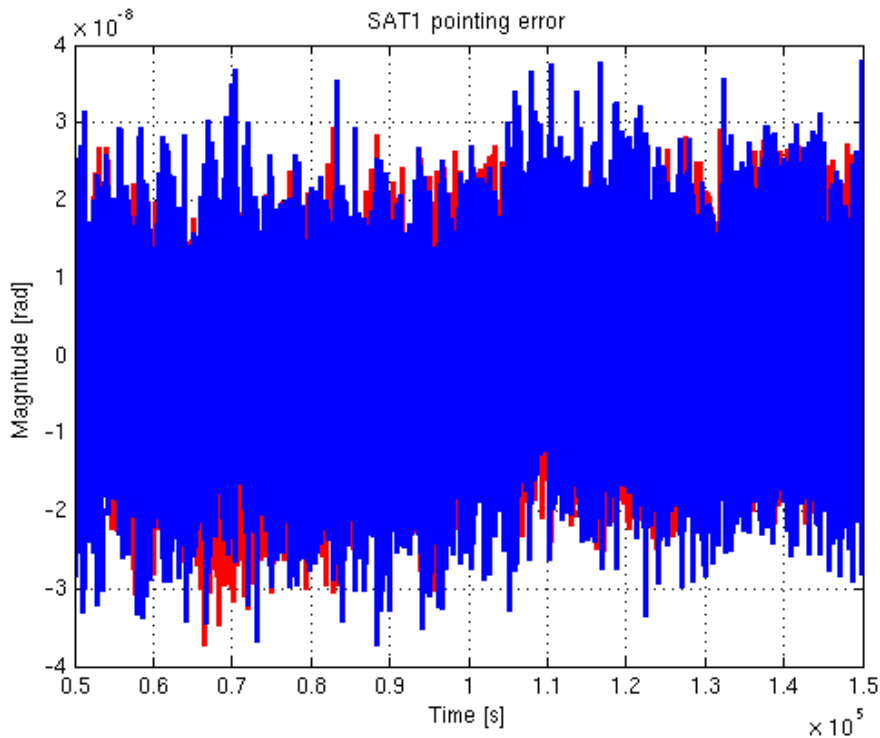


Figure 4.4-30 Pendulum formation - Time serie of the Satellite 1 pointing errors (Y and Z axes).

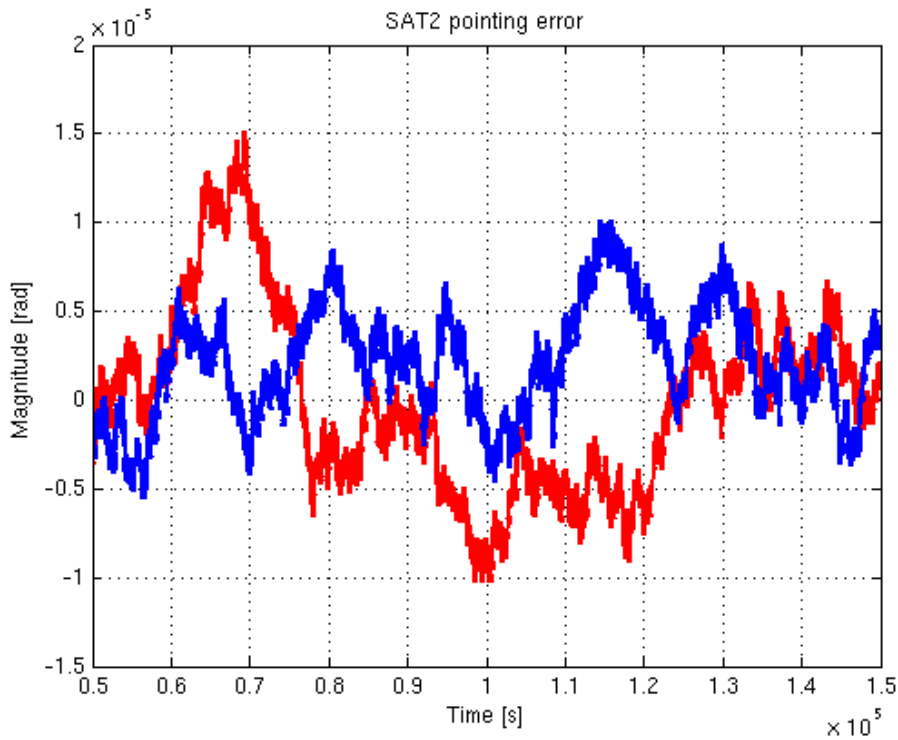


Figure 4.4-31 Pendulum formation - Time serie of the Satellite 2 pointing errors (Y and Z axes).

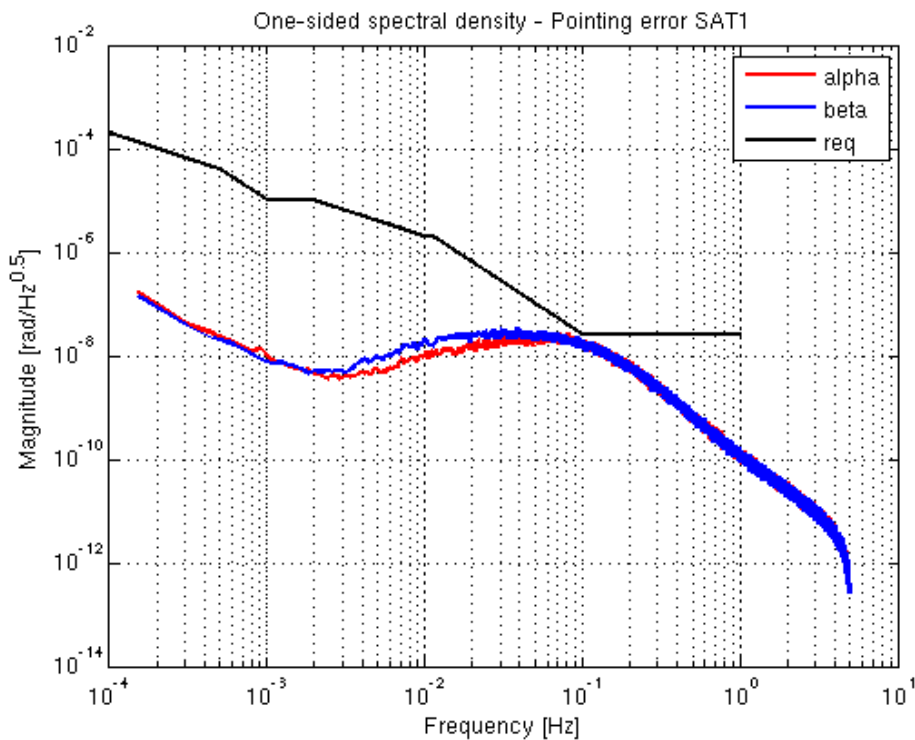


Figure 4.4-32 Pendulum formation - One-sided spectral of the Satellite 1 pointing errors (alpha=>Z, beta=>Y).

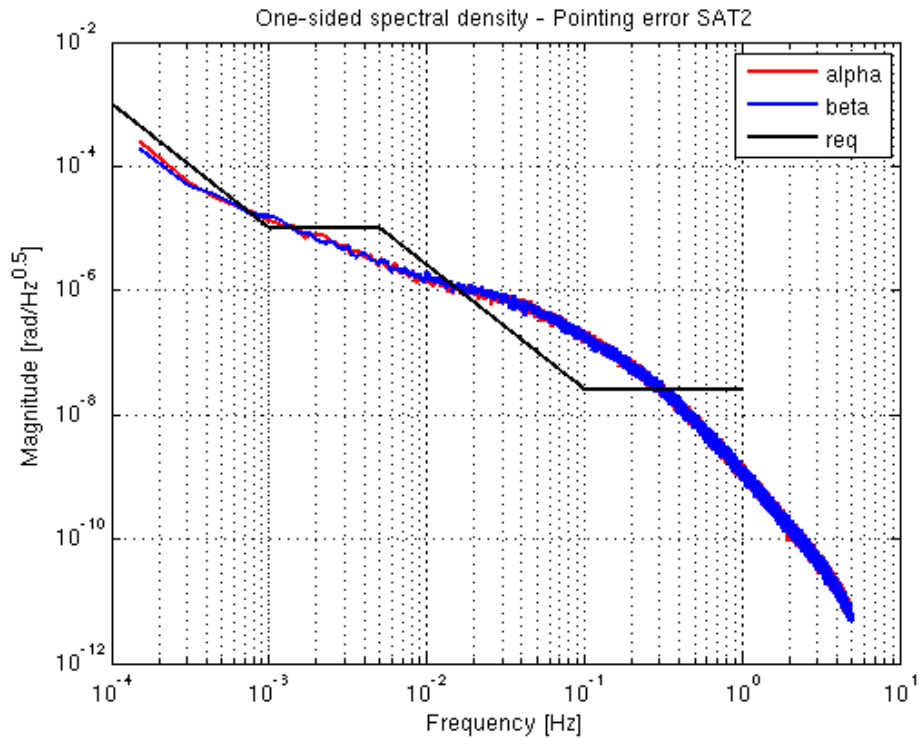


Figure 4.4-33 Pendulum formation - One-sided spectral of the Satellite 2 pointing errors (alpha=>Z, beta=>Y).

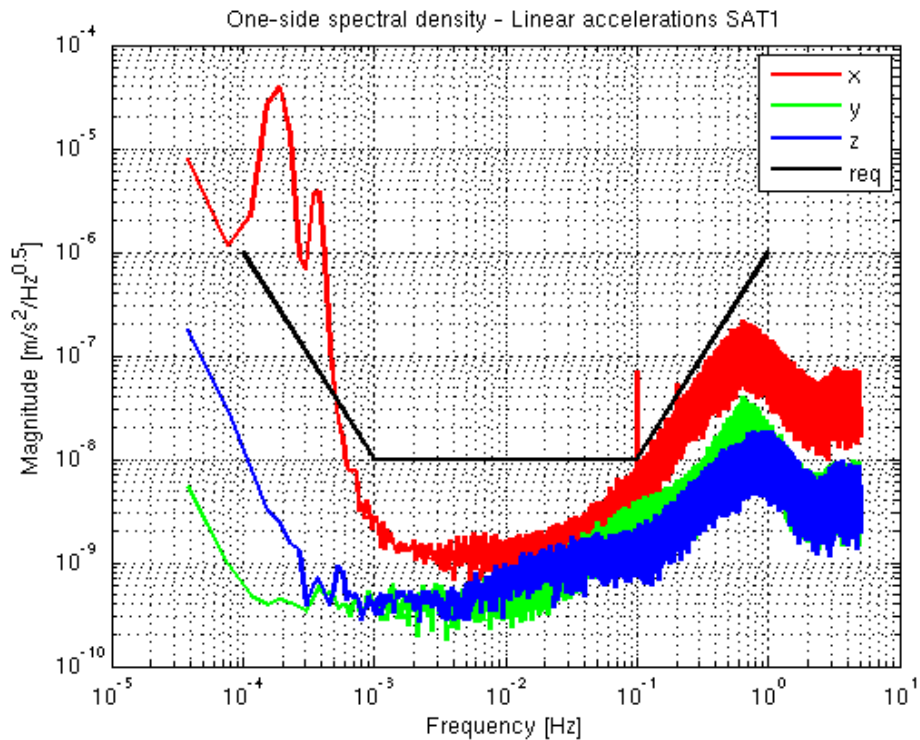


Figure 4.4-34 Pendulum formation - One-sided spectral density of the SAT1 linear acceleration in SAT1 body reference frame (requirement considered in previous study phase).

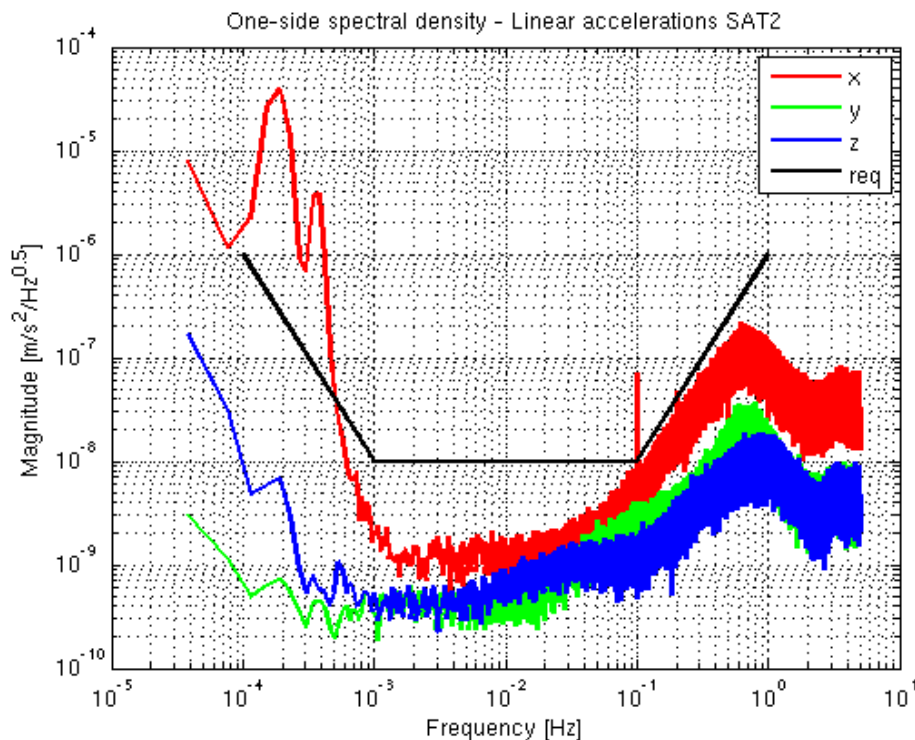


Figure 4.4-35 Pendulum formation - One-sided spectral density of the SAT2 linear acceleration in SAT2 body reference frame (requirement considered in previous study phase).

## 5. NEW STAR-TRACKER MODEL

### 5.1 Introduction

As clearly stated in previous chapters, the low-frequency performances of the attitude control and angular rate reconstitution are strongly dependent on the star-tracker attitude errors.

The star-tracker low-frequency attitude errors, named also Field-of-View errors (FoV) are due to:

- residual from focal plane calibration;
- uncertainty on star colour;
- residual from differential aberration compensation;
- S-shape;
- star-tracker thermo-elastic deformation.

Above errors become random biases in inertial pointing. In Earth observation application, the star-tracker images almost the same sky-regions in subsequently orbits, giving rise to harmonic errors. In mission GOCE like (about 16 orbit/day and 1 deg/day precession), the above errors may be considered as harmonic on time span of several orbit periods.

The problem was addressed in preliminary way in [RD-26] to put the attention on the star-tracker gyroscope data-fusion problem for Earth observation application. Depending on the

considered equipment, the standard deviation of the FoV errors may be also greater than the temporal error. Moreover, the temporal noise spectral density is extended up to the Nyquist frequency and, on the other hand, the spectrum of the FoV errors is mainly concentrated at low-frequency (actually, the frequency extension grows with the star image velocity).

Star-tracker manufacturer provides information about the performance of the equipment in terms of standard deviation or confidence level, without clarify their spectrum. To support the NGGM activities, the in-flight quaternion time series provided by GOCE (3 Advanced Stellar Compass by Technical University of Denmark star-trackers) has been use to estimate the error spectral density.

## 5.2 Computation of the spectral density of attitude error

The GOCE star-tracker attitude error spectral densities have been estimated considering:

- uncorrelated the star-tracker errors on each axis;
- the power spectral density on X and Y axes (Z axis is the boresight) equal;
- the error on the star-trackers are uncorrelated.

The covariance matrix of the attitude errors in star-tracker measurement reference frame reads:

$$\mathbf{S}_{STR}(f) = \begin{bmatrix} S_{XY}(f) & 0 & 0 \\ 0 & S_{XY}(f) & 0 \\ 0 & 0 & S_Z(f) \end{bmatrix}$$

At each sample step  $k$ , the measured attitude quaternions  $\tilde{\mathbf{q}}_i(k)$  and  $\tilde{\mathbf{q}}_j(k)$  provided by star-tracker  $i$  and  $j$  respectively are available. From that, it is possible to build the relative attitude  $\tilde{\mathbf{q}}_{ij}(k)$  time series, to compute the average rotation  $\bar{\mathbf{q}}_{ij}$  (representative of the actual relative attitude between star-trackers) and the attitude error time series  $\delta\mathbf{q}_{ij}(k)$ :

$$\tilde{\mathbf{q}}_{ij}(k) = \bar{\mathbf{q}}_{ij} \delta\mathbf{q}_{ij}(k)$$

From  $\delta\mathbf{q}_{ij}$  it is possible to compute the power spectral density matrix  $\mathbf{S}_{ij}(f)$ . The link between the spectral density of the star-tracker attitude errors and the  $\mathbf{S}_{ij}(f)$  reads:

$$\mathbf{S}_{ij} = \mathbf{S}_{STR} + \bar{\mathbf{R}}_{ij} \mathbf{S}_{STR} \bar{\mathbf{R}}_{ij}^T$$

$$\bar{\mathbf{R}}_{ij} = (2\bar{q}_{ij\_4} - 1)\mathbf{I} + 2\bar{\mathbf{q}}_{ij\_123} \bar{\mathbf{q}}_{ij\_123}^T + 2\bar{q}_{ij\_4} [\tilde{\mathbf{q}}_{ij\_123}]$$

$$\bar{\mathbf{q}}_{ij} = \begin{bmatrix} \bar{q}_{ij\_123} \\ \bar{q}_{ij\_4} \end{bmatrix} \quad \bar{\mathbf{q}}_{ij\_123} = \begin{bmatrix} \bar{q}_{ij\_1} \\ \bar{q}_{ij\_2} \\ \bar{q}_{ij\_3} \end{bmatrix} \quad [\tilde{\mathbf{q}}_{ij\_123}] = \begin{bmatrix} 0 & -\bar{q}_{ij\_3} & \bar{q}_{ij\_2} \\ \bar{q}_{ij\_3} & 0 & -\bar{q}_{ij\_1} \\ -\bar{q}_{ij\_2} & \bar{q}_{ij\_1} & 0 \end{bmatrix}$$

Two different sets of data have been used:

- data acquired at November 3rd, 2009, by STR1 and STR2 (172799 samples at 2Hz);
- data acquired at December 10th, 2009, by STR1 and STR3 (79199 samples at 2Hz).

Figure 5.2-1 and Figure 5.2-2 show the estimated spectral densities. It is possible to see that the low-frequency spectral density is about ten times greater than the high-frequency spectral density linked to the temporal noises. Changing the length of the time interval on which the spectral density is computed, it is possible to see the harmonic nature of the low-frequency errors.

To provide a realistic scenario for the simulation, a new mathematical model of star-tracker errors has been developed starting from above in-flight data and analysis. The model takes into account bias, random and harmonic errors. Figure 5.2-3 shows the spectral density of the simulated star-tracker attitude errors.

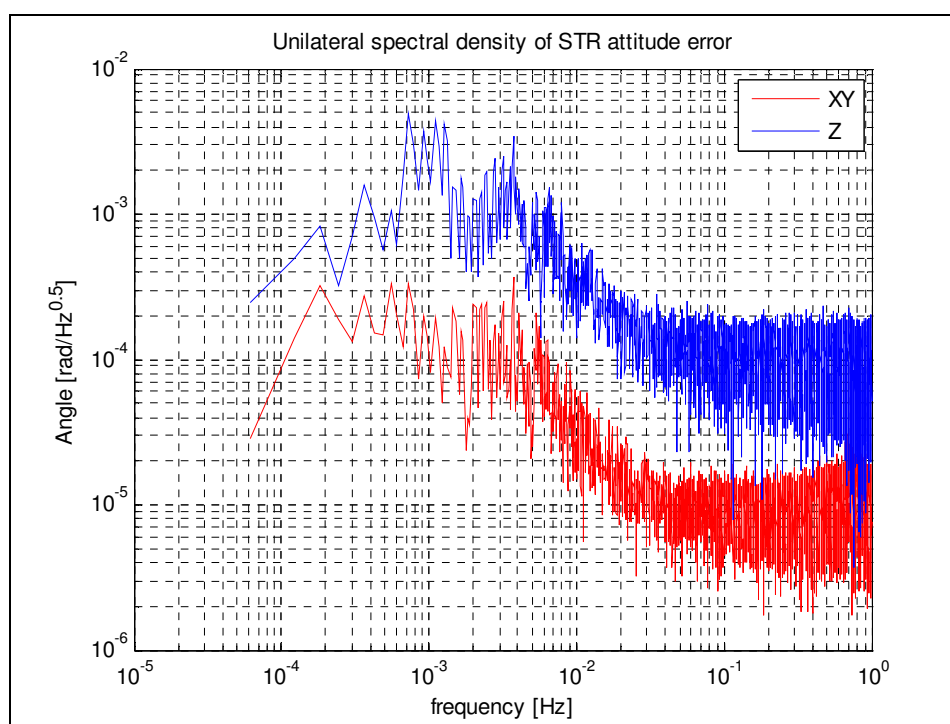


Figure 5.2-1 Estimated one-sided spectral density of star-tracker attitude errors. GOCE STR1 and STR2 time series (Nov 3rd, 2009).

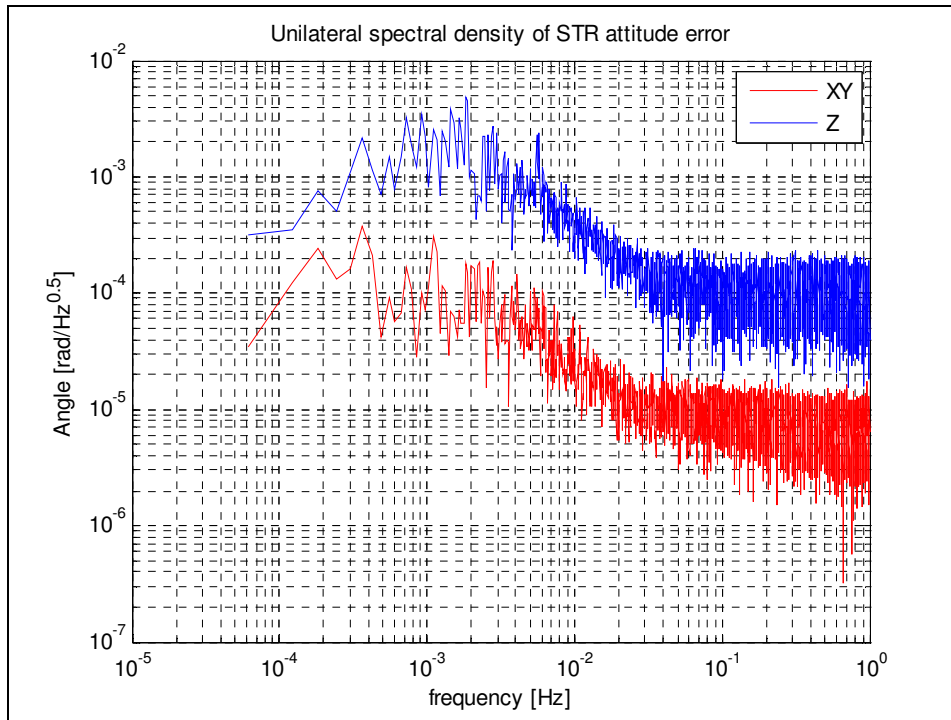


Figure 5.2-2 Estimated one-sided spectral density of star-tracker attitude errors. GOCE STR1 and STR3 time series (Nov 10th, 2009)

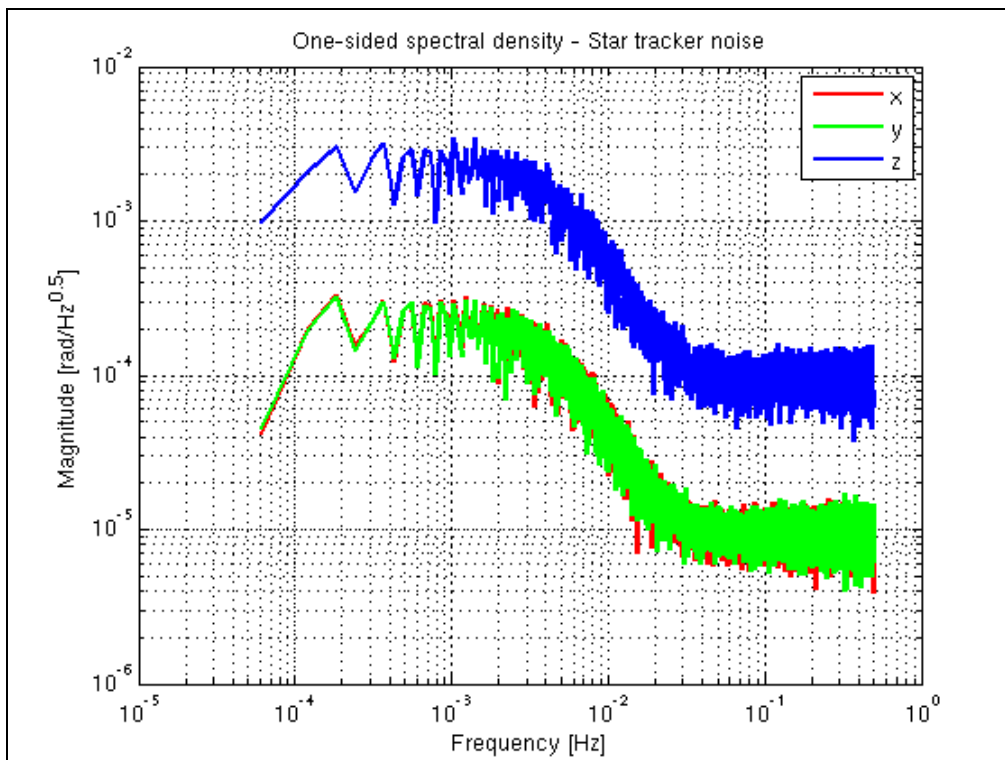


Figure 5.2-3 One-sided spectral density of simulated star-tracker attitude errors

## 6. POST-PROCESSING EMULATOR

### 6.1 Introduction

In the frame of the study, to improve the fidelity of the E2E up to Level 1b, an emulator of the algorithms for angular rate and attitude reconstitution has been developed. Those variables are computed for each satellite in the formation.

### 6.2 Algorithm description

The emulator inputs are:

- actual satellite attitude;
- actual angular rate;
- attitude errors as from star-tracker noise properties and mounting solution;
- accelerometers' linear acceleration noises.

The emulator outputs are:

- estimated angular rate;
- estimated attitude.

The sampling time step is equal to 1s. At each sampling step  $i$ , the estimated angular rate and attitude quaternion are computed according the following formulas:

$$\hat{\omega}(i) = \bar{\omega}(i) + \delta\omega(i)$$

$$\hat{q}(i) = \bar{q}(i) dq(i)$$

being:

$\hat{\omega}$  : estimated angular rate;

$\bar{\omega}$  : actual angular rate;

$\delta\omega$  : additional error on angular rate derived by data-fusion of noises;

$\hat{q}$  : estimated attitude quaternion;

$\bar{q}$  : actual attitude quaternion;

$dq$  : additional quaternion to take into account the additional noise due to data-fusion;

$$\delta\omega(i) = \begin{bmatrix} \delta\omega_x(i) \\ \delta\omega_y(i) \\ \delta\omega_z(i) \end{bmatrix}$$

$$dq(i) = \begin{bmatrix} \frac{\delta\vartheta_X(i)}{2} \\ \frac{\delta\vartheta_Y(i)}{2} \\ \frac{\delta\vartheta_Z(i)}{2} \\ \sqrt{1 - \frac{(\delta\vartheta_X^2(i) + \delta\vartheta_Y^2(i) + \delta\vartheta_Z^2(i))}{4}} \end{bmatrix}$$

For each axis, the pair of correlated estimation errors  $\begin{bmatrix} \delta\vartheta(i) \\ \delta\omega(i) \end{bmatrix}$  is carried out from the data fusion filter.

The data fusion filter embeds the following discrete time state equation:

$$\begin{bmatrix} x_0(i+1) \\ x_1(i+1) \\ x_2(i+1) \\ x_3(i+1) \\ x_4(i+1) \\ x_5(i+1) \end{bmatrix} = \begin{bmatrix} 1-k_0 & 1 & 0 & 0 & 0 & k_0 \\ -k_1 & 1 & 1 & 0 & 0 & k_1 \\ -k_2 & 0 & 1 & 1 & 0 & k_2 \\ -k_3 & 0 & 0 & 1 & 1 & k_3 \\ -k_4 & 0 & 0 & 0 & 1 & k_4 \\ 0 & 0 & 0 & 0 & 0 & k_5 \end{bmatrix} \begin{bmatrix} x_0(i) \\ x_1(i) \\ x_2(i) \\ x_3(i) \\ x_4(i) \\ x_5(i) \end{bmatrix} + \begin{bmatrix} 0 & 0 \\ 1 & 0 \\ 0 & 0 \\ 0 & 0 \\ 0 & 0 \\ 0 & 1-k_5 \end{bmatrix} \begin{bmatrix} \delta\tilde{\omega}(i) \\ \delta\tilde{\vartheta}(i) \end{bmatrix}$$

$$\begin{bmatrix} \delta\vartheta(i) \\ \delta\omega(i) \end{bmatrix} = \begin{bmatrix} x_0(i) \\ x_1(i) \end{bmatrix}$$

$\delta\tilde{\omega}(i)$  : angular acceleration noise computed starting from the linear acceleration noises provided by the simulator;

$\delta\tilde{\vartheta}(i)$  : attitude error as provided by the simulator.

**The gains have been selected according to the pole placement method, in order to approximate the better data-fusion condition taking into account sensors noise properties. Current selected gains are reported in**

In the in-line formation, Satellite 2 may track the LORF allowing the same attitude control architecture described in [RD-22].

Table 4.4-1.

**Table 6.2-1 Preliminary parameters considered for data-fusion filters.**

Axis	Gain	Value
------	------	-------

Axis	Gain	Value
X	$k_0$	2.500000e-03
	$k_1$	2.500000e-06
	$k_2$	1.250000e-09
	$k_3$	3.125000e-13
	$k_4$	3.125000e-17
	$k_5$	1.000000e-04
Y	$k_0$	1.000000e-03
	$k_1$	4.000000e-07
	$k_2$	8.000000e-11
	$k_3$	8.000000e-15
	$k_4$	3.200000e-19
	$k_5$	1.000000e-04
Z	$k_0$	2.500000e-03
	$k_1$	4.000000e-07
	$k_2$	8.000000e-11
	$k_3$	8.000000e-15
	$k_4$	3.200000e-19
	$k_5$	1.000000e-04

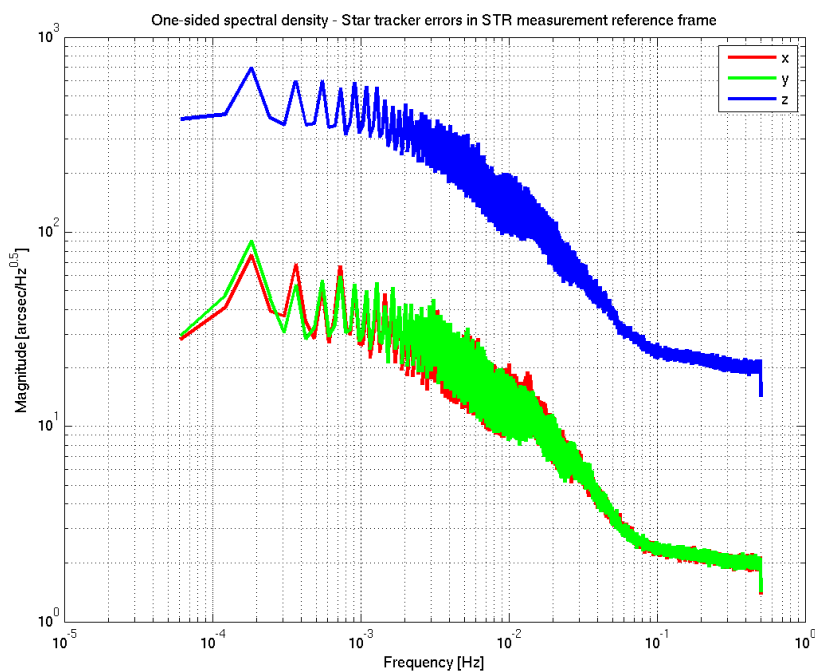


Figure 6.2-1 One-sided spectral density of the star-tracker errors in the equipment measurement reference frame.

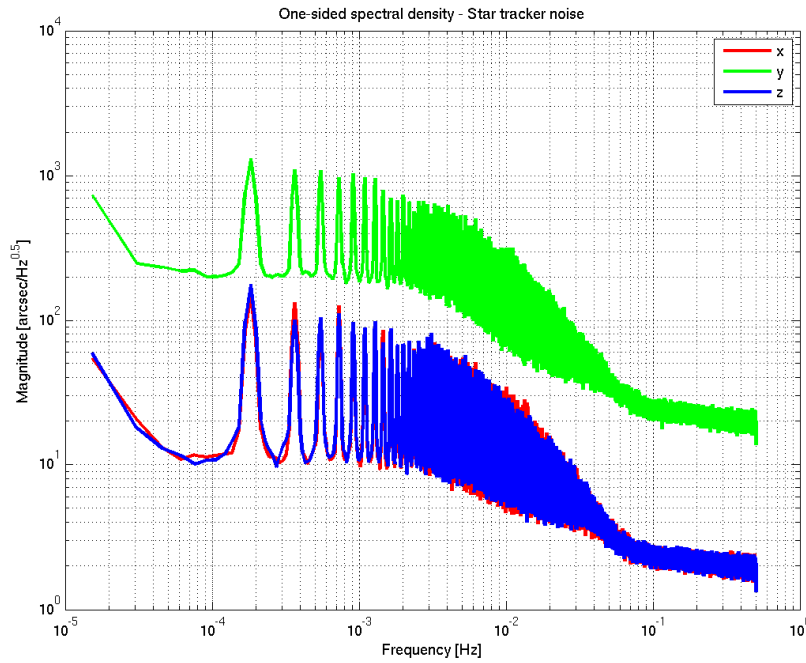


Figure 6.2-2 One-sided spectral density of the star-tracker errors in the data-fusion reference frame (considered coincident with the body reference frame).

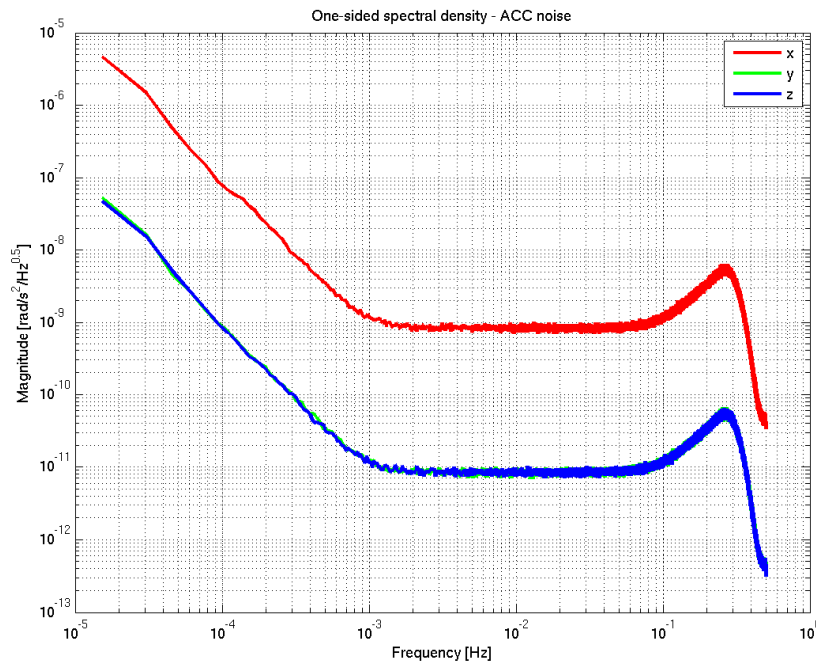


Figure 6.2-3 One-sided spectral density of the simulated angular acceleration errors in the equipment measurement reference frame).

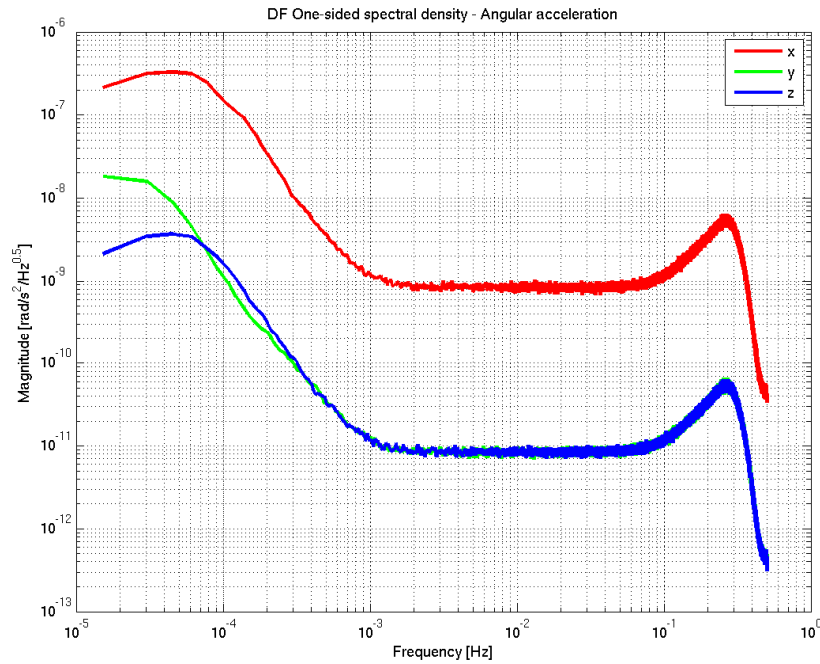


Figure 6.2-4 One-sided spectral density of the estimated angular acceleration error

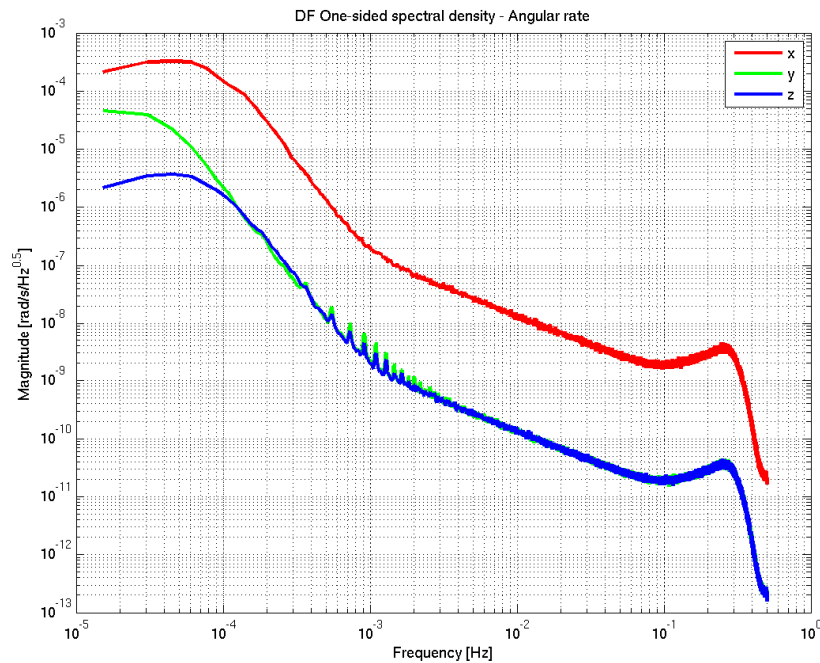


Figure 6.2-5 One-sided spectral density of the estimated angular rate error.

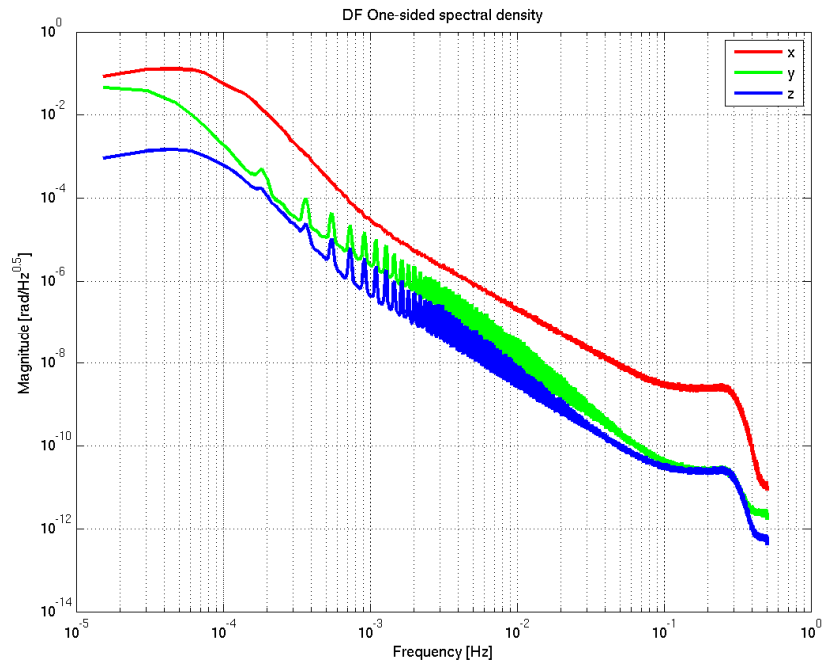


Figure 6.2-6 One-sided spectral density of the estimated attitude error.

## 7. EQUIPMENT REQUIREMENT

### 7.1 Thrusters requirements

The derivation of the thrusters requirement is a complex and delicate activity. To provide reliable values, it is necessary to define the mission scenario (orbit, epoch, formation geometry) and satellite configuration.

Requirements provided on Main thrusters (called also Mini Thrusters) and Lateral thrusters (Micro Thrusters) in the frame of the previous study phase shall be reviewed as consequence of:

- additional formation geometries (e.g. pendulum and cartwheel);
- laser pointing executed by attitude control;
- thrusters assembly modification.

In the following, thruster requirements will be provided considering the thruster assembly as shown in Figure 7.1-1. It is clear that the shown assembly may be considered a good solution for in-line formation geometry, but it shall be deeply reviewed in case of pendulum and cart-wheel formation.

Due to the uncertainty on mission profile and satellite configuration, all provided values shall be considered as preliminary and they shall be reviewed between Mission Architecture Review and Final Presentation.

Moreover, the maximum thrust has been derived considering the scientific observation operating mode only. It means that all requirements shall be provided at the same time (e.g. noise figures and maximum/minimum thrust). Possible additional requirements related to formation acquisition maneuvers (amplitude and timing) have not taken into account at this study phase.

The considered environmental conditions have been:

- operating altitude in the range 300÷350 km;
- maximum and minimum solar activity.

For the in-line formation, at first approximation, the requirement carried out during previous study phase (see [RD-22][RD-23]) may be still considered valid (TBC). The impact on thruster requirement due to formation control has been reduced, and the laser pointing by satellite attitude is not too much significant.

As already written, the pendulum formation requires a different assembly design. At the time being and still considering the assembly provided in Figure 7.1-1, requirements given in Table 7.1-1 and Table 7.1-2 may be considered. The non optimality of the assembly is clearly shown from the fact that there are not significant differences on maximum required thrust between Mini and Micro thrusters. Instead, the Micro thrusters resolution is very little (15 bit are needed).

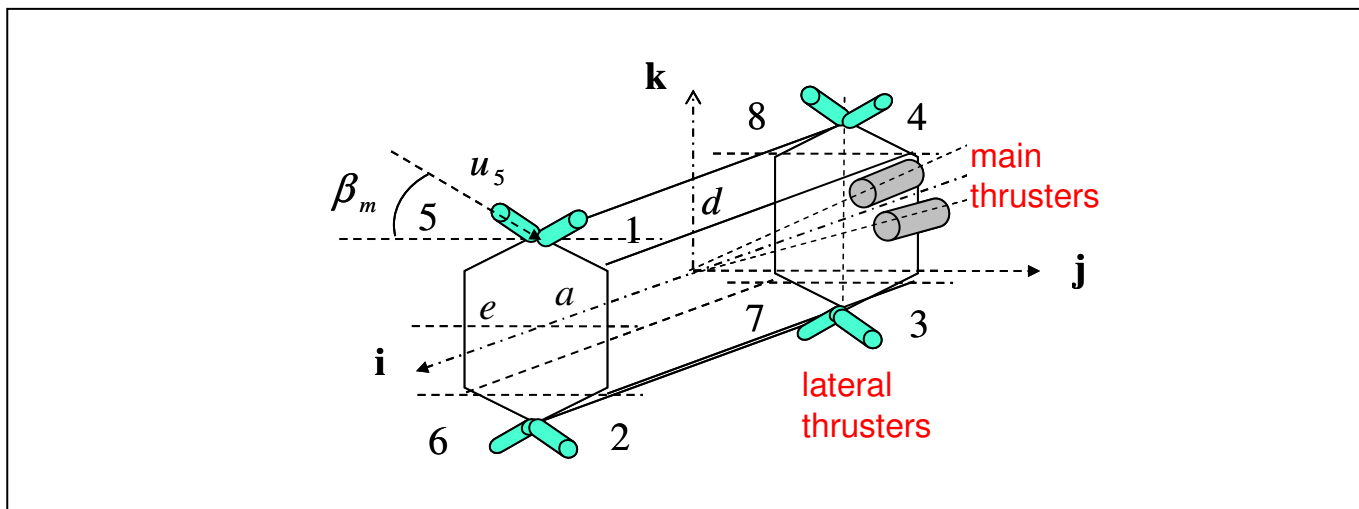


Figure 7.1-1 Sketches of satellite thrusters assembly.

Table 7.1-1 Main thrusters (Mini-thruster) requirement

Parameter	Value	Unit	Comments
Minimum thrust	0.3	mN	
Maximum thrust	15	mN	
Thrust resolution	4	$\mu$ N	
Thrust noise	see figure below		with leakage
Bandwidth	10	Hz	to be transformed in response time
Slew rate	5	mN/s	0.5mN in 0.1s
Update command rate	10	Hz	
Thrust non linearity	< 2%		
Lifetime	> 10 years		
Total impulse			
Specific impulse			
Thrust direction stability			

Table 7.1-2 Lateral thrusters (Mini-thruster) requirement

Parameter	Value	Unit	Comments
Minimum thrust	0.05	mN	
Maximum thrust	12	mN	
Thrust resolution	0.5	$\mu$ N	
Thrust noise	see figure below		with leakage
Bandwidth	10	Hz	to be transformed in response time
Slew rate	5	mN/s	0.5mN in 0.1s
Update command rate	10	Hz	
Thrust non linearity	< 2%		
Lifetime	> 10 years		
Total impulse			
Specific impulse			
Thrust direction stability			

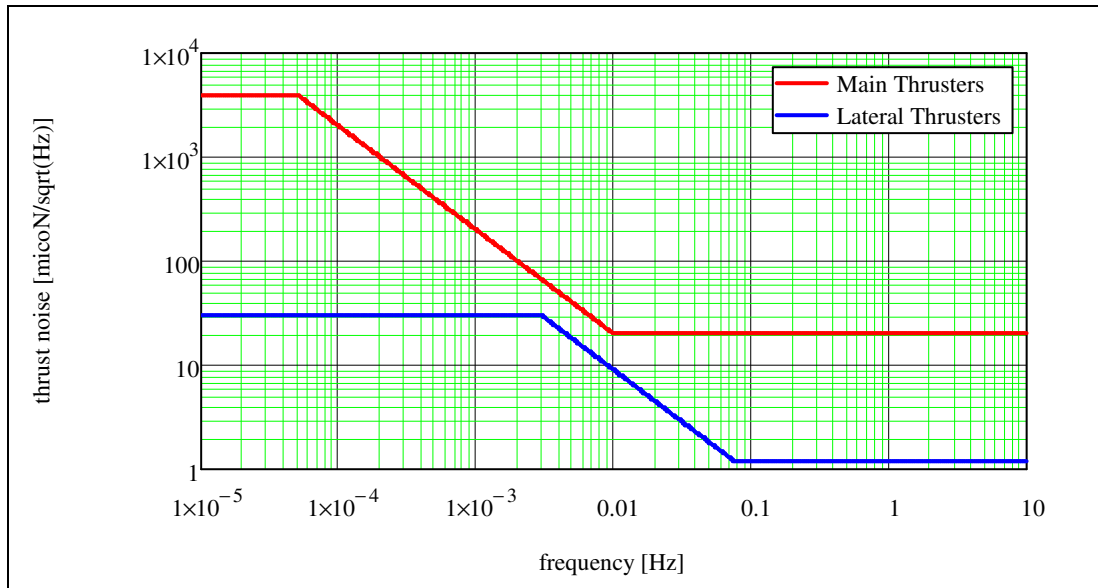


Figure 7.1-2 Thruster noise profile.

## 8. CONCLUSIONS

This document has been submitted in fulfilment of WP 2220 of the Next Generation Gravity Mission (NGGM) study.

The document summarises the work and the results concerning the new design of attitude and orbit control concepts introduced in the frame of the study. These start from the considered new formation geometries like in-line with baseline up to 100km (10km in previous study phase), pendulum and cartwheel. Moreover, the laser pointing mechanism has been cancelled leaving laser pointing function in charge of the attitude control.

The proposed algorithm solutions have shown to be able to cope with the objective of the study, i.e. to support the performance prediction under a more realistic environment. In any case, they should be object of refinement and robustness analysis. This may be subject of a dedicated study in future.

The angular metrology, that is necessary for the laser beam pointing by satellite in pendulum formation, provides accuracy that is not enough to cope with residual angular acceleration requirement for frequency higher than 0.02Hz.

Preliminary thruster requirements update has been done; this will be reviewed and consolidated between Mission Architecture Review and Final Presentation, after consolidation of mission profile and satellite configuration.

## 9. APPENDIX A – ATTITUDE MOTION IN PENDULUM FORMATION

### 9.1 Justification of the attitude motion

The attitude motion observed in pendulum formation on the Satellite 1 and 2, when substituting the beam steering mechanism, will be justified in the following.

Starting from simulation results on relative position and velocity in pendulum formation, the reference attitude to be tracked has been computed according to the formulas provided in chapter 4.4.2.2 is hereafter reported.

At each sample time, the attitude matrix  ${}_I \mathbf{R}_{TARGET1}$  linked with the reference attitude to be maintained by the Satellite 1 (and Satellite 2) reads:

$${}_I \mathbf{R}_{TARGET1}(i) = ({}_I \mathbf{R}_{LORF1}(i)) ({}_{LORF1} \mathbf{R}_{TARGET1}(i))$$

$${}_I \mathbf{R}_{LORF1}(i) = \begin{bmatrix} \frac{\mathbf{v}_1(i)}{\|\mathbf{v}_1(i)\|} & \frac{\mathbf{r}_1(i) \times \mathbf{v}_1(i)}{\|\mathbf{r}_1(i) \times \mathbf{v}_1(i)\|} & \frac{\mathbf{v}_1(i)}{\|\mathbf{v}_1(i)\|} \times \frac{\mathbf{r}_1(i) \times \mathbf{v}_1(i)}{\|\mathbf{r}_1(i) \times \mathbf{v}_1(i)\|} \end{bmatrix}$$

$${}_{LORF1} \mathbf{R}_{TARGET1}(i) = \begin{bmatrix} \hat{\mathbf{n}}_{21}^{LORF1}(i) & \left( \frac{\hat{\mathbf{n}}_{21}^{LORF1}(i) \times \mathbf{v}_1(i)}{\|\hat{\mathbf{n}}_{21}^{LORF1}(i) \times \mathbf{v}_1(i)\|} \right) & \left( \hat{\mathbf{n}}_{21}^{LORF1}(i) \times \frac{\hat{\mathbf{n}}_{21}^{LORF1}(i) \times \mathbf{v}_1(i)}{\|\hat{\mathbf{n}}_{21}^{LORF1}(i) \times \mathbf{v}_1(i)\|} \right) \end{bmatrix}$$

$$\hat{\mathbf{n}}_{21}^I(i) = \frac{\mathbf{r}_2^I(i) - \mathbf{r}_1^I(i)}{\|\mathbf{r}_2^I(i) - \mathbf{r}_1^I(i)\|}$$

$$\hat{\mathbf{n}}_{21}^{LORF1}(i) = ({}_I \mathbf{R}_{LORF1}(i))^T \hat{\mathbf{n}}_{21}^I(i)$$

The reference angular rate has been computed considering the following equation at the first differences:

$$[\tilde{\omega}_{TARGET1}(i)] = ({}_I \mathbf{R}_{TARGET1}(i))^T \left[ \frac{{}_I \mathbf{R}_{TARGET1}(i) - {}_I \mathbf{R}_{TARGET1}(i-1)}{T_s} \right]$$

$T_s$  sampling step.

Figure 9.1-1 and Figure 9.1-2 show the reference angular rate and its spectral density respectively. In the same way, Figure 4.2-3 and Figure 4.2-4 show the actual satellite angular rate and its spectral density.

It is possible to see that the observed movement is in line with the reference trajectory. The differences are very small and not significant in terms of corruption of the performance at frequency close to 1mHz.

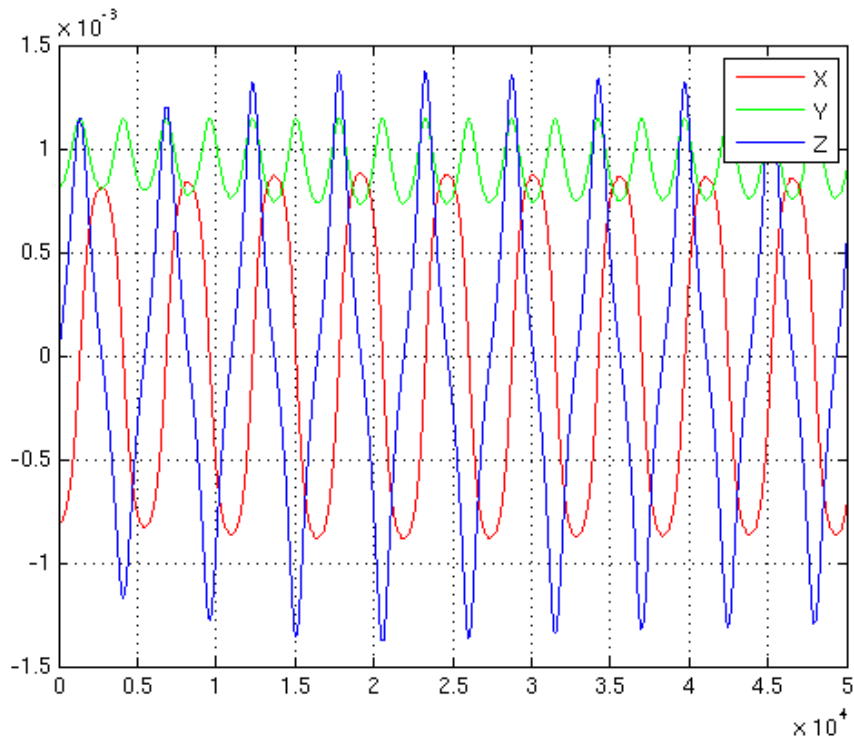


Figure 9.1-1 Reference angular rate.

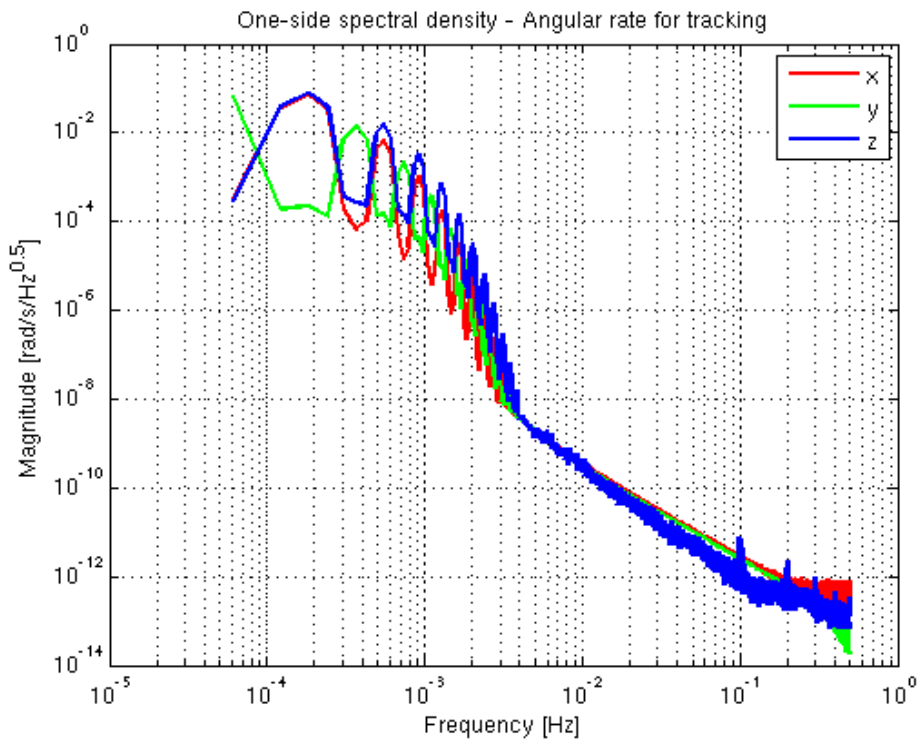


Figure 9.1-2 One-sided spectral density of the reference attitude rate.

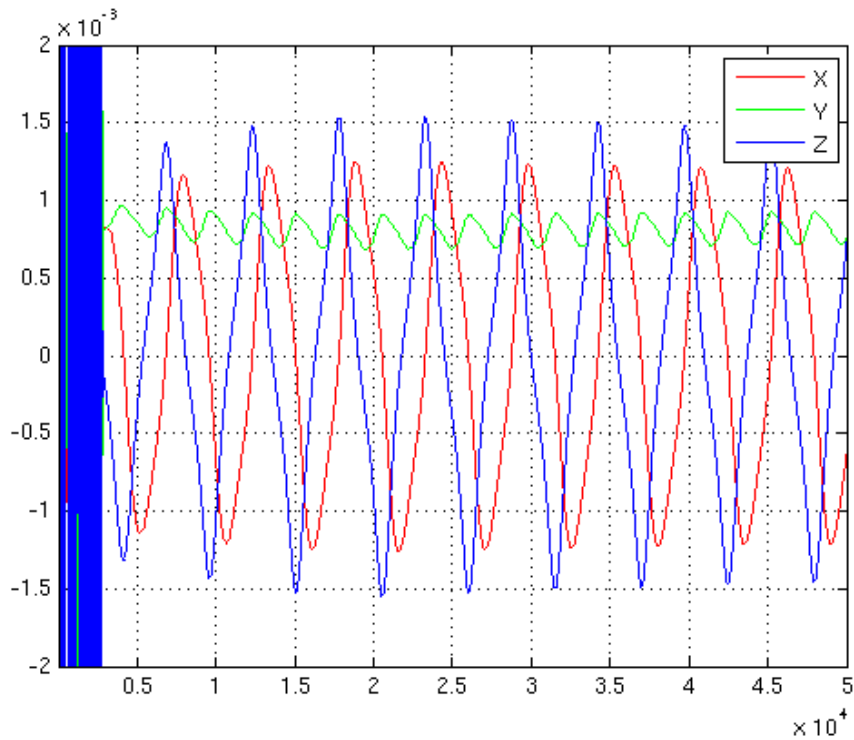


Figure 9.1-3 Satellite 1 angular rate (the init transient is due to the not correct attitude and rate initialization).

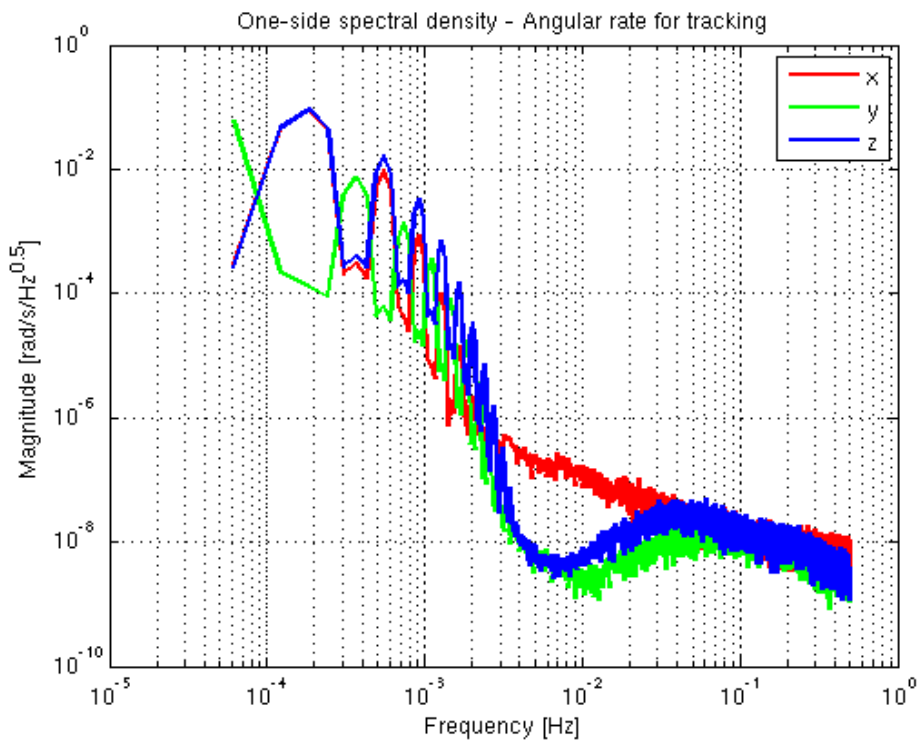


Figure 9.1-4 One-sided spectral density of the Satellite 1 angular rate.

## 10. ACRONYMS

AD	Applicable Document
BOL	Beginning of Life
BSM	Beam Steering Mechanism
C/C	Carbon-Carbon (composite)
CHAMP	CHAllenging Minisatellite Payload
COM	Centre of Mass
DFAC	Drag-Free and Attitude Control
E2ES	End-to-End Simulator
EOL	End of Life
FF	Formation Flying
GNSS	Global Navigation Satellite System
GOCE	Gravity field and steady-state Ocean Circulation Explorer
GPS	Global Positioning System
GRACE	Gravity Recovery And Climate Experiment
HCW	Hill-Clohessy-Wiltshire
INRIM	Istituto Nazionale di Ricerca Metrologica
ITT	Invitation To Tender
KBR	K-Band Ranging
LEO	Low Earth Orbit
II-SST	low-low Satellite to Satellite Tracking
LORF	Local Orbital Reference Frame
LPM	Laser Pointing Mechanism
LRR	Laser Retro Reflector
MBW	Measurement Bandwidth
MIMO	Multi Input Multi Output
MST	Mission Simulation Tool
NGGM	Next-Generation Gravity Mission
P/L	Payload
POD	Precise Orbit Determination
PSD	Power Spectral Density
RD	Reference Document
RF	Radio Frequency
RMS	Root Mean Square
S/C	Spacecraft
SLR	Satellite Laser Ranging
SQUID	Superconducting Quantum Interference Device
SSO	Sun Synchronous Orbit
SST	Satellite to Satellite Tracking
TAS-I	Thales Alenia Space Italia
TBC	To Be Confirmed
TBD	To Be Defined

**END OF DOCUMENT**